Southern California Earthquake Center
an NSF+USGS center
University of Southern California, 3651 Trousdale Parkway, Suite 169, Los Angeles, CA 90089-0742
Phone: 213-740-5843 Fax: 213-740-0011 E-Mail: scec@usc.edu Web: www.scec.org

USC-SCEC/CEA Technical Report #9

for
Milestone 3d

Submitted to

California Earthquake Authority
801 K Street, Suite 1000
Sacramento, CA 95814

From the

University of Southern California
Southern California Earthquake Center
3651 Trousdale Parkway, ZHS 169
Los Angeles, CA 90089-0742

Principal Investigator: Thomas H. Jordan
Director, SCEC

Project 1 Manager: Edward H. Field
United States Geological Survey

Projects 2/3 Manager: Paul Somerville
URS Corporation

November 12, 2007
Rev 2

Summary and Introduction

The objective Project 3 is to improve loss estimates in Southern California using realistic earthquake scenarios. CEA sets its rate schedules using probabilistic hazard maps, but significant earthquake losses occur in discrete events. Approximately 70% of the risk in the CEA's current portfolio is concentrated in Southern California. Better ground-motion scenarios for anticipated large earthquakes will improve CEA's ability to evaluate this risk. Current scenario maps use simplified methods that result in smooth "bull's-eye" patterns of ground motion shaking level which do not contain the variability from one location to the next found for actual earthquakes. For example, the 1994 Northridge earthquake produced concentrations of damage and large recorded ground motion levels in Santa Monica and Sherman Oaks that are not predicted by these simplified methods. In this Project, we will conduct a pilot study to (a) produce more realistic earthquake ground motion scenario maps by including more realistic representations of the earthquake source, seismic wave propagation from the source to the ground surface, and local site geology, and (b) perform simulations of the structural damage to specific index woodframe buildings using the ground motion time histories from these scenarios. The pilot study will focus on scenarios for the Puente Hills blind thrust system, which has only recently been characterized by SCEC scientists and represents a significant hazard that is not portrayed in the 1997 Uniform Building Code. The goal is a capability for end-to-end simulation of the earthquake process that can be used for statewide risk assessment.

This report contains Milestone 3d, whose goal is provide the response of residential index structures to simulated ground motion for scenario ruptures of the Puente Hills fault.

Project 3 Management

The End-to-End project is managed through the SCEC Implementation Interface. Paul Somerville is Project Manager and coordinates activities with CUREE through R. Reitherman, PEER through J. Moehle, the NSF SPUR Project through G. Fenves, and the USGS through W. Ellsworth. T. Jordan acts as Principal Investigator, responsible for the overall success of the project; he provides the CEA with a single point of contact for project management.

Index Woodframe Houses and their Response to Puente Hills Scenario Earthquakes

Keith Porter, Robert Graves, Evan Reis and Paul Somerville

SUMMARY

End-to-end modeling of the scenario earthquake. To produce ground motion time histories for use in the analysis of the response of woodframe buildings, we generated ground motion time histories that represent the potential ground shaking hazard posed by a M7.15 scenario earthquake occurring on the Puente Hills fault system. We selected 648 locations near the fault to examine. We designed six distinct index buildings to examine. Then we generated dynamic models of the fault rupture, propagated the seismic waves through the earth's crust to each location, and input the resulting 3-dimensional waveforms (accelerograms) at each location into nonlinear dynamic structural analysis of each index building. Each analysis produced an estimate of the maximum force and deformation of every structural member of each building, based solely on a mathematical model of the physics involved in the propagation of waves from the rupture to the structural member, hence the term "physics-based modeling." Because the wave passage was modeled from its source at the fault rupture to termination at the building, the analysis is also called "end-to-end (E2E)." The mathematical model is an idealization of a complex reality and therefore involves a number of uncertain inputs that contribute to uncertainty in the outputs (the member forces and deformations in the index buildings). Some means of propagating these uncertainties through from the inputs to the outputs was required.

Uncertainty propagation through moment matching. For this pilot test, we selected four uncertain inputs that from past experience appeared to be most likely to contribute the majority of the uncertainty in the outputs, and varied them. (There are more than four uncertainties that contribute to the uncertainty in the output, but to ensure practical computational effort it was necessary to limit the number of uncertain inputs.) We chose two top seismological variables (rupture velocity and rise time) and two structural ones (one representing both member strength and stiffness, the other representing viscous damping; we also varied building orientation for one of the index buildings.)

We then selected and weighted nine combinations of these variables, i.e., nine sets of particular values of these variables, each with an associated probability-like weight. In general the sample points are (1) each variable set at its median value; (2) all variables but one set at their median values and the remaining variable set at its 96th percentile (i.e., $\mu + 1.732\sigma$) value; (3) all variables set to their median but one set at its 4th percentile ($\mu - 1.732\sigma$) value; (4-9) steps 2 and 3 repeated for each of the remaining three variables. In general the weight applied to each sample depends on the number of variables and samples per variable; here they –0.333 for sample 1 and +0.1667 for samples 2 through 9. As a result, the first five moments of the weighted sample set of input variables (the vector mean, variance, skewness, kurtosis, and 5th moment) match the same moments of

the joint continuous distribution of the input random variables, hence the term *moment matching*.

The output variable (here, the drift in each wall of each index building at each gridpoint) is calculated for each sample vector of the input variables. That is to say, we perform a full end-to-end simulation for each of the nine combinations of the seismological and structural variables. This produces nine sample outputs for each structural member in each index building at each gridpoint. Thus, we perform approximately 9 x 6 x 648 = 34,992 end-to-end analyses. The sample output is then assigned the same weight as the corresponding input set. Thus the first 5 moments of the input samples *exactly* match the moments of the continuous input random variables, while the moments of the sample outputs *approximate* the moments of the output that would have been calculated if the inputs had been continuously sampled. The approximation yields high accuracy: for example, if one matches 5 moments of the input variables, the estimate of the mean drift equals a 5^{th}-order Taylor Series expansion about the mean of drift, and lower-order accuracy of higher moments. As shown in an appendix, moment matching requires orders of magnitude less computational effort than Monte Carlo simulation to achieve the same accuracy, for various smooth and non-smooth functions[1].

Despite the new name, the reader should not assume moment matching is highly novel and untested. It was first suggested for use in earthquake engineering by Rosenblueth (1975). It has been the subject of several peer-reviewed archival journal articles by Julier and his colleagues (e.g., Julier and Uhlmann 2002). And it is related to Gauss quadrature (see e.g., Hornbeck 1975), which has many structural engineering applications, such as finite-element analysis of plates and solids (e.g., Hoit 1995). The moment matching approach allows for correlated basic variables, although the variables we judged to be most important here appear to be uncorrelated, continuous, unimodal, and smooth.

Comparison with an NGA-based approach. By these means, we performed a pilot test of end-to-end simulation of several index buildings through the area affected by a hypothetical M7.15 Puente Hills Thrust Fault earthquake, including propagation of key uncertainties. We then compared the results with a more traditional loss-estimation approach employing empirical seismic attenuation relationships rather than physics-based modeling of ground motion. To do so, we first calculated the mean and coefficient of variation (COV) of shaking intensity by the next-generation attenuation (NGA) relationships. Shaking intensity was measured at each gridpoint in terms of 5%-damped spectral acceleration response at 0.3-second period (denoted here by S_a). For each index building and gridpoint, we found samples from the E2E simulations whose S_a values approximately matched (within ±5%) the NGA-based S_a value at NGA's 4%, 50%, and

[1] The sophisticated reader can independently test these assertions by performing simple spreadsheet calculations. For example, consider a Gaussian input x with zero mean and unit standard deviation, and then consider several smooth and non-smooth functions of x: $y(x) = x^2$, $y(x) = x^3$, $y(x) = x$ if $|x| < 1$ and x^3 otherwise, $y(x) = \Phi(x)$, and $y(x) = x^3$ if $|x^3| < 1$, otherwise 1 x sign(x^3). Apply the trapezoidal rule at the 0.5%, 1.5%, 2.5%, … 99.5% nonexceedance probability values of x. In each case, moment matching produces the same mean as the trapezoidal rule within ±1%, and the variances agree within 13%, *all for 3% of the computational effort*. Monte Carlo simulation generally requires *more* effort than applying the trapezoidal rule to achieve the same accuracy.

96% nonexceedance probabilities. We then scaled the sample drift outputs by the ratio of NGA-based S_a to the E2E-based S_a (i.e., scaling drifts up or down by no more than a factor of 1.05, to reduce sampling error) and calculated the mean and COV of the resulting drifts using the weights 1/6, 2/3, 1/6 (again matching five moments of S_a).

Thus we were able to estimate the mean and COV of each output under an NGA-based approach, and then compare them with E2E. Note that the same inputs, physical models, and structural analyses were used to estimate the moments of the NGA-based outputs as were used for the moments of the E2E outputs, so the comparison of the two approaches is truly an apples-to-apples one.

The differences in the moments of drift under NGA vs. E2E result when one "forgets" details of the rupture and wave propagation. NGA forgets and E2E remembers these details. They principally include directionality and the local 3-D velocity structure of the Los Angeles basin. The NGA relationships ignore directionality, and only reflect the 3D velocity structure in a single basin term that appears in only one of the NGA relationships. Because the E2E analyses account for this additional knowledge and NGA do not, one would expect E2E to produce lower uncertainty in structural response. One would also expect NGA to underestimate structural response in areas with forward directivity and underestimate it elsewhere. Indeed, that is what we found. As shown in Figure A, NGA appears to underestimate drift on the hanging wall by a factor of 2, relative to E2E, and overestimate it elsewhere by a factor of up to 2. As shown in Figure B, E2E appears to reduce the COV of drift by a factor of 2 or more, relative to NGA.

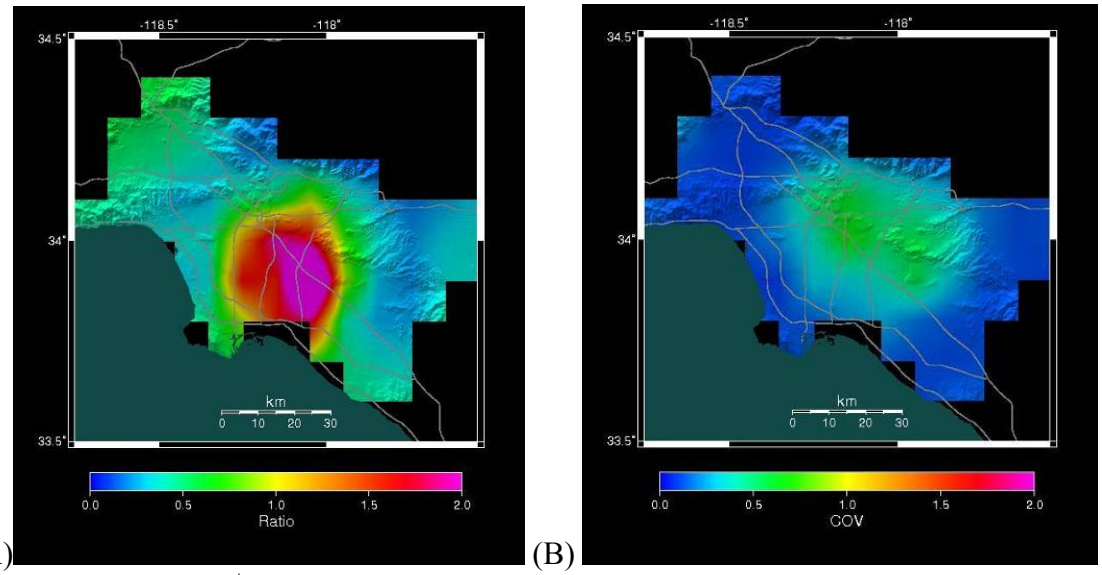

(A) (B)

Ratioaverage-wall 1st-story mean drifts for 1940s-1950s house

Conclusions and value of the study for the CEA. Numerous studies have shown that estimated seismic performance of buildings strongly depends on ground motion variability. It seems unlikely that further work on empirical models such as NGA will reduce these uncertainties. Thus the main opportunity for reducing the uncertainty in

ground motion estimates for scenario earthquakes lies in the further development of the simulation-based methods. Toward that end, this study achieved the following results: it successfully pilot-tested E2E modeling on woodframe buildings; examined a number of new index buildings; examined sensitivity of drift to five top sources of uncertainty; performed NGA-based assessment in addition to end-to-end; examined whether E2E offers advantages over NGA in terms of reduced uncertainty and detection of bias; and supported the hypothesis that E2E seems to reduce uncertainty and to detect bias in the attenuation approach. If our results are further validated, E2E offers the promise of great value to the CEA and its policyholders. For example, reduced COV of loss implies reduced probability of high portfolio losses, and reduced need for (or at least fair price of) reinsurance. Furthermore, directionality could be an important rating factor: the pure premium for locations not on the hanging wall of blind thrust faults may have had their pure premiums calculated too high, and therefore warrant premium reductions. Conversely, policyholders living in houses on the hanging wall of such faults may be paying too little.

Study limitations and recommendations. Though the results tend to support our hypotheses, they are not definitive. Many limitations remain.

Order of moment matching. We do not know how sensitive these results are to the order of the moment matching, and recommend further tests to determine whether 5-point, 7-point or higher order moment matching produces significantly different outputs for the same input, or in other words when moment matching converges on a single stable result.

Comparison with Monte Carlo simulation (MCS). We have not tested these results relative to the more familiar MCS approach. We recommend testing to determine the number of MCS simulations required to converge on a single stable result, and to test whether that result is the same as the one produced by moment matching (MM). With new SCEC peta-scale computing capabilities, it will be practical to perform the large numbers of MCS simulations necessary to compare MM with MCS.

Effect of other important and readily apparent building features. We do not how applicable these results are for index buildings with important structural differences such as: site slope (say > 30%); different foundation types (e.g., post-and-pier or mixed foundations); shiplap siding (horizontal boards nailed to the studs, as opposed to plywood or OSB); or lath-and-plaster walls. We therefore strongly recommend modeling addition index buildings with these and other potentially important and readily apparent features, which could then be available for use as rating factors.

Inventory of important features. The previous point begs the question of how common are homes with these features. The inventory is only indirectly relevant to E2E vs. NGA modeling, but it is necessary to know these statistics if one

wishes to do statewide risk assessment with either method. We therefore recommend undertaking a study of these statistics.

Loss. We do not know how significantly the estimated repair cost or insured losses might differ between E2E and NGA approaches. We recommend further study of these and other index building to determine the impact on loss of the modeling approach.

Other seismological uncertainties. We examined the effects of uncertain rupture velocity, rise time, and high-frequency content on drift. We believe these to be the most important seismological uncertainties in the present case. However, there are other (probably lesser) seismological uncertainties whose effects we do not know. We therefore recommend addition study to estimate the effect of uncertainties in slip distribution, hypocenter location, geological structure, seismic velocity structures, anelastic attenuation (Q of media), near-surface site response, and possibly others. In addition, we used NGA relationships that were still in flux at the time of the study. Because of subsequent revisions, we recommend a study to determine whether these changes significantly impact our findings.

Other structural uncertainties. Though we examined the effect on drift from uncertainties in member strength and stiffness, damping ratio, and orientation, we have not yet examined the effects of various other structural uncertainties. We therefore recommend further study of non-strength-related hysteretic parameters in the structural model, random extreme structural deficiencies such as lack of required hold-downs, long missing lines of connectors, or imperfect correlation in member strength and stiffness.

Claims-adjustment practice. Past studies we have performed for the CEA have carried NGA-type analyses through to loss, but assumed perfect knowledge on the part of the claims adjuster of what damage was and was not earthquake induced. We have anecdotal evidence that even when accompanied by a structural engineer, claims adjusters overpaid Northridge earthquake insurance claims by a factor of 2 on average for one insurer and 7 for another. The effect may be that observed losses and the empirical vulnerability functions derived from them are much higher than the actual earthquake-induced physical damage, primarily because of claims-adjustment practices. Though the relative merits of E2E vs. NGA-style analysis is independent of how claims are adjusted, the difference in uncertainties between the two may be small compared with the bias and increased uncertainty resulting from claims-adjustment practice. We strongly recommend the CEA undertake a study of claims-adjustment practice on modeled losses.

Statewide risk assessment with E2E modeling. If the methodology employed here is validated through MCS, SCEC's peta-scale computing capability will enable us to leverage the efficiency of moment matching to perform E2E modeling of large numbers of scenario earthquakes and index buildings. This is as opposed to the single Mw 7.15 Puente Hills scenario rupture and six index building examined

here. We will be able to perform physics-based PSRA for an insurance portfolio, propagating E2E's uncertainty reduction to overall portfolio risk. Reducing uncertainty means reducing the estimated probability of high losses. This would reduce reinsurance needs and thus potentially allow the CEA to provide the same insurance at lower cost.

PUENTE HILLS SCENARIO EARTHQUAKE GROUND MOTIONS

With the summary provided above as preface, we turn now to the details of the analysis. Recent studies have identified the seismic potential of the Puente Hills fault system, which lies directly beneath downtown Los Angeles. The geometry and slip rate of the system were defined by Shaw et al. (2002), and four large-slip paleoearthquakes on this system were identified by Dolan et al. (2003). The seismic potential of this fault system was manifested by the 1987 Whittier Narrows earthquake, which occurred on the Santa Fe Springs segment of the Puente Hills blind thrust (Shaw et al., 2002). Figure 1 shows a map view of the Los Angeles region indicating the location of the Puente Hills fault system. This section provides a brief description of the broadband (0-10 Hz) ground motion simulations for scenario earthquakes on the Puente Hills fault system. For each rupture scenario, broadband ground motion time histories have been simulated at 648 sites covering the Los Angeles, San Fernando and San Gabriel basin regions (Figure 1).

Rupture Models

Five primary rupture scenarios were considered, consisting of median estimates of rupture velocity and rise time, and combinations of median and +/- 1.732σ values. These five rupture scenarios are designed to represent the random variability in the ground motions for a specified earthquake magnitude on the Puente Hills Blind Thrust, due to random variations in the median values of rupture velocity and rise time in a given earthquake. These five scenarios were designed in coordination with the planning for structural response analysis, described later in this report. For each of these scenarios, the hypocenter is the same and the slip distribution is randomized with a K^{-2} fall-off. The moment magnitude of these scenarios is Mw 7.15. Table 1 summarizes these scenarios, and Figure 2 plots the rupture models.

Table 1. Rupture variables

Name	Rupture velocity (percent of Vs)	Rise time (sec)
CEA_PH-01	80%	1.4
CEA_PH-02	80%	0.9
CEA_PH-03	80%	2.1
CEA_PH-04	70%	1.4
CEA_PH-05	92%	1.4

Ground Motion Results

Figures 3 to 7 plot ground motion maps for the simulations at PGA, PGV, and SA of 0.3 s, 1.0 s and 3.0 s, respectively. The results of six scenarios are show in each figure. Five of the scenarios are described above, and the sixth (PH_All2, lower right panel in each figure) represents an earlier simulation which used a high dynamic stress drop at the high frequencies (variant of CEA_PH-01 and CEA_PH-02).

Figures 8 to 10 plot the simulated ground velocity time histories at sites of Los Angeles, Downey and Long Beach, respectively.

INDEX BUILDINGS

We have developed index buildings for use in the Puente Hills seismic loss model. This involved the following steps:

- Identifying five building types representative of actual detached single family housing styles in the Los Angeles area. The building types represent a range of construction ages and configurations. A trip to the area was made to confirm the choice of building types.

- Identifying the structural elements and characteristics of the index buildings that are likely to affect earthquake performance and building loss. These include the foundation system, bracing and anchorage; wall sheathing; parking under living space; split level configuration; ratio of interior walls to gross square footage; etc. For each building type, one or more possible configurations of these and other elements have been identified.

- For each index building, providing simple building sketches noting the presence and location of these elements, for incorporation into the structural models.

This section of the report summarizes the development of the index houses.

Selection of Housing Locations

The index houses were chosen from actual, typical housing stock in the areas most likely to be affected by the strong ground shaking. Three communities expected to be within the area of strong ground shaking were selected from which to draw the index housing stock: Cypress, Bellflower and Downey. These communities are representative of other communities in the region and contain large tracts of single family homes built over a range of years from the early 1940's to the present. The locations of these communities are shown in Figures 11 and 12.

Selection of Housing Types

The current study is a limited pilot project; therefore only a select number of housing types were to be evaluated. There are dozens of unique broad housing styles that might have been chosen to represent the typical housing stock in the region. Based on experience and the inventory of housing in the area, however, three age categories were selected:

- 1940's – 1950's
- 1960's – 1970's
- 1980's – 2000's

The inventory of housing in the area older than 1940 is relatively small, and the age grouping reflects houses of similar architectural and construction styles.

Housing built in the 1940's and 1950's typically consists of one-story buildings, 1,000 to 1,600 square feet, with two to three bedrooms and one to two baths. Rooms are typically small and ceilings are commonly eight-foot throughout. Windows are typically small. Garages may be one or two cars wide. This age of housing was typically built with more traditional, union labor practices and without the benefit of sophisticated seismic codes.

Housing built in the 1960's and 1970's typically reflects a more spacious floor plan of ranch style construction and consists of medium sized one-story or two-story buildings, 1,500 to 2,200 square feet, with three to four bedrooms and two to three baths. Floor plans often contain separate bedroom and living/dining "wings." Common rooms are typically larger and may have sloping cathedral ceilings. The second floor, if it exists may extend over only a portion of the house and may sit partially over the garage. There are typically larger windows in the first story. Garages are generally two cars wide. This age of housing was typically built with non-union labor in a faster development style with many houses constructed at the same time. These buildings were also commonly built without the benefit of sophisticated seismic codes.

Housing built in the 1980's through the present commonly contain a spacious floor plan of modern architectural style and consist of larger two-story buildings, 2,000 to 3,000 square feet, with three to four bedrooms and two to three baths or more. Floor plans often contain bedrooms upstairs and spacious living/dining areas downstairs with few partitions walls separating the rooms. Common rooms are typically large and may have high cathedral ceilings extending into the second floor space. The second floor typically extends over most of the footprint of the house including the garage. Large windows and French doors predominate. Garages are generally two or three cars wide. This age of housing was typically built with non-union labor in a faster development style with many houses constructed at the same time. These buildings were also typically built with the benefit of sophisticated seismic codes; however, the older types of these homes lack special detailing at the garages, at walls with many windows and in connections between floors that the newer types of homes contain.

Figures 13, 14 and 15 shows photographs of many houses reflective of the styles above. These houses were found using the Internet to search real estate listings in the Cypress, Downey and Bellflower communities.

Six particular houses were considered that reflect common features of the three age groups above, with summary features listed in Table 2.

Table 2. Matrix of index buildings

Era	Story	Siding	Shape	Found.	Slope	Roof
1940-1950s	1	Shingle on skip sheathing	L	Stemwall	Flat	Light
1960-1970s	1	Stucco/plywood	T	Slab	Flat	Light
1960-1970s	2	Stucco/plywood	T	Slab	Flat	Light
1960-1970s	2	T1-11 nailed at lap	T	Slab	Flat	Light
1980-2000s	2	Stucco/OSB	4	Slab	Flat	Heavy
1980-2000s	2	Stucco/OSB, steel frame, strongwalls	4	Slab	Flat	Heavy

Slab: slab on grade

A caution regarding generalization

It was *not* an objective of the present study that the index houses be statistically representative of all houses of the given eras. The Internet search we performed did not constitute a statistical study of the joint probability distribution of features that are important to the seismic performance of houses. Such a study would be required before one could make strong assertions that a set of index houses are statistically representative of the joint distributions of important features. In ATC-50, the Applied Technology Council (in press) offers a long list of features that are potentially important to the seismic performance of woodframe houses. These include such issues as:

- Foundation type (slab on grade, stemwall, cripple wall, post and pier, mixed, etc.). The CEA's portfolio contains a significant number of buildings with raised foundations (stemwalls, cripple walls, etc.); none of the index buildings examined here have raised foundations.
- Site slope (e.g., fraction of houses on >30% slope). A significant number of California houses, and probably of the CEA's portfolio, stand on steep slope; none of those examined here do.
- Shearwall materials (e.g., stucco, plywood, OSB, T1-11, etc.). No statistical data is readily available either on the general population of housing or the CEA's portfolio with which to compare the index buildings examined here.
- Plan and vertical irregularities (e.g., L, U, C, T or other plan shapes). No statistics for comparison either with the population of houses or the CEA's portfolio.
- Relative stiffness and strength in the two perpendicular directions of the house. No statistics for comparison.
- Masses (heavy versus light roofing materials, etc.). No statistics for comparison.

It would be valuable to pursue the goal of statistically representative sample houses in the future. With enough sample houses analyzed by PBEE methods, one could create analytical performance models for populations of houses, e.g., by era of construction, number of stories, foundation type, wall type, etc. One could then make strong assertions about the extent and effects of variability in characteristics on the earthquake performance of populations of houses.

Absent such a study, it is improper to assume that the performance of these particular index buildings should match that of the general population of housing, especially when the performance trends of the population being compared may reflect hidden variables such as claims adjustment practice.

Figure 16 shows the location of specific properties reflecting these housing types.

Figures 17, 18, 21, 24, 27 and 28 show photographs of individual houses reflective of the above building types. A site tour of the building locations and the aerial photographs of the surrounding neighborhoods confirmed that these houses are indeed reflective of

housing styles in the area expected to be affected by strong ground motion from the Puente Hills Fault.

Figures 19, 22, 25, 29 and 30 are tables describing the primary structural characteristics of each building type. The elements are those that are expected to impact the seismic performance. These descriptions are based on experience with the construction of these types of houses, requirements of codes in effect during the era of construction, site observation of typical housing styles and discussions with others knowledgeable in housing construction.

Several of the houses shown or nearby houses of similar construction were toured to develop typical floor plans. The floor plans of typical houses of each style are shown in Figures 20, 23, 26 and 31. The floor plans reflect best estimates of dimensions and floor plan layouts based on observation and experience. Each figure contains information and a wall section describing typical construction details and the structural elements of the buildings. These elements should be incorporated into the computer model of the buildings developed by SCEC. The structural details should be considered common in buildings of each style. However, these elements in individual houses will of course be present in a lesser or greater extent, and architectural styles and thus earthquake performance will be unique to each house.

STRUCTURAL MODELS

The index building designs described above are used to develop structural models for use in structural response analysis.

What is a structural model? By "structural model" is meant a mathematical idealization of the house, in which individual structural members are modeled using mathematical springs whose stiffness (the amount of force required to deform the spring by a fixed amount) depends on the member's materials and connections. The technical reader should know that plywood, OSB, T1-11, stucco, and gypsum wallboard walls are represented by spring-type members with Wayne Stewart degrading stiffness hysteresis.

Structural model parameters. In general, median strength and stiffness parameters for each structural element (each plywood shearwall, for example) were calculated based on the wall's length and per-unit-length values recommended by FEMA 356 (ASCE 2000), or from laboratory tests such as Pardoen et al. (2000), or calculated using the finite-element software CASHEW (Folz and Filiatrault 2000). CASHEW models a woodframe shearwall panel as a collection of rigid linear studs and plates, linear elastic rectangular sheathing panels, and nonlinear connectors, and calculates the equivalent parameters for a single nonlinear spring. See Appendix 1 for an example calculation of the strength and stiffness parameters for a particular combination of sheathing and nailing. In particular, we examine an 8-ft high woodframe shearwall sheathed with T1-11 siding, nailed at the lap with ¼-in edge distance.

PROPAGATION OF UNCERTAINTY

The structural analyses involve a number of uncertain variables. As noted earlier, rise time and rupture velocity are uncertain for a given fault rupture location and magnitude. Furthermore, numerous laboratory tests and field observations have shown that structural parameters such as damping, member strengths, and member stiffnesses are also uncertain. The orientation of the building relative to the fault is another uncertain variable. Several methods are available to treat these uncertainties:

(1) One could ignore them, and model the system using only best-estimate values. This approach however would provide no insight into uncertainty in seismic performance, nor permit comparison between performance estimates using end-to-end simulation and performance estimates using seismic attenuation relationships.
(2) Use Monte Carlo simulation. In this approach, all the uncertain variables are randomly simulated a large number of times. This approach is straightforward but can be computationally expensive, potentially requiring tens of thousands or more simulations and potentially terabytes of storage to achieve reasonable accuracy for a problem of the size addressed here.
(3) Use numerical integration. There are several possible methods to perform numerical integration. In one method, referred to here as *moment matching*, points are carefully selected from the distribution of each uncertain variable so that the moments of the selected points (mean, variance, skewness, etc.) match those of the continuous uncertain variables. Moment matching is far more efficient than Monte Carlo simulation, allowing comparable accuracy to Monte Carlo approaches using with a more-practical number of simulations. Viewed another way, moment matching provides superior accuracy for the same number of simulations. Moment matching is the approach used here.

How moment matching works. The theory behind moment matching is briefly discussed a little later, but for present purposes it is sufficient to summarize the math. Say one is interested in estimating moments of the distribution of an uncertain variable of interest, such as the mean and variance of drift along a column line of a woodframe dwelling. Let the uncertain drift be denoted by Y, which can be calculated as a function of one or more other uncertain variables X, whose distributions are known (or can be estimated). In the present case, X includes earthquake rupture velocity, rise time, member strengths and stiffnesses, etc., which all feed into the structural analyses used to calculate drift, Y. Let μ_Y and σ_Y denote the estimates of mean and standard deviation of Y; these are calculated as

$$\mu_Y = \sum_{i=1}^{N} w_i Y_i$$
$$\sigma_Y = \sqrt{\left(\sum_{i=1}^{N} w_i Y_i^2 \right) - \left(\mu_Y \right)^2} \qquad (1)$$

where Y_i denotes the drift calculated by assuming a particular simulation of the uncertain variables X, denoted by X_i, and w_i denotes a weight associated with the set X_i.

Comparison of moment matching and Monte Carlo simulation. In Monte Carlo simulation, the X_i values are selected at random from the distributions of X and the weights are all equal ($1/N$). In moment matching, the choice of X_i is more deliberate and the w_i values are generally not all equal. In the present case, X_1 represents a simulation in which all of the variables in X are taken as their median values, and the remaining simulations X_2, X_3, … X_N have all the variables at their median except one, which is taken either at a low value (here, its 4^{th} percentile) and a high one (its 96^{th} percentile). In simulations X_2, X_3 … X_N, the low and high values for each variable in X is sampled once, with all the others at their medians.

The main benefit here from moment matching is its efficiency (crucial for present purposes), but a side benefit is that one can see how sensitive Y is to each variable in X, because one sees how Y changes when one changes one of the variables in X from its median, to a lower bound, to an upper bound. If the change in Y is small, Y is said to be not very sensitive to that uncertain variable in X, so in the future one might simply assume that that variable is fixed rather than uncertain, without significantly underestimating the uncertainty in Y.

For more insight into the accuracy and superiority of moment matching versus Monte Carlo simulation, see, e.g., Rosenblueth (1975) or Julier and Uhlman (2002). A briefer technical treatment is contained in Appendix 3 of the present document, but in summary, the same variability of input data can be captured using moment matching as with Monte Carlo simulation. Both require the modeler to select which variables should be treated as random, and both require the modeler to specify the distributions of the basic random variables (though neither requires parametric distributions). There is no difference in the objectivity or admissibility of the methods. The main difference is that moment matching converges much more quickly than Monte Carlo, and provides sensitivity information along the way as an informative byproduct. For a simple illustration of the accuracy of moment matching, see Figure A3-1 in Appendix 3.

How moment matching is applied here. In the present application of moment matching, 18 nonlinear time-history structural analysis were initially performed for each index building at each of 648 gridpoints shown in Figure 1, as summarized in Table 3. For example, in simulations 8, 9, 17, and 18, nominal values of initial stiffness, yield strength, and ultimate strength for all members are all scaled by a single factor (e.g., 0.6 in simulations 8 and 17), namely the strength-and-stiffness factor, while all the fault-rupture variables and damping ratios were taken at their nominal value. (The other extreme, taking all member strength and stiffness values as uncorrelated or even negatively correlated would probably result in an underestimated drift variance.) After the 1940-1950s house was examined, it appeared that drift is not particularly sensitive to building orientation (at least for this house in this earthquake scenario), so for efficiency's sake only simulations 1 through 9 were performed for the other houses.

Table 3. Simulation matrix

Sim *i*	Fault rupture[a]	Structural variables[b]	X-axis[c]	Weight w_i[d]
1	Nominal	Nominal	0°	-0.1667
2	0.9 sec rise time	Nominal	0°	0.0833
3	2.1 sec rise time	Nominal	0°	0.0833
4	0.7 Vs rupture velocity	Nominal	0°	0.0833
5	0.92 Vs rupture velocity	Nominal	0°	0.0833
6	Nominal	5% damping ratio	0°	0.0833
7	Nominal	18% damping ratio	0°	0.0833
8	Nominal	0.6 x strength and stiffness	0°	0.0833
9	Nominal	1.6 x strength and stiffness	0°	0.0833
10	Nominal	Nominal	90°	-0.1667
11	0.9 sec rise time	Nominal	90°	0.0833
12	2.1 sec rise time	Nominal	90°	0.0833
13	0.7 Vs rupture velocity	Nominal	90°	0.0833
14	0.92 Vs rupture velocity	Nominal	90°	0.0833
15	Nominal	5% damping ratio	90°	0.0833
16	Nominal	18% damping ratio	90°	0.0833
17	Nominal	0.6 x strength and stiffness	90°	0.0833
18	Nominal	1.6 x strength and stiffness	90°	0.0833

(a) Nominal fault rupture velocity = 0.8 Vs; rise time = 1.4 sec
(b) Nominal damping ratio = 10%; nominal strength and stiffness = 1.0 x calculated
(c) Direction of the index building's X-axis, relative to north
(d) Weight for Equation 1. After assessing the 1940s-1950s house, we ignored orientation, using 0°-orientation only. For these buildings, only samples 1-9 are used and weights are doubled.

Basis for structural model parameters. As noted above, nominal values of structural model parameters were determined using FEMA 356 (ASCE 2000), where applicable, or CASHEW or other data where FEMA 356 is insufficient. Coefficients of variation were determined using laboratory test data, for example the City of Los Angeles-UC Irvine shearwall tests performed by Pardoen et al. (2002). Low and high values are taken as median $\pm$ 1.73σ, or more precisely $\exp(\lambda \pm 1.73\beta)$, where λ denotes the mean of the natural logarithm of the uncertain variable, and β denotes the standard deviation of its natural logarithm. This reflects the assumption that the variables treated here are lognormally distributed.

The use of the lognormal distribution is justified several ways. First, observations of their values in real buildings tend to fit the lognormal distribution, see for example Porter et al. (2002) which found the distribution of damping ratio at low excitation tended to fit the lognormal distribution. Second, there is strong precedent: an ANSI standard that helped to set the stage for load and resistance factor design (Ellingwood et al. 1980) supports the use of lognormal distributions for strength in many structural elements. Finally, a strong theoretical reason: information theory says that when a variable is positive and constrained only by its median and logarithmic standard deviation, the lognormal

distribution is the "maximum-entropy" or least-knowledge distribution, meaning that it assumes the most uncertainty possible.

Basis for damping ratios. The damping ratios and coefficients of variation shown in the foregoing table may seem high to the engineering reader more familiar with concrete or steel design, but they are solidly based in the observed seismic performance of actual woodframe buildings in several earthquakes, and independently supported by several sources. A technical treatment of this issue is contained in Appendix 2. In brief, the mean, variance and distribution of damping ratios are derived from system-ID analysis of seismic records for instrumented woodframe buildings, documented in recent work by Camelo et al. (2001) for the CUREE-Caltech Woodframe Project. They generally agree with other published sources, some of which suggest elastic damping ratios lower than 5% or greater than 18%, including, notably, Newmark and Hall's 1982 EERI monograph (whose suggested damping ratios were adopted by the developers of the HAZUS-MH software) and FEMA 356 (ASCE 2000; see Sec 1.6.1.5.3). The idealized distribution (lognormal) passes a formal goodness-of-fit test. Finally, it was calculated that drift is only moderately sensitive to variability in the damping ratio. The other sources of variability—rise time, etc.—dominate the variance in drift.

NONLINEAR TIME-HISTORY STRUCTURAL ANALYSES

Structural analysis software used. Structural analyses were performed using Ruaumoko 2D (Carr 2001). Ruaumoko is a powerful general-purpose structural analysis software package developed at the University of Canterbury. It can perform static and dynamic, linear and nonlinear structural analyses, including both material and geometric nonlinearities. It offers a wide variety of options for damping, structural member types, stiffness and strength degradation, applied loads, and methods for time-history integration. It is capable of 2-D or 3-D structural analysis, though 2-D "pancake" models were used here.

What is meant by 2-D structural analysis, and which 2Ds were used. The reader should note that the 2 Ds in question in a pancake model may not be the familiar ones: as shown in Figure 32, which schematically illustrates a pancake model, the 2 Ds are the two horizontal axes, not one horizontal and one vertical. That is, the software is looking down at the building from above, not looking at one column line from the side. In a pancake plan model, shearwalls are represented as zero-height springs connecting a fixed base to a 2-D roof or floor diaphragm, or connecting the 1st-floor diaphragm to the roof diaphragm.

This approach explicitly models torsion and asymmetric plan (and elevation), though it does not capture P-delta effects, which is potentially relevant at high drifts, especially for houses with post-and-pier foundations (none of the index buildings has these). The analysis thus *explicitly calculates* out-of-plane deformations such as stresses and deformations and twists caused by torsion, and thus captures the important effects on inter-story drift from unsymmetrical floor-plan shapes. Diaphragms are treated as flexible, using the shear modulus proposed by FEMA 356. We judged torsion and plan irregularities more important to capture than P-delta, so the choice of a pancake model

(versus an elevation model) seemed the more reasonable of the two choices of which 2 Ds to use. Of course it would be preferable to use full 3D modeling, but this would have been prohibitively expensive in terms of computer time, given the number of simulations required to produce maps and to capture uncertainty to a reasonable extent. To perform the same number of 3-D structural analyses as were performed here for 2-D would have taken months or more of dedicated computer time.

Structural models and periods of vibration. Figures 33 through 36 depict the structural models configurations. The structural models for all the index buildings are available for review and use by others at www.risk-agora.org/archive.htm. Table 4 lists 1st- and 2nd-mode periods of the index buildings with all-nominal values. Periods generally agree with empirical observation by Camelo et al. (2001). The effect of the largely unbraced garage opening in the 1940s-1950s house is evident in the relatively high 1st-mode period. The very open floor plan of the 1980s-2000s house has a similar effect: with high mass and few walls, the period of this 2-story house is substantially greater than for either 2-story 1960s-1970s house; the effect on drift will be clear shortly. Perhaps because floor and roof diaphragms are treated here as flexible, the special seismic details on the north and south walls have minimal effect on period, though they will be shown to reduce average drifts.

Table 4. Periods of index buildings

Index building	1st mode (sec)	2nd mode (sec)
1940s-1950s	0.18	0.13
1960s-1970s 1-story ("1960a")	0.14	0.14
1960s-1970s 2-story ("1960b)	0.19	0.16
1960s-1970s 2-story, T1-11, no stucco ("1960d")	0.15	0.13
1980s-2000s 2-story ("1980a")	0.28	0.23
1980s-2000s 2-story, special seismic detailing ("1980b")	0.28	0.23

Judging by periods, one would expect 1960a and 1960d to have the lowest drifts, the 1980s houses to have the highest ones, and the 1940s and 1960b house to have intermediate drifts, relative to the others; an expectation borne out in the structural analyses.

Number of structural analyses. Nine nonlinear time-history structural analyses were performed for each of six index buildings at each of 648 gridpoints, for a total of 35,000 nonlinear time-history structural analysis. Each analysis took on the order of 30 seconds on a laptop PC, for a total of approximately 300 hours, or 12 days, of computer time.

GEOGRAPHIC MAPS OF RESPONSE: END-TO-END SIMULATION

Outputs from Structural Analysis

The point of these structural analyses was to calculate interstory drift along each column line and at each story under end-to-end modeling (E2E). (Accelerations in each direction

along each column line were also calculated, although they are less interesting in the present case, where loss is dominated by damage to walls, which are sensitive to drift, as opposed to content and roof-tile damage, which are more sensitive to acceleration. The accelerations are available for use in a later study, but for brevity's sake are not presented here.) Rather than trying to map drift on all walls at all stories, we mapped drift only on the 1st story (which tends to dominate damage and loss in 1- and 2-story woodframe houses), for the "worst wall," i.e., the one with the greatest drift, and the "average wall," meaning the average of the drift along all column lines. E2E maps contained here include:

- ***Worst-wall 1st-story E2E drift simulations.*** This is the drift on the worst 1st-story wall (sometimes called a column line) by E2E simulation, i.e., the wall of the 1st story with the largest drift under a given simulation of rupture rise time, rupture velocity, damping, strength and stiffness. These maps can be compared between simulations to see how sensitive the worst-wall drift might be to a given uncertainty in the rupture or structural model. We do not present maps of 2nd story walls here because in 2-story buildings, it appears to be the 1st story that dominates losses. These maps are contained in Appendix 4.
- ***Average-wall 1st-story E2E drift simulations.*** This is the drift on the average 1st-story wall or column line in a given simulation. These maps can be compared between simulations to see how sensitive the average-wall drift might be to a given uncertainty in the rupture or structural model. These maps are contained in Appendix 5.
- ***Expected value of worst-wall and average-wall 1st-story wall E2E drift.*** These are the weighted average drift of the worst and average 1st-story wall, considering all the uncertainties in rupture rise time, rupture velocity, member strengths and stiffness, and damping. These maps are contained in Appendix 6.
- ***Coefficient of variation of worst-wall and average-wall 1st-story E2E drift***. The coefficient of variation (denoted by COV) is the standard deviation divided by the mean, so it represents a sort of plus-or-minus multiplier to indicate uncertainty. Here, it is the multiplier for drift on the worst 1st-story wall. COV = 0.25, for example, means that the drift on the 1st story varies by ± 25%, roughly speaking, considering all those uncertainties. (Actually the ± term is a more complex, because drifts tend to be lognormally distributed. They can have COVs of 1, 1.5, or 2, which doesn't mean drift uncertainty of ±100%, ±150%, or ±200%.) These maps are also shown in Appendix 6.
- ***Bottom-line maps.*** The maps that really matter for purposes of comparing the average effect on estimated drift by using E2E versus attenuation are those that show the average-wall 1st-story drift under E2E and under attenuation, and the ratio of the former to the latter. The maps that matter in testing whether E2E produces lower drift uncertainty than attenuation show the coefficient of variation of average-wall 1st-story drift under the two approaches, and the ratio of the two. These are discussed shortly.

Worst-Wall 1st-story Drift Results

Appendix 4 shows the worst-wall drifts for each index building in Table 2 and each simulation in Table 3. Note that in the 1940s-1950s index building, the garage is largely unbraced in the plane of the garage door opening, so sway of that wall is substantially higher than for the rest of the building. These figures suggest the following:

- Uncertainty in rise time, rupture velocity, strength, and stiffness can have a substantial effect on the worst 1st story drift;
- By comparison, viscous damping (not hysteretic) was observed to have modest effect on drift, and building orientation was observed to have relatively negligible effect, so negligible that simulations 10 through 18 were only performed for the 1940s-1950s building, and none of the others.

The coefficient of variation of worst-wall-line roof drift in the 1940s-1950s building can be substantial: typically on the order of 1.0, when conditioned on rupture magnitude and location, and building design and location.

The 1960s 1-story index building with stucco and plywood sheathing (labeled "1960a" for brevity) experiences much lower drifts than the 1940s-1950s index building, generally less than 0.5 inches with a coefficient of variation generally less than 0.75. These results agree qualitatively with intuition: because of its stucco and plywood, the 1960a house is much stiffer than the 1940s-1950s house, whose lateral strength and stiffness is primarily provided by the gypsum wallboard interior wall finishes alone.

The 1960s 2-story house with stucco and plywood sheathing (labeled "1960b" for brevity) has greater mass than 1960a, because of the 2nd story, without significantly different 1st-story stiffness, which increases mass and hence fundamental period. The change in period probably explains the substantially greater 1st-story drift, compared with 1960a, with some locations experiencing expected drift in excess of 2 inches.

The 1960s 2-story house with T1-11 siding and no stucco is labeled "1960d," rather than "1960c," because a 1-story version with T1-11 and no stucco was anticipated but not ultimately created; the label 1960c was reserved for it. As might be expected from its lower period, 1960d is estimated to experience lower worst-wall drifts than 1960b. One might expect the drifts to be higher, not lower, because T1-11 tends to be more flexible than plywood, and the lack of stucco should also make 1960d more flexible. Probably the reduced weight of 1960d compared with 1960b is responsible for the lower period.

Estimated drifts in the 2-story 1980s-2000s house without special seismic detailing (labeled "1980a") are very high, with houses across most of the San Gabriel Valley and much of the Los Angeles basin estimated to experience worst-wall 1st-story drift in excess of 2 inches, which would likely cause such a house to be a complete loss and potentially to collapse. These high drifts are to be expected: the house has large openings and relatively small length of shearwall for its weight, compared with the 1960b building.

Drifts are somewhat lower for the 2-story 1980s-2000s index building with special seismic detailing (labeled "1980b") than in 1980a, owing to the stiffness added by the

strongwalls and steel frame. The special seismic detailing does not fully compensate for the openness and high weight-to-wall area ratio in this index building, and so drifts are still substantially higher than in 1960b.

Average-Wall 1st-Story Drift Results

Appendix 5 contains maps of the average 1st story wall drifts. Again, by "average 1st-story wall drift" is meant the equally weighted average of peak transient drifts along each 1st story wall. It reflects a sort of overall average displacement of the roof (in 1-story houses) relative to the foundation, or of the 2nd floor (in 2-story houses) relative to the foundation. It is indicative of the average damage to 1st-story walls, where damage would tend to be concentrated in 1- and 2-story houses without raised foundations as is the case here.

Trends in these buildings are similar to the worst-wall drifts, though generally lower. The average-wall drift is generally 30% to 70% that of the worst-wall drift. Table 5 shows the average value of this ratio by index building. The table reflects the average over all gridpoints for the all-nominal simulations. It shows for example that the special seismic details in the 1980s-2000s house tend to reduce torsional effects.

Table 5. Average wall vs. worst wall 1st-story drift

Index building	Ratio
1940s-1950s 1-story	0.7
1960s-1970s 1-story	0.4
1960s-1970s 2-story stucco and plywood	0.4
1960s-1970s 2-story T1-11 no stucco	0.4
1980s-2000s 2-story	0.3
1980s-2000s 2-story special seismic details	0.5

GEOGRAPHIC MAPS OF RESPONSE: ATTENUATION APPROACH

Method for Comparison

In the foregoing analyses, accelerograms at each gridpoint were calculated by a end-to-end approach, i.e., a dynamic time history structural analysis of the earth wherein the analyst calculates the passage of seismic waves between the fault rupture and each gridpoint and produces accelerograms particular to that rupture and travel path.

E2E employs a great deal of information about the rupture and travel path beyond what is involved in a more traditional attenuation-based approach. In the attenuation-based approach, one uses attenuation relationships that reflect regression analyses of intensity observations from numerous historical recordings at disparate sites in past earthquakes.

It is hypothesized here that compared with E2E, the traditional approach introduces greater uncertainty in structural response, and under some circumstances could produce error in the mean estimate of structural response. We can test this hypothesis by

performing the structural analysis both ways: by the end-to-end and traditional approaches, and then mapping the ratio of the mean structural response under the two approaches (to test for bias) and mapping the ratio of the coefficient of variation of structural response of the two approaches (to test for uncertainty reduction).

We wish to perform an apples-to-apples comparison of NGA vs. E2E. That means limiting the differences between the two methods to the one being tested: better information about the rupture and path. To do so, we use the same ground motions and same structural analyses in both the E2E and NGA analyses. In the NGA-based approach we "forget" the path the waves traveled to reach the building site. That is, for an NGA-based analysis at any gridpoint, we consider any E2E analysis (of the same index building) whose S_a value matches the NGA S_a within ±5%. We do this as follows:

1. ***Calculate S_a(0.3 sec, 5%) at each gridpoint using attenuation relationships***. A SCEC researcher, Nitin Gupta, used the OpenSHA software with the same rupture surface and magnitude as in the end-to-end approach, along with Next-Generation Attenuation (NGA) relationships by Boore and Atkinson (2006), Campbell and Bozorgnia (2006), and Chiou and Youngs (2006), to calculate for each gridpoint the mean and standard deviation of the 0.3-sec, 5% damped elastic spectral acceleration response, denoted by S_a for brevity. Results of the three NGA relationships were weighted equally to produce estimated mean and coefficient of variation of S_a at each gridpoint, as follows:

$$\mu'_{S_a} = \frac{1}{3}\sum_{i=1}^{3}\mu_i$$
$$\sigma'^2_{S_a} = \frac{1}{3}\left(\sum_{i=1}^{3}\sigma_i^2 + \sum_{i=1}^{3}\left(\mu'_{S_a} - \mu_i\right)^2\right) \quad (2)$$

   where μ_i denotes the mean S_a from attenuation relationship i, μ'_{Sa} denotes the weighted average mean S_a, σ_i denotes the standard deviation of S_a from attenuation relationship i, and σ'_{Sa} denotes the combined standard deviation of S_a.

2. ***Tabulate drift vs. S_a from end-to-end simulations***. Here, for each index building, we tabulate the average-wall 1st-story drift for each E2E simulation and gridpoint, along with the corresponding value of S_a and simulation weight. This table represents a pool of data from which to regress mean and COV of drift as functions of S_a, knowledge of which gridpoint or simulation produced the drift and S_a pair. (We must keep the weight information, because the simulations are not equally likely.)

3. ***Calculate attenuation-approach mean and standard deviation of drift by gridpoint.*** Let μ_R and σ_R denote these two values, respectively. Let r and a denote particular values of drift and S_a, respectively. Let $f_{R|Sa}(r|a)$ denote the probability density function of drift R given that $S_a = a$, and let and $f_{Sa}(a)$ denote the probability density function of S_a evaluated at a. One could then calculate:

$$\mu_R = \int_{a=0}^{\infty}\int_{r=0}^{\infty} r \cdot f_{R|S_a}(r\,|\,a)\, f_{S_a}(a)\, dr da$$
$$\sigma_R^2 = \int_{a=0}^{\infty}\int_{r=0}^{\infty} (r-\mu_R)^2\, f_{R|S_a}(r\,|\,a)\, f_{S_a}(a)\, dr da \quad (3)$$

We can perform this integration numerically, using data already in hand. Let us denote by $\mu_{R|Sa=a}$ and $\sigma_{R|Sa=a}$ the mean and standard deviation of drift given that $S_a = a$. These are values of the inner integrals of Equation (3), estimated by

$$\mu_{R|S_a=a} \cong \frac{\sum_{i=1}^{N} w_i r_i(a)}{\sum_{i=1}^{N} w_i}$$
$$\sigma^2_{R|S_a=a} \cong \frac{\sum_{i=1}^{N} w_i \left(r_i(a) - \mu_{R|S_a=a}\right)^2}{\sum_{i=1}^{N} w_i} \quad (4)$$

In this equation, $r_i(a)$ denotes a sample of drift in the database from step 2 where the S_a from the end-to-end simulation is approximately equal to a, w_i is the weight associated with sample number i, and N is the total number of samples with $S_a \approx a$. A reasonable definition of $S_a \approx a$ is that $S_a = a \pm 0.05$g. Then with 3-point quadrature (a form of moment matching),

$$\mu_R = \frac{1}{6}\mu_{R|S_a=a_L} + \frac{2}{3}\mu_{R|S_a=a_M} + \frac{1}{6}\mu_{R|S_a=a_H}$$
$$\sigma_R^2 = \frac{1}{6}\sigma^2_{R|S_a=a_L} + \frac{2}{3}\sigma^2_{R|S_a=aM} + \frac{1}{6}\sigma^2_{R|S_a=a_H} \quad (5)$$
$$+\frac{1}{6}\left(\mu_{R|S_a=a_L} - \mu_R\right)^2 + \frac{2}{3}\left(\mu_{R|S_a=a_M} - \mu_R\right)^2 + \frac{1}{6}\left(\mu_{R|S_a=a_H} - \mu_R\right)^2$$

where a_L, a_M, and a_H are 4th, 50th, and 96th percentile values of S_a at that gridpoint, calculated using the moments of S_a from Equation (2) and assuming S_a at the gridpoint is lognormally distributed, as is common.

Results of Comparison

Figure 37 depicts the mean of S_a under the E2E and NGA approaches, respectively, and the ratio of the former to the latter. The two approaches generally agree, though E2E has slightly higher S_a than NGA above the fault rupture and slightly lower elsewhere. Figure 38 compares the coefficient of variation (COV) of S_a under the two approaches; values from the E2E approach are on the order of ½ those of NGA.

Figures 39 and 40 compare the E2E versus NGA estimates of mean and coefficient of variation of 1st story average-wall drift for the 1940s-1950s index building. Figure 39 suggests that E2E captures of ground motion directionality better than does NGA, as it

shows building drifts on the part of the hanging wall at the upper edge of the rupture substantially greater than elsewhere. The drift pattern from the NGA approach tend to match the surface projection of the fault, but do not suggest directionality of motion. Figure 40 reflects much lower uncertainty in drift under the E2E than under NGA, generally on the order of ½, with greater difference far from the rupture. Figures 41 through 50 reflect similar outcomes for the other index houses.

IMPLICATIONS FOR REGIONAL VULNERABILITY

End-to-end (E2E) modeling appears to capture directionality in motion better than the attenuation approach does. One would expect to see greater drifts on the hanging wall of a blind thrust fault than elsewhere. This effect is produced by end-to-end modeling of all six index buildings, but not reflected in the attenuation approach in which only S_a matters. The implication for an insurer is that an attenuation approach, even using next-generation attenuation (NGA) relationships, may not capture an important seismological risk factor. Here, the NGA approach systematically underestimates drift (and hence risk) to homes on the hanging wall of a blind thrust fault (of which southern California has many), and overestimates risk elsewhere.

E2E modeling appears to reduce uncertainty in drift (and hence risk) by a factor of approximately ½, owing to detailed knowledge of the rupture and path of seismic wave propagation that is missing from the NGA approach. Note that this difference is not because the E2E approach was in some way more deterministic than NGA: its top two seismological uncertainties (rupture velocity and rise time) were treated probabilistically, and the same motions and structural analyses were used in both E2E and NGA approaches. The difference is that the NGA approach pools ground motion intensity from diverse earthquakes and seismic settings, many of which may be very different from the one under consideration. The result is much greater uncertainty in S_a, uncertainty that may in some cases be avoided.

This study is of course far from definitive. Only one earthquake rupture scenario was used, though important uncertainties were reflected. Only six index buildings were studied, and though they were diverse, they were not intended to be somehow statistically representative of southern California construction. Some important structural features were not reflected in any of the models, such as sloping site, the effects of foundation type, and other potentially important building features on seismic risk. Only one structural engineer's structural models were used, and though they reflected uncertainty in damping, strength, and stiffness, they were not tested for sensitivity to alternative modeling approaches such as different hysteretic rules.

Nonetheless, the study showed systematic results consistent with our initial intuition: It appears from this limited study that E2E may better capture risk on the hanging wall of a blind thrust fault. Since the effect can be significant (with drifts 50% greater than those elsewhere but at similar fault distance), this attribute could be used as a rating factor.

The study also showed systematically lower uncertainty in structural response calculated using in end-to-end simulation, on the order of ½, relative to an attenuation-based approach. Lower uncertainty is structural response results in lower uncertainty in loss, which tends to reduce the upper tails of the probability distribution of loss. This could have implications for portfolio risk and reinsurance needs.

These results apply to individual buildings in a single scenario. We do not know to what extent the effects on risk in this scenario would apply to total probabilistic risk to single buildings considering all earthquake faults and event sizes, much less to the CEA's portfolio of houses. But the results are promising enough to warrant further testing with a statistically representative sample of houses and a larger number of earthquakes.

RECOMMENDATIONS

We recommend that further study be pursued to examine open questions of end-to-end simulation:

- Test sensitivity of results to number of moment matching points. This would involve duplicating the analyses described here except with more samples of each input variable, say 5 or 7 points per variable rather than 3.
- Compare Monte Carlo simulation with moment matching. It is been argued that MM is far more efficient than MCS, but it would be valuable to test that assertion by finding how many MCS simulations are required to converge on a results with the same accuracy as MM.
- Explore the effects on seismic risk of site slope, foundation type, shiplap or other board-like siding, lath-and-plaster interior walls, and other potentially important and relatively apparent building features.
- Estimate the relative quantities of these features in California construction, so as to prepare for E2E-based statewide risk analysis.
- Test sensitivity of results to other seismological uncertainties: slip distribution, hypocenter location, geological structure, seismic velocity structures, anelastic attenuation (Q of media), near-surface site response, and possibly others.
- Test sensitivity of results to the revised NGA relationships produced since our study.
- Test sensitivity of results to non-strength-related hysteretic parameters in the structural model, structural deficiencies such as lack of hold-downs, long missing lines of connectors, or imperfect correlation in member strength and stiffness.
- Investigate whether claims-adjustment practices produce substantial bias in loss estimates or swamp uncertainty benefits from using E2E vs. NGA.
- Perform statewide risk assessment with E2E modeling. E2E modeling holds to potential to reduce uncertainty on site loss and thus the probability of high portfolio losses, relative to NGA approaches. Reduced probability of high loss can mean lower reinsurance needs and thus lower costs. The savings could conceivably be passed along to policyholders and the state.

REFERENCES CITED

(ASCE) American Society of Civil Engineers, 2000. *FEMA-356: Prestandard and Commentary for the Seismic Rehabilitation of Buildings,* Washington, DC, 490 pp.

Camelo, V.S., Beck, J.L., and Hall, J.F., 2001, *Dynamic Characteristics of Woodframe Structures,* Consortium of Universities for Research in Earthquake Engineering, Richmond, CA, 68 pp.

Carr, A.J., 2001. *Ruaumoko 2-D*, University of Canterbury, Christchurch, New Zealand.

Ellingwood, B., T.V. Galambos, J. G. MacGregor, and C.A. Cornell, 1980. *Development of a Probability-Based Load Criterion for American National Standard A58,* National Bureau of Standards, Washington, DC, 222 pp.

Hoit, M., 1995. Computer-Assisted Structural Analysis and Modeling. Prentice Hall, Englewood Cliffs NJ, 440 pp.

Hornbeck, R.W., 1975. Numerical Methods. Quantum Publishers, Inc., New York, 310 pp.

Julier, S.J. and J.K. Uhlmann, 2002. Reduced sigma point filters for the propagation of means and covariances through nonlinear transformations. *Proc American Control Conference*, May 8-10, Anchorage Alaska, 6 pp.

Pardoen, G.C., R.P. Kazanjy, E. Freund, C.H. Hamilton, D. Larsen, N. Shah, and A. Smith, 2000. Results from the City of Los Angeles-UC Irvine shear wall test program. *Proc., 6th World Conf on Timber Engineering*

Porter, K.A., J.L. Beck, and R.V. Shaikhutdinov, 2002. Sensitivity of building loss estimates to major uncertain variables. *Earthquake Spectra*, 18 (4), 719-743, http://keithp.caltech.edu/publications.htm

Rosenblueth, E., 1975. Point estimates for probability moments. *Proceedings of the National Academy of Sciences of the United States of America*, 72 (10), (Oct., 1975), 3812-3814

Carr, A.J., 2001. *Ruaumoko 2-D*, University of Canterbury, Christchurch, New Zealand

Ching, JY., K.A. Porter, and J.L. Beck, 2004. *Uncertainty Propagation and Feature Selection for Los Estimation in Performance-based Earthquake Engineering*, http://caltecheerl.library.caltech.edu/443/01/EERL-2004-02.pdf

Folz, B., and A. Filiatrault, 2000. *CASHEW Version 1.0. A Computer Program for Cyclic Analysis of Wood Shear Walls*. Report No. SSRP – 2000/10. Department of Structural Engineering, UC San Diego

Fonseca, F.S., S.K. Rose, S.H. and Campbell, 2002, *CUREE-Caltech Woodframe Project Task 1.4.8.1 – Nail, Wood Screw and Staple Fastener Connections,* Consortium of Universities for Research in Earthquake Engineering (CUREE), Richmond, CA, 160 pp

Hart, G.C., and Vasdevan, R., 1975, Earthquake Design of Buildings: Damping, *Journal of the Structural Division,* 101 (ST1), Jan 1975, 11-29.

Isoda, H., B. Folz, and A. Filiatrault, 2001. *Seismic Modeling of Index Woodframe Buildings on Research Task 1.5.4.,* Consortium of Universities for Research in Earthquake Engineering, Richmond, California, 144 pp.

Julier, S.J. and J.K. Uhlmann, 2002. Reduced sigma point filters for the propagation of means and covariances through nonlinear transformations. *Proc American Control Conference*, May 8-10, Anchorage Alaska, 6 pp., http://www.cs.unc.edu/~welch/media/pdf/ACC02-IEEE1358.pdf

Kennedy, R.P., 1999. Overview of methods for seismic PRA and margin analysis including recent innovations. *Proceedings of the OECD-NEA Workshop on Seismic Risk*, Tokyo Japan, 10-12 August 1999

McVerry, G.H., 1979, *Frequency Domain Identification of Structural Models for Earthquake Records, Report No. EERL 79-02,* California Institute of Technology, Pasadena, CA, http://caltecheerl.library.caltech.edu/documents/disk0/00/00/02/23/00000223-00/7902.pdf, 221 pp.

Newmark, N.M. and W.J. Hall, 1982. *Earthquake Spectra and Design,* EERI Monograph MNO-3, Earthquake Engineering Research Institute, Oakland, California.

Pardoen, G.C., R.P. Kazanjy, E. Freund, C.H. Hamilton, D. Larsen, N. Shah, N., A. and Smith, 2000. Results from the City of Los Angeles-UC Irvine shear wall test program. *Proc., 6th World Conf on Timber Engineering* http://timber.ce.wsu.edu/Resources/papers/1-1-1.pdf

Porter, K.A., J.L. Beck, H.A. Seligson, C.R. Scawthorn, L.T. Tobin, and T. Boyd, 2002. *Improving Loss Estimation for Woodframe Buildings,* Consortium of Universities for Research in Earthquake Engineering, Richmond, CA, 136 pp., http://resolver.caltech.edu/caltechEERL:2002.EERL-2002-01 (main report) and http://resolver.caltech.edu/caltechEERL:2002.EERL-2002-02 (appendices).

Porter, K.A., R.P. Kennedy, and R.E Bachman, 2007. Creating fragility functions for performance-based earthquake engineering. *Earthquake Spectra*. 23 (2), May 2007

Rose, J., 2000. Re: T-111. *Discussion Archive of Structural Engineers Association International*. http://www.euken.com/group/seaoc/seaoc.shtml

Rosenblueth, E., 1975. Point estimates for probability moments. *Proceedings of the National Academy of Sciences of the United States of America*, 72 (10), (Oct., 1975), 3812-3814

FIGURES

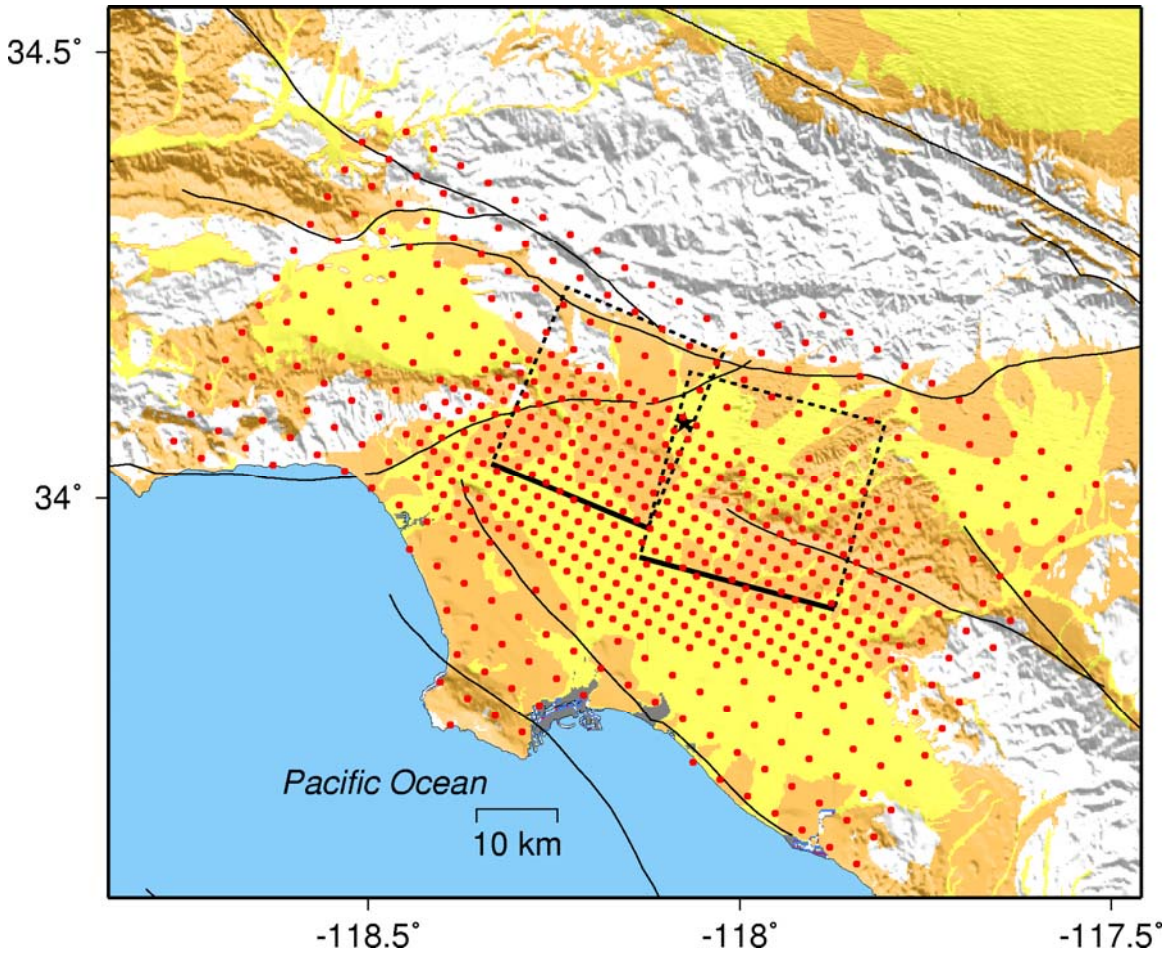

Figure 1. Map showing the Puente Hills Blind Thrust fault model (black rectangles, with solid line indicating the top edge) and the grid of stations (red dots) at which ground motions were simulated.

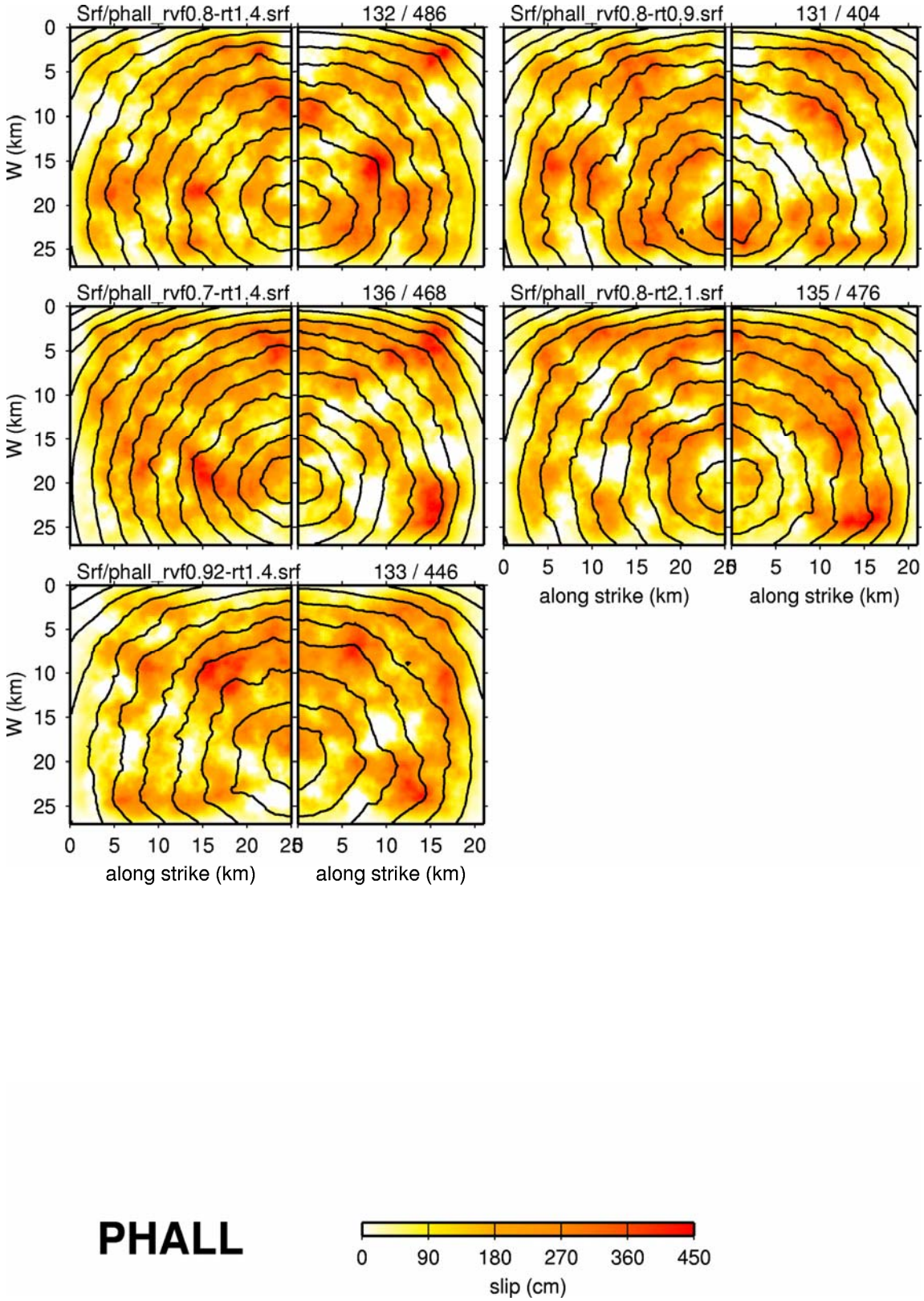

Figure 2. Rupture models of five scenario earthquakes on the Puente Hills Blind Thrust.

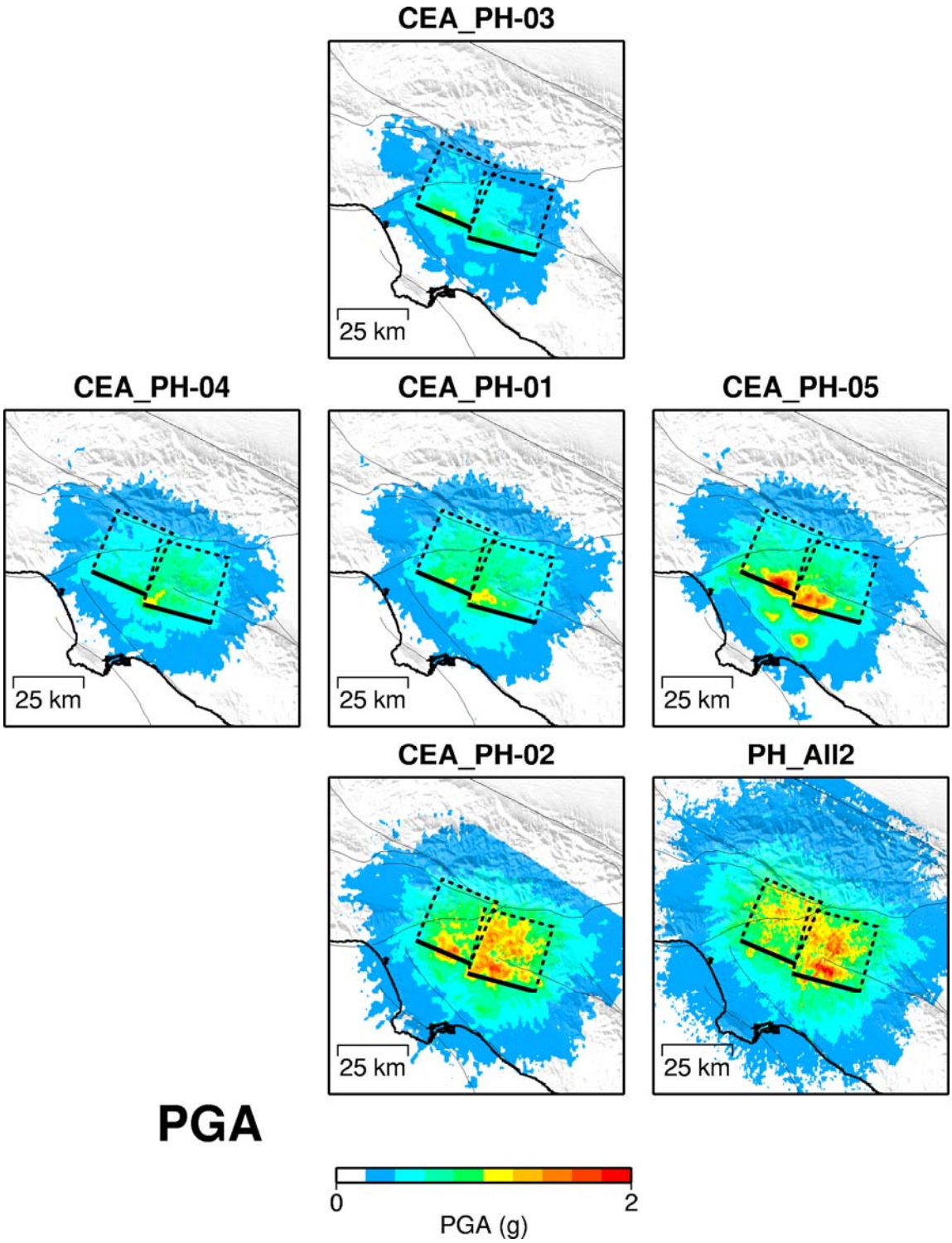

Figure 3. Ground motion maps for the simulated peak acceleration from six scenarios

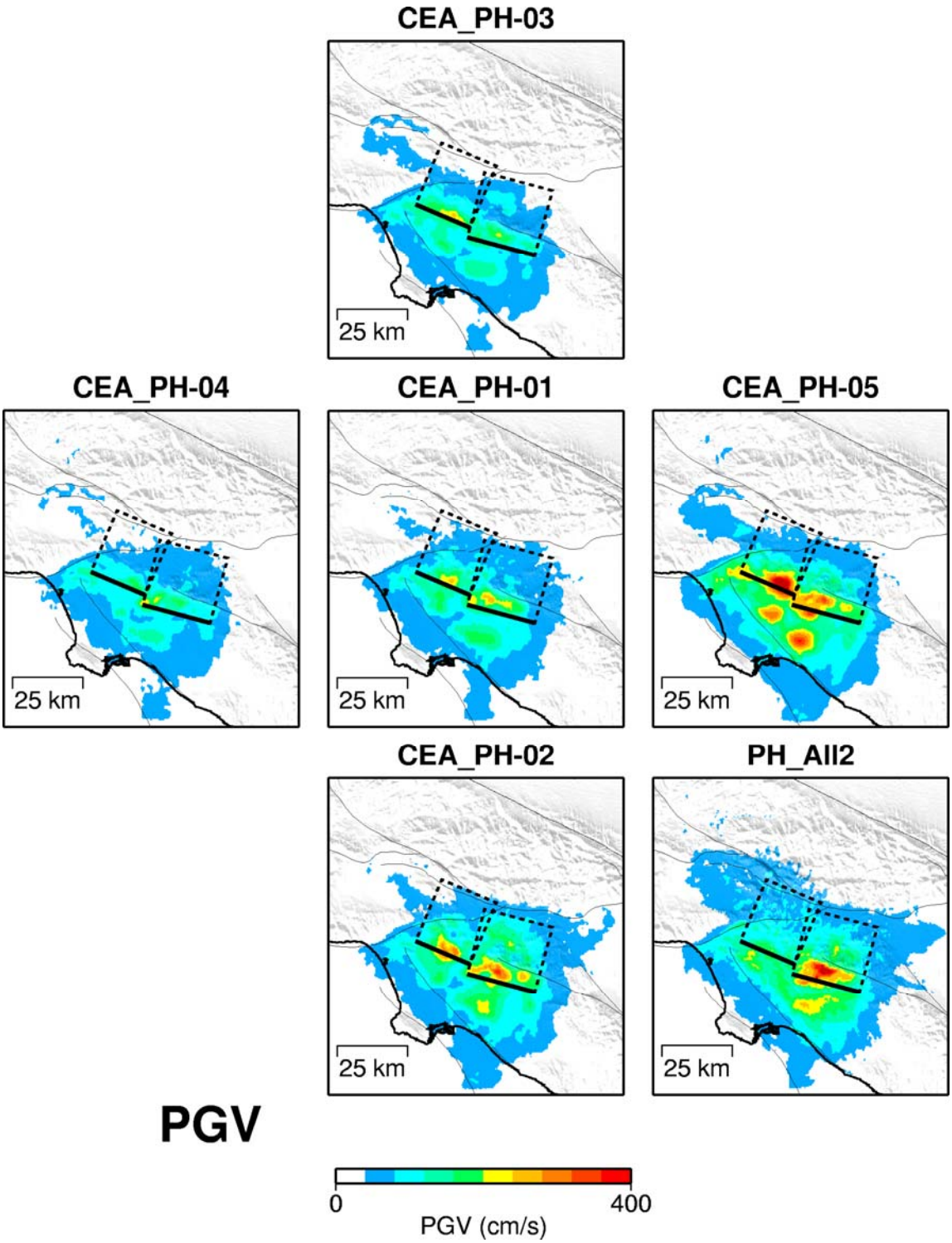

Figure 4. Ground motion maps for the simulated peak velocity from six scenarios

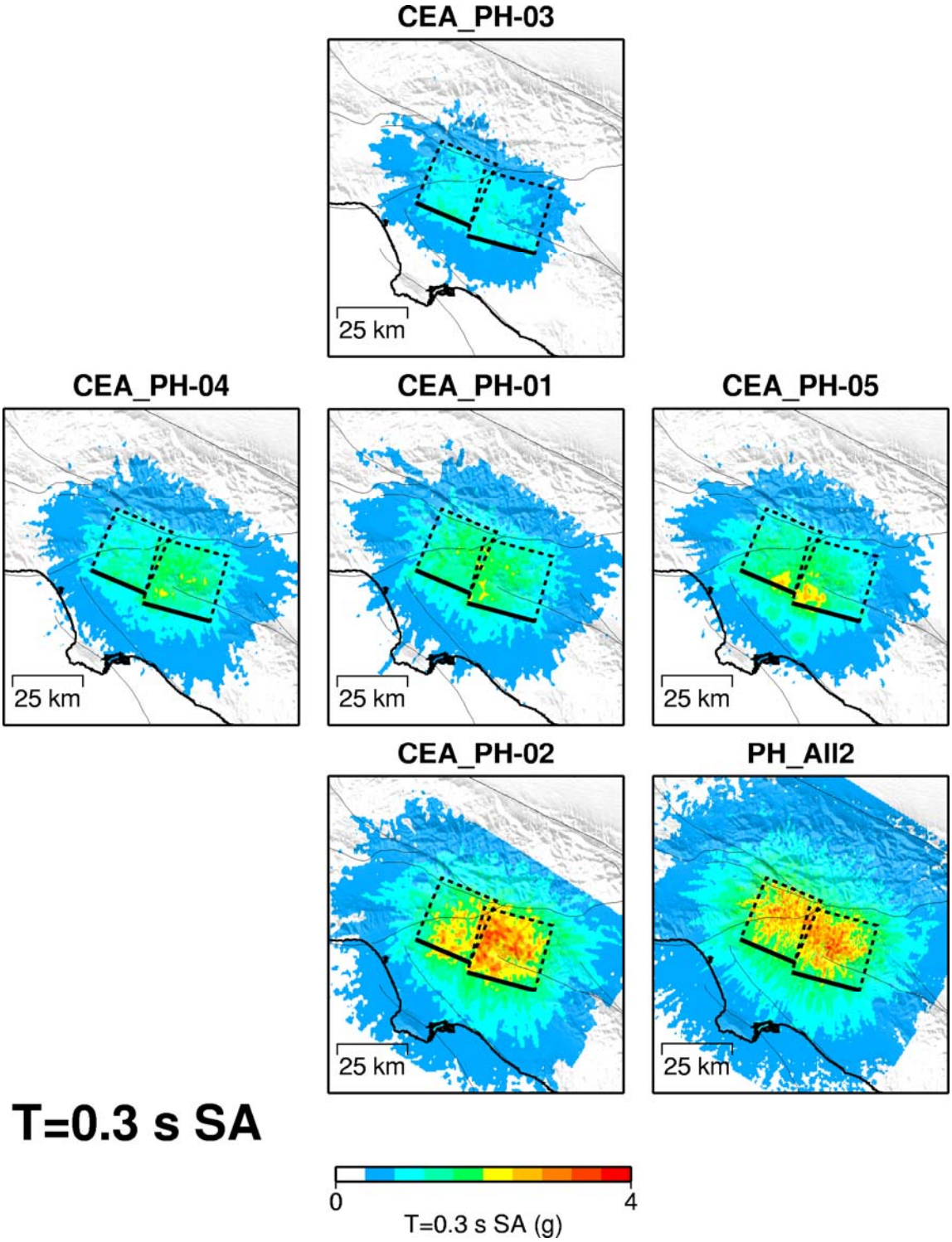

Figure 5. Ground motion maps for the simulated response spectral acceleration at a period of 0.3 seconds from six scenarios

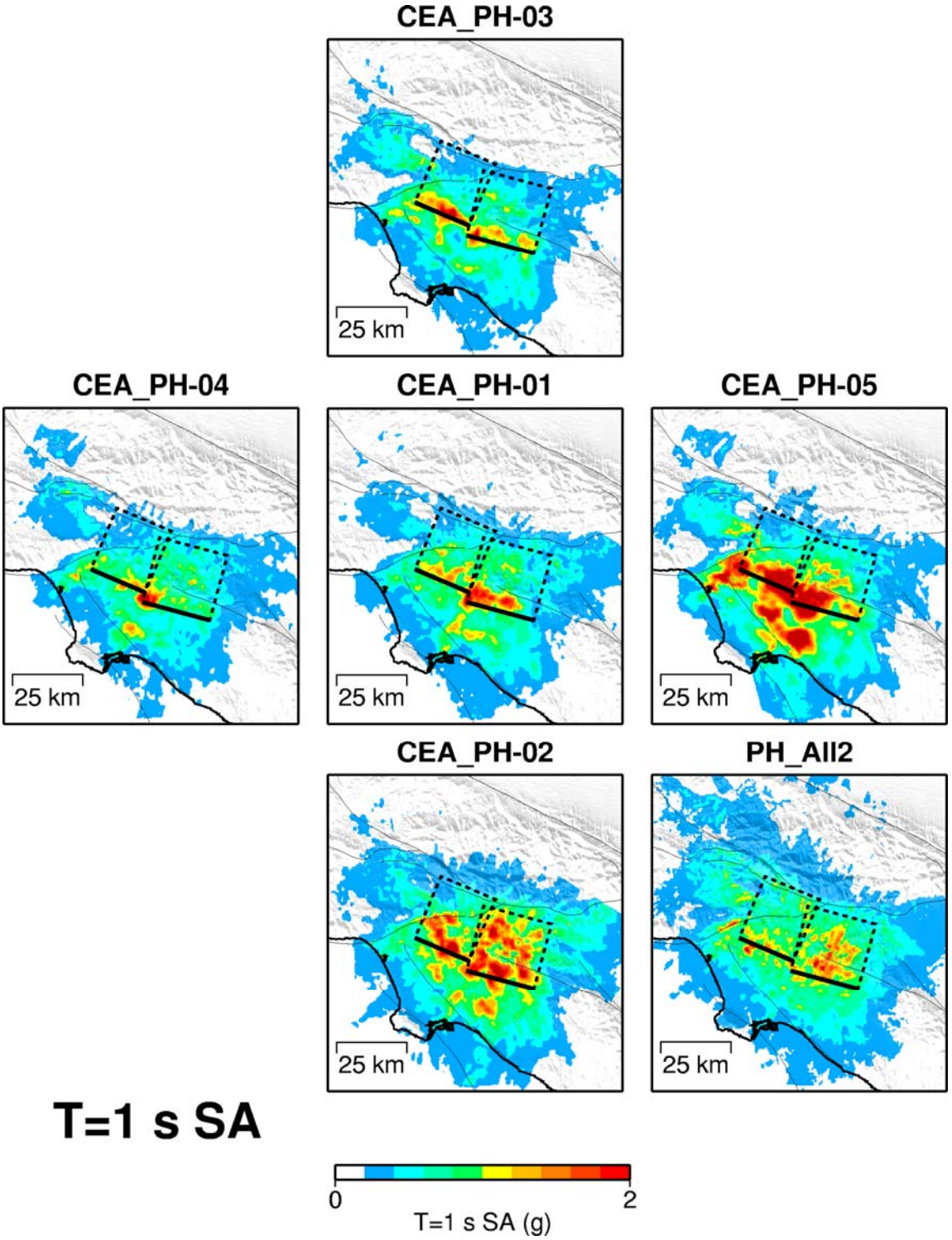

Figure 6. Ground motion maps for the simulated response spectral acceleration at a period of 1 second from six scenarios

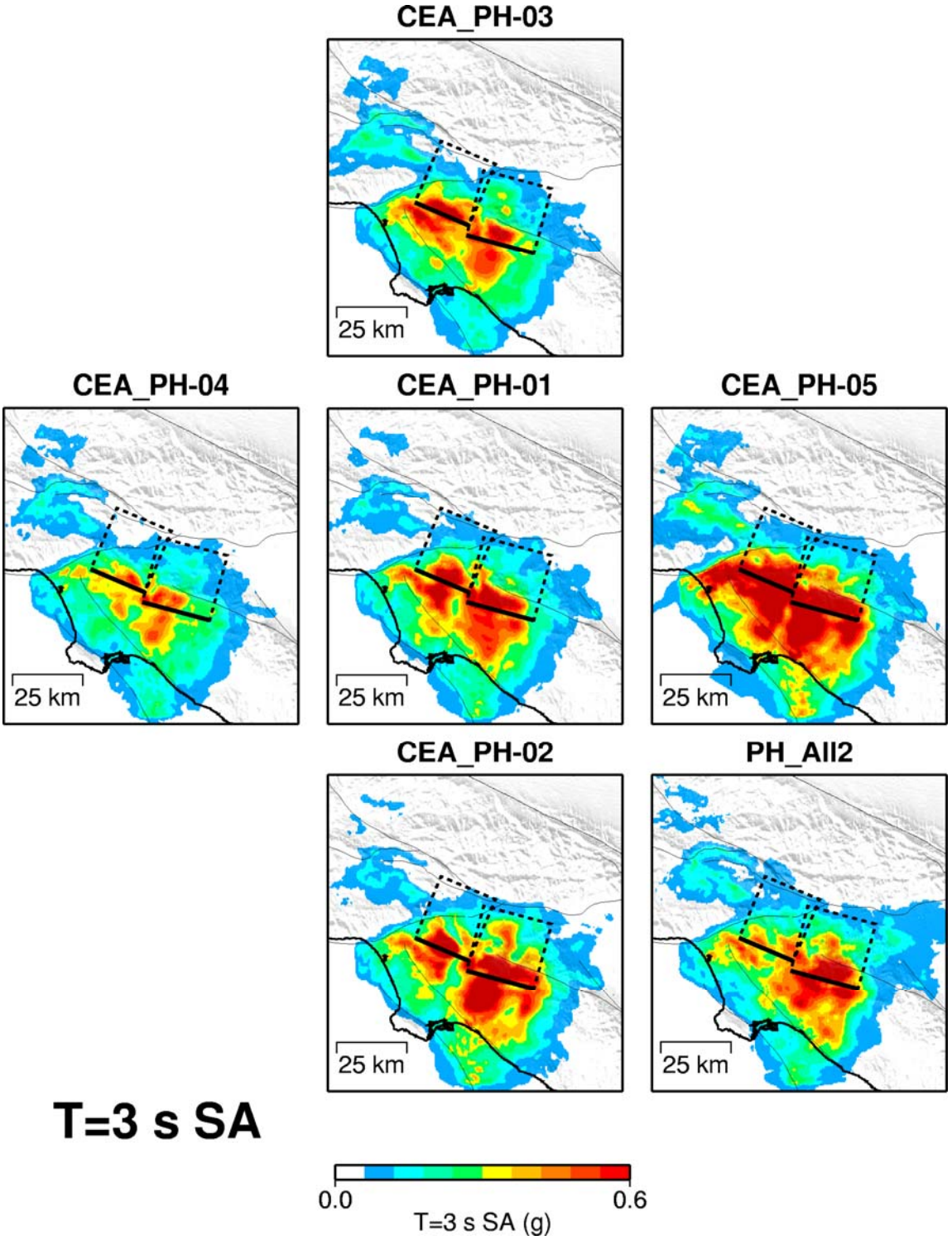

Figure 7. Ground motion maps for the simulated response spectral acceleration at a period of 3 seconds from six scenarios

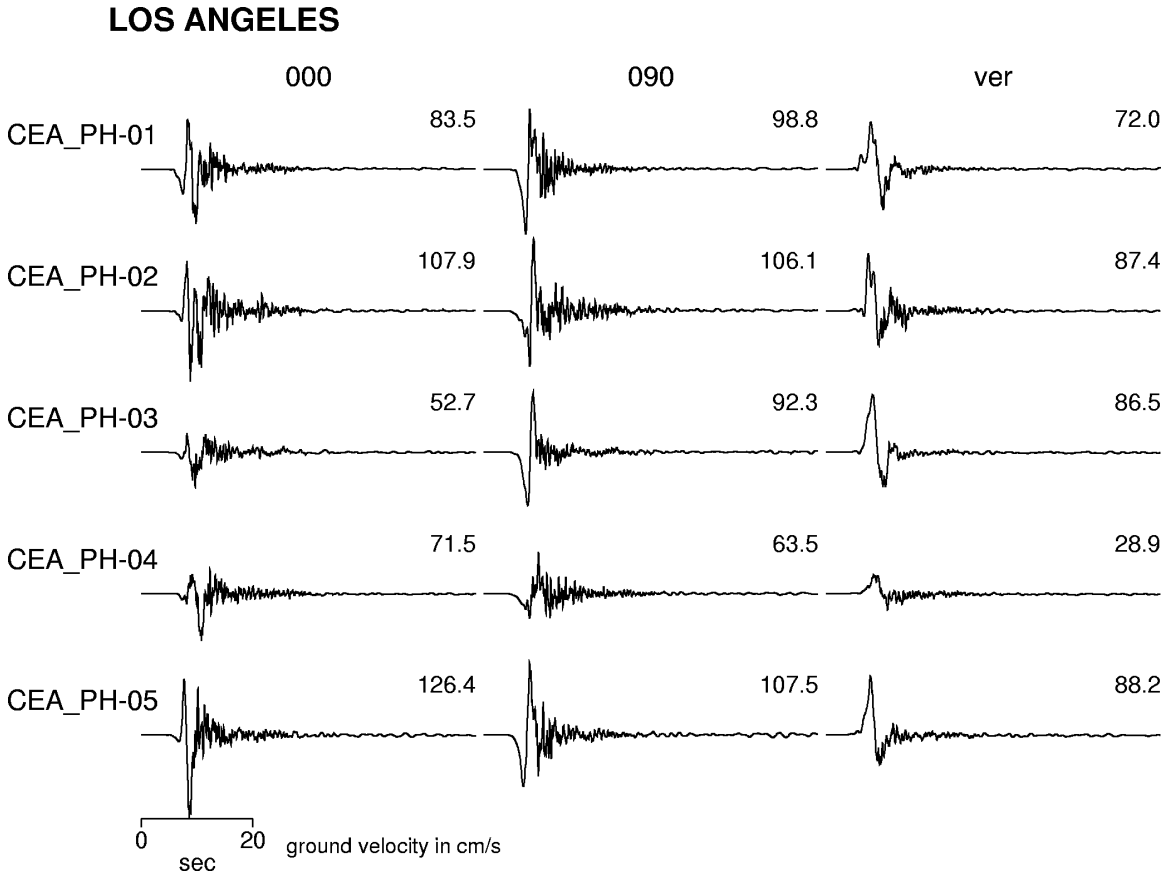

Figure 8. Simulated ground velocity time histories in downtown Los Angeles.

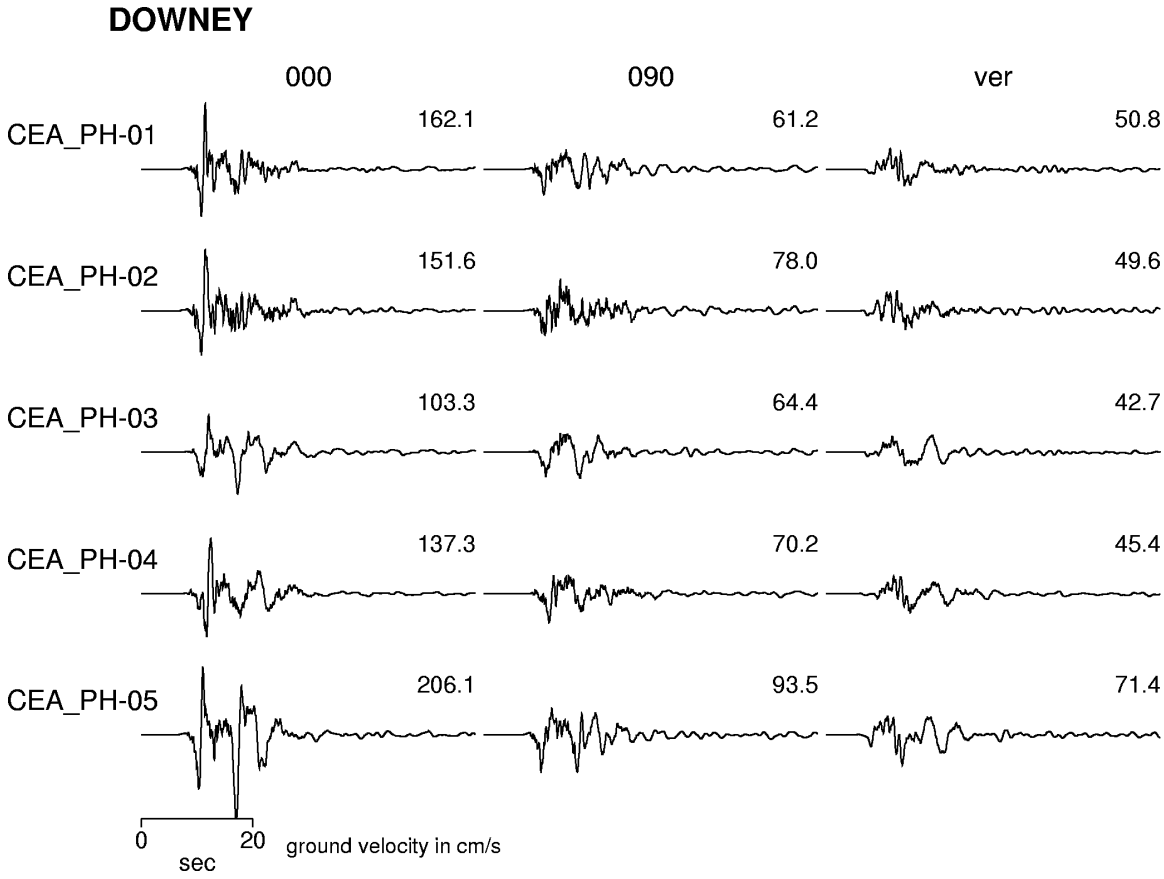

Figure 9. Simulated ground velocity time histories at a site in Downey

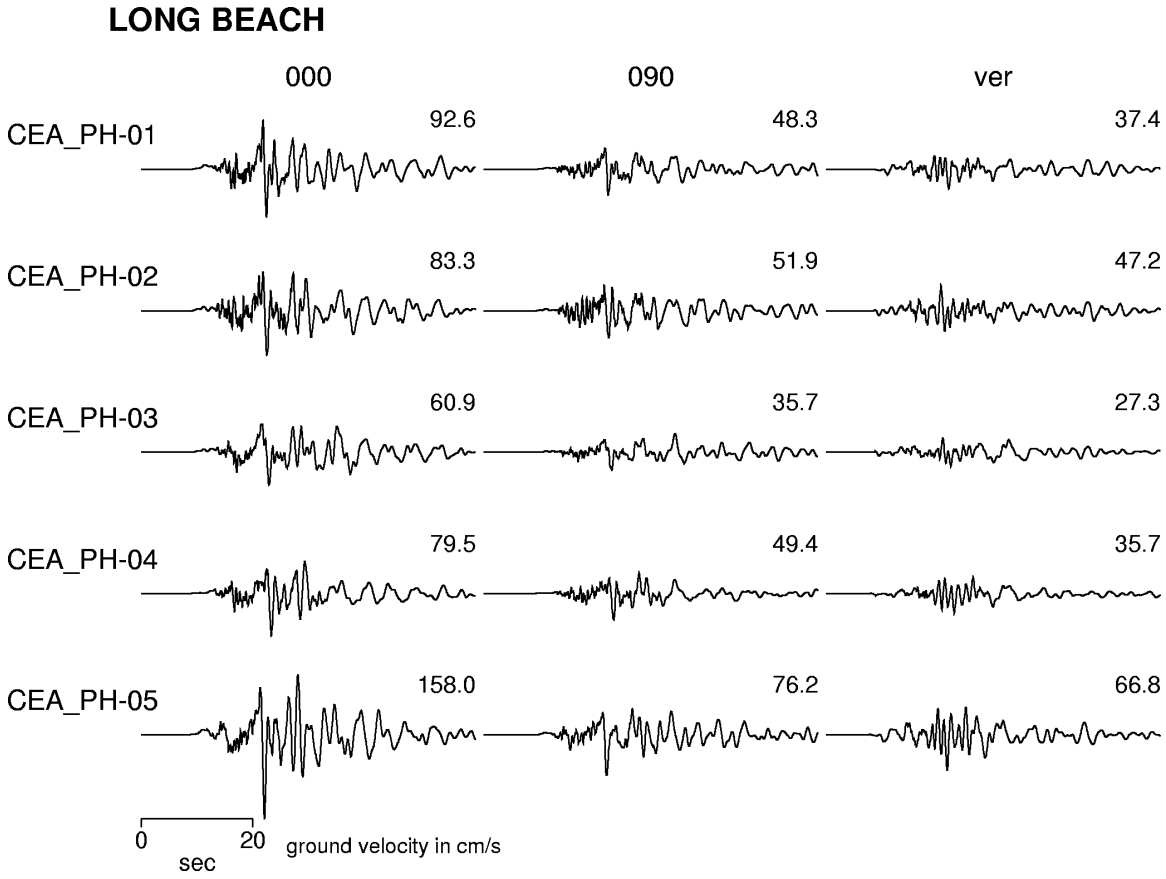

Figure 10. Simulated ground velocity time histories at a site in Long Beach.

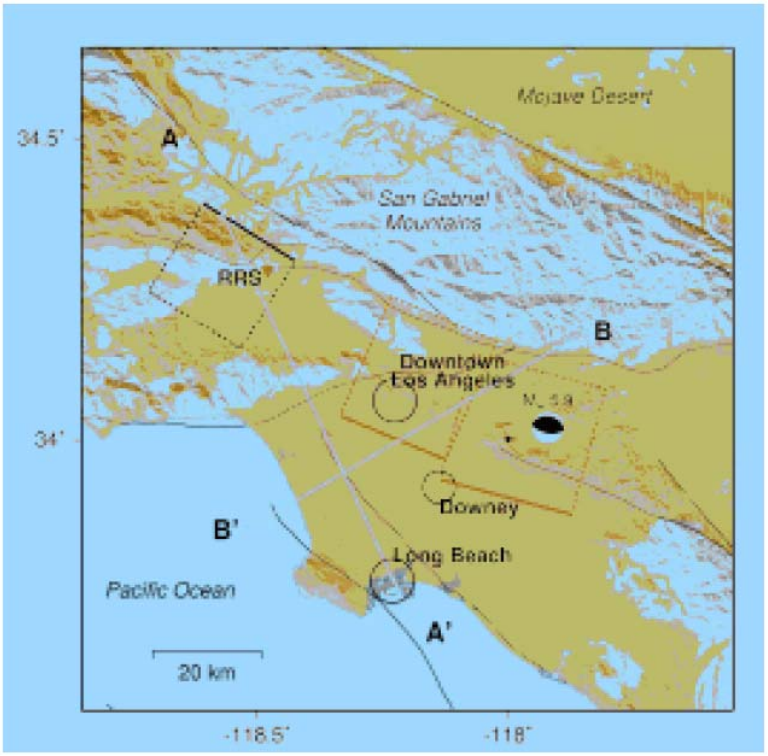

Figure 11. Puente Hills fault system

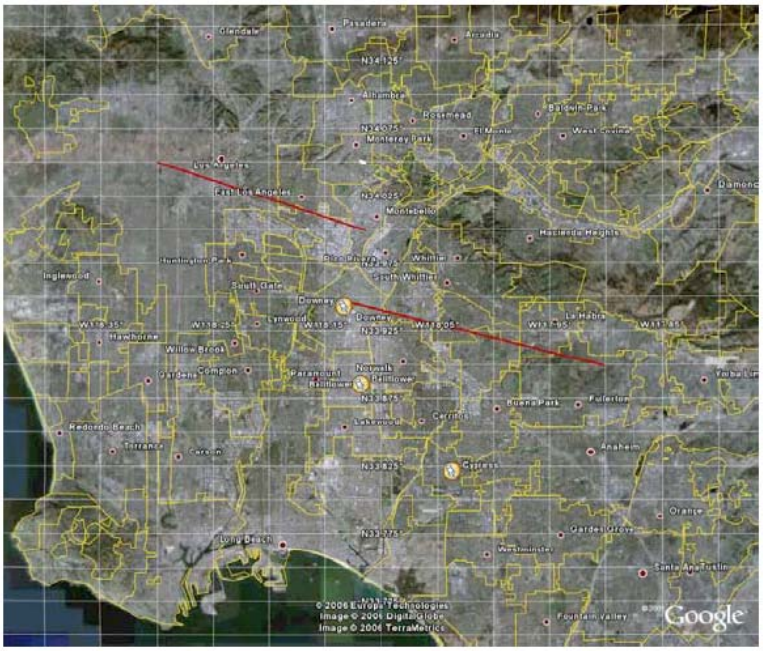

Figure 12. Selected cities within strong motion area

10049 Arthurdale St, Bellflower -1954

$520,000
10049 Arthurdale St
Bellflower, CA
Beds: **4**
Baths: **2**
Sq.Ft.: **1,231**
Acres: **0.13**

7838 Springer St, Downey, CA - 1940

$549,000
7838 Springer St
Downey, CA
Beds: **2**
Baths: **1**
Sq.Ft.: **861**
Acres: **0.17**

15212 Cornuta Ave, Bellflower - 1948

$552,000
15212 Cornuta Ave
Bellflower, CA
90706
Beds: **3**
Baths: **1**
Sq.Ft.: **1,230**
Acres: **0.17**

7838 Springer St, Downey, CA - 1940

$549,000
7838 Springer St
Downey, CA
Beds: **2**
Baths: **1**
Sq.Ft.: **861**
Acres: **0.17**

Downey, CA - 1940

$430,000
Downey, CA
Beds: **3**
Baths: **1**
Sq.Ft.: **1,085**
Acres: **0.13**

9053 Eglise Ave, Downey, CA - 1950

$515,000
9053 Eglise Ave
Downey, CA
Beds: **2**
Baths: **1**
Sq.Ft.: **840**
Acres: **0.13**

10537 Pangborn Av, Downey, CA - 1950

$650,000
10537 Pangborn Av
Downey, CA
Beds: **3**
Baths: **2**
Sq.Ft.: **1,239**
Acres: **0.17**

Figure 13. Various 1940's – 1950's properties in selected cities

9430 Rose St, Bellflower, CA - 1961

$1,300,000
9430 Rose St
Bellflower, CA 90706
Beds: **3**
Baths: **2**
Sq.Ft.: **1,914**
Acres: **0.36**

11680 Tarawa St, Cypress, CA - 1972

$739,900
11680 Tarawa St
Cypress, CA
Beds: **4**
Baths: **3**
Sq.Ft.: **2,136**
Acres: **0.12**

5112 Citation Ave, Cypress, CA - 1963

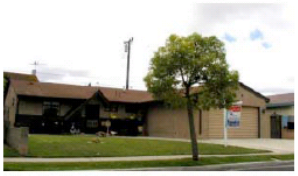

$575,000
5112 Citation Ave
Cypress, CA
Beds: **4**
Baths: **2.5**
Sq.Ft.: **1,291**
Acres: **0.14**

Downey, CA 90241 - 1969

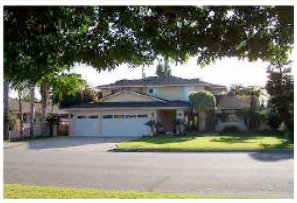

$1,257,777
Downey, CA
Beds: **4**
Baths: **3**
Sq.Ft.: **3,340**
Acres: **0.22**

4467 Via Largo, Cypress, CA - 1967

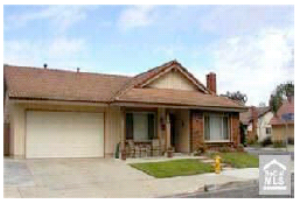

8745 Dorian St, Downey, CA - 1970

$685,000
8745 Dorian St
Downey, CA
Beds: **4**
Baths: **3**
Sq.Ft.: **2,197**
Acres: **0.12**

4342 Nestle Ave, Cypress, CA - 1964

$625,900
4342 Nestle Ave
Cypress, CA
Beds: **3**
Baths: **2**
Sq.Ft.: **1,500**
Acres: **0.14**

12015 Morning Ave, Downey, CA - 1964

$979,900
12015 Morning Ave
Downey, CA
Beds: **4**
Baths: **4**
Sq.Ft.: **2,781**
Acres: **0.22**

9823 Newville Ave, Downey, CA - 1969

$1,259,000
9823 Newville Ave
Downey, CA 90240
Beds: **4**
Baths: **3.5**
Sq.Ft.: **3,049**

Downey, CA 90242 - 1969

$799,000
Downey, CA
Beds: **4**
Baths: **3**
Sq.Ft.: **2,378**
Acres: **0.12**

Figure 14. Various 1960's – 1970's properties in selected cities

9432 Cedar St, Bellflower, CA - 2004

$550,000
9432 Cedar St
Bellflower, CA
Beds: **3**
Baths: **2.5**
Sq.Ft.: **1,620**
Acres: **0.45**

Bellflower, CA - 1980

$795,000
Bellflower, CA
Beds: **4**
Baths: **3**
Sq.Ft.: **2,199**
Acres: **0.11**

4960 Ariano Dr, Cypress, CA - 1991

$845,000
4960 Ariano Dr
Cypress, CA
Beds: **3**
Baths: **2.5**
Sq.Ft.: **2,300**
Acres: **0.11**

9450 Arbor Ln, Cypress, CA - 1995

$650,000
9450 Arbor Ln
Cypress, CA
Beds: **4**
Baths: **2.5**
Sq.Ft.: **1,948**
Acres: **0.09**

8814 La Salle, Cypress, CA - 2005

$650,000
8814 La Salle
Cypress, CA
Beds: **3**
Baths: **2.5**
Sq.Ft.: **1,795**
Acres: **0.09**

8950 Serapis Av, Downey, CA - 1990

$599,900
8950 Serpis Ave
Downey, CA
Beds: **4**
Baths: **3**
Sq.Ft.: **1,705**
Acres: **0.11**

Downey, CA - 2000

$740,000
Downey, CA
Beds: **4**
Baths: **2.5**
Sq.Ft.: **2,294**
Acres: **0.14**

Downey, CA - 1989

$799,000
Downey, CA
Beds: **4**
Baths: **3**
Sq.Ft.: **2,378**
Acres: **0.12**

9709 Downey Ave, Downey, CA - 1993

$1,397,000
9709 Downey Ave
Downey, CA
Beds: **5**
Baths: **4**
Sq.Ft.: **3,700**
Acres: **0.19**

Figure 15. Various 1980's – 2000's properties in selected cities

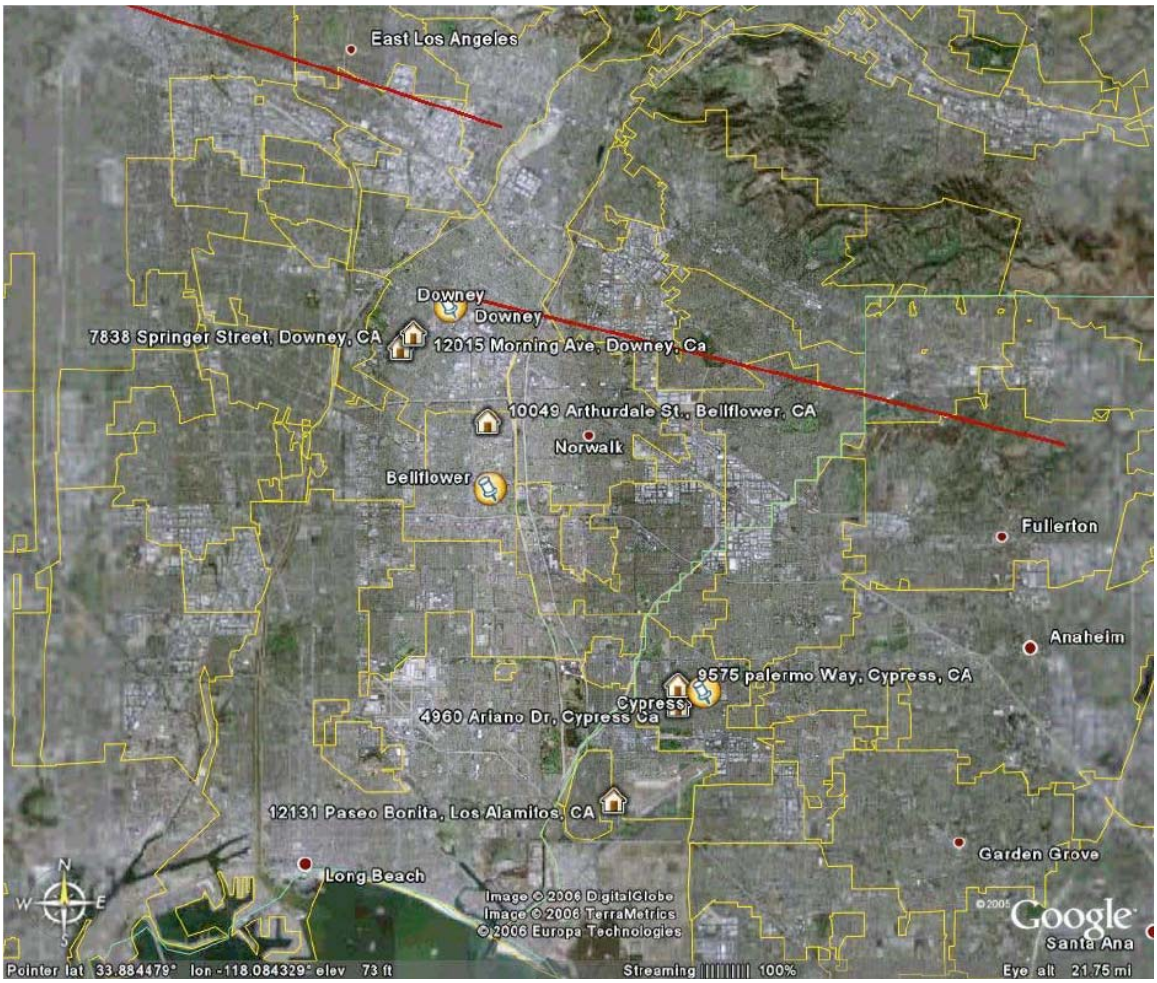

Figure 16. Selected representative properties

7838 Springer St, Downey, 1940, 1sty, 1000 sf

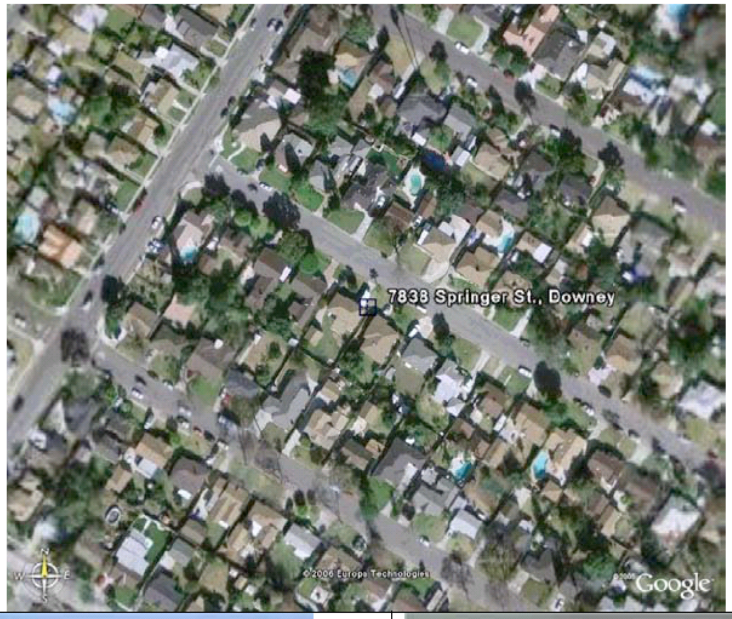

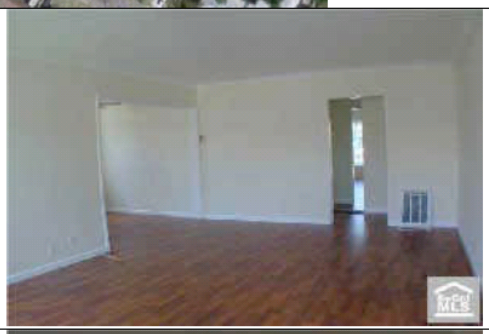

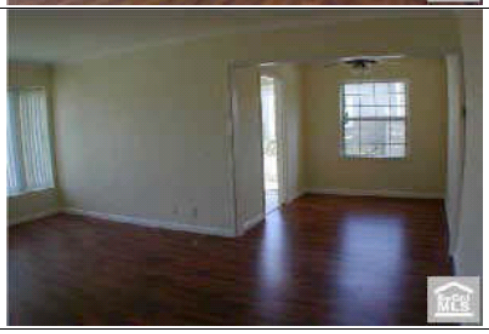

- Single Family Property
- Lot 6,500 SF
- Year Built: 1940
- Approximately 1,000 SF

- 2 total bedroom(s)
- 1 total bath(s)
- One Level
- 2 car attached garage
- Composition roofing
- Floor Furnace

Figure 17. 1940's – 1950's property

10049 Arthurdale St, Bellflower, CA 1954, 1sty, 1231 sf

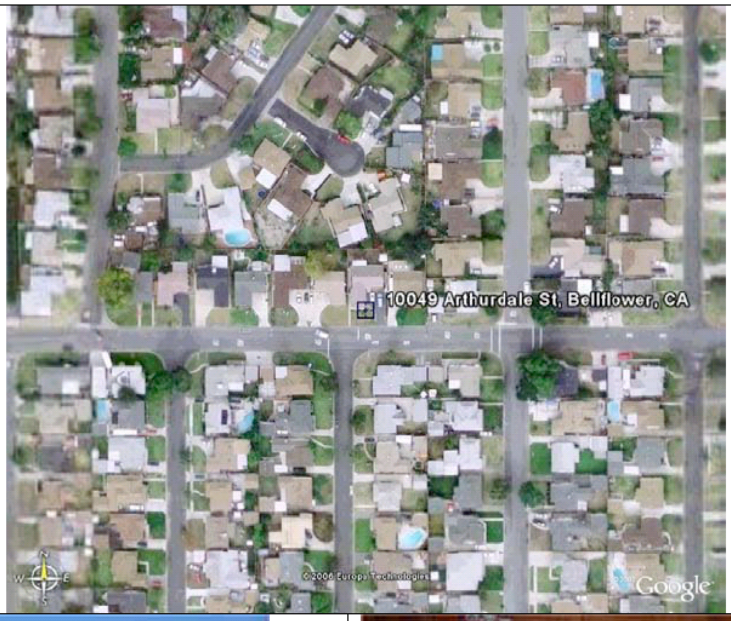

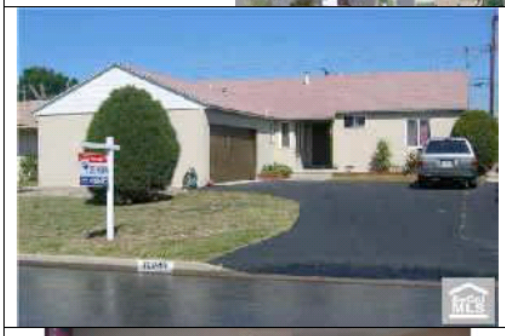

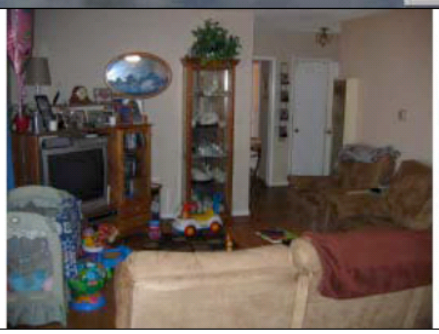

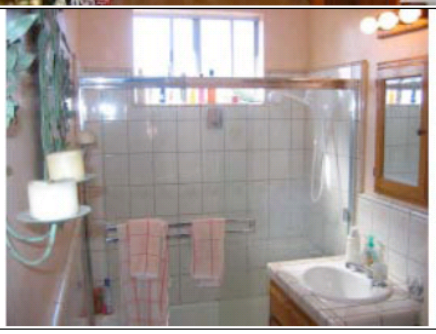

- Single Family Property
- Lot 5,600 SF
- Year Built: 1954
- Approximately 1231 SF
- 4 total bedroom(s)
- 2 total bath(s)
- Dining room
- Hardwood floors
- 2 car attached garage
- Formal Dining Rm,
- Composition roofing

Figure 18. 1940's – 1950's property

Element	Description
Foundation:	Lightly reinforced strip footing around perimeter and at garage.
Garage slab:	4” concrete slab on grade with wire mesh. Not doweled into footings.
Sill plate:	3x6 with 3/8” anchor bolts at 6’-0” oc
Crawl space:	2x6 floor joists @16” oc sit directly on sill plate. Span to 4x girders supported on wood posts and precast footing piers. All elements only toenailed to each other. Rim joist on sides perpendicular to joists end nailed into joists and toenailed to sill plate.
First floor:	1x diagonal sheathing with 2-10d nails to each joist. Hardwood floor over sheathing.
Exterior walls:	2x4 studs @ 16” oc to eight foot ceilings. Paper nailed to studs with 1x4 furring strips at ~7” oc. Shingles nailed directly to furring. No solid straight sheathing. Diagonal 2x4 let in bracing on exterior walls from sill to top pl., but heavily interrupted by doors and windows. Bracing nailed to studs w/ 2-16d.
Interior walls:	½” gypsum wallboard with cooler nails at ~6” oc ends. Walls are nailed to floor sheathing with 2-16d @ 16” oc.
Ceiling:	2x4 joists @ 16” oc spanning to exterior walls and some interior partition walls or built up 2x4 beams. Joists toenailed into wall top plates.
Roof:	2x4 roof rafters @ 16” oc spanning to exterior walls and to non load bearing ridges. Some intermediate truss elements to stiffen rafters. Rafters bird-mouthed and nailed to ceiling joists and toenailed to top plate. 2x4 blocking with vent holes at perimeter.
Roofing:	1x4 skip sheathing with 2-8d per rafter with wood shingles.

Figure 19. 1940’s – 1950’s house structural features

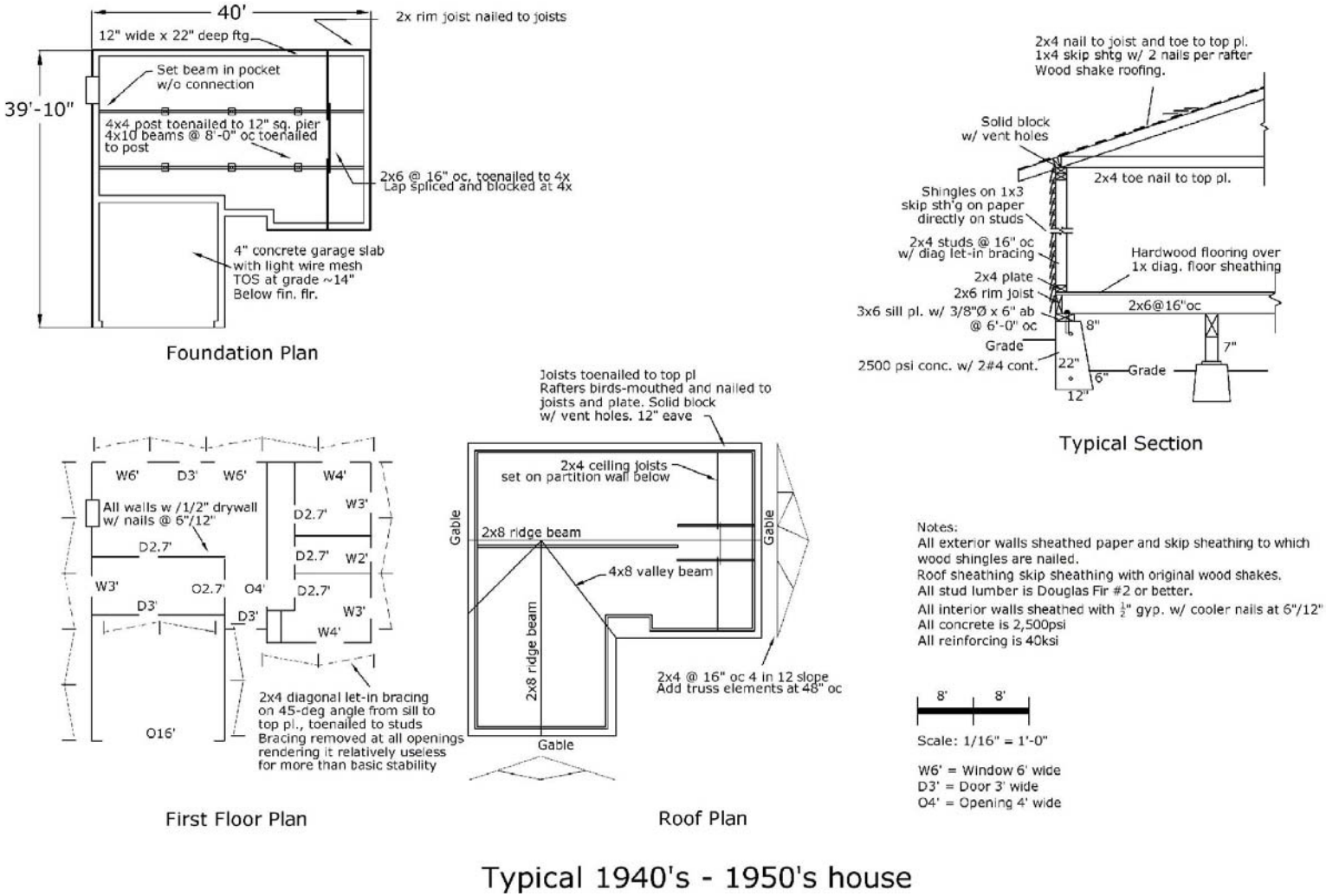

Figure 20. 1940's – 1950's property, building sketches

12131 Paseo Bonita, Los Alamitos, 1963, 1sty, 1,660 sf

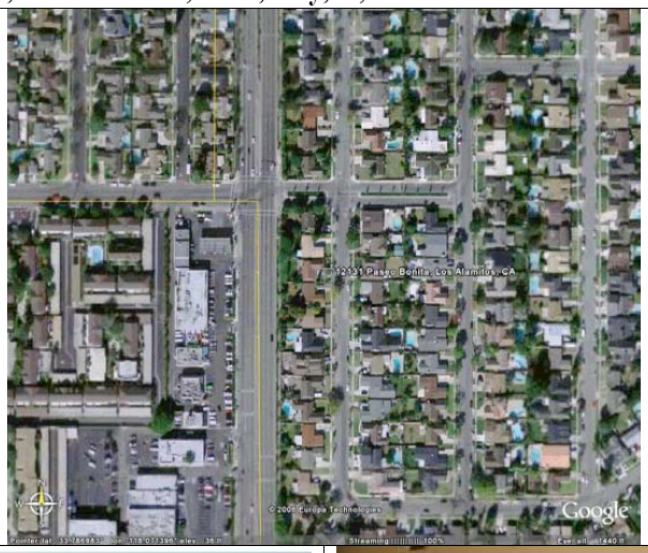

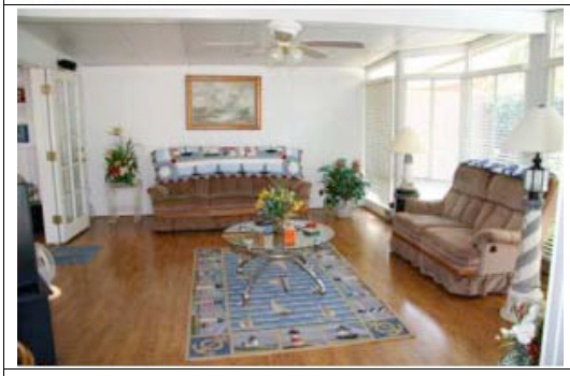

- Single Family Property
- Year Built: 1963
- Lot 6,000 SF
- Approximately 1,660 SF
- Master bedroom
- Living room
- 4 bed + 2 bath
- Family
- Kitchen,
- Recreation Rm
- Composition/Shingle roofing
- 2 car attached garage

Figure 21. 1960's – 1970's property

Element	Description
Foundation:	5” slab on grade with turned-down footing at perimeter and bearing walls
Sill plate:	3x4 with 1/2” anchor bolts at 4’-0” oc
First floor:	Slab on grade under hardwood planking
Exterior walls:	2x4 studs @ 16” oc to eight foot ceilings. 3/8” plywood or hardboard nailed to all exterior wall faces with 8d @ 6”/12”. Stucco applied to exterior of wall with wire nailed flat to wall sheathing. No special hold downs or strapping details.
Interior walls:	½” gypsum wallboard with screws at ~6” oc ends. Walls are nailed to floor sheathing with 2-16d @ 16” oc.
Ceiling:	2x6 joists @ 16” oc spanning to exterior walls and some interior partition walls Joists toenailed into wall top plates.
Roof:	2x6 rafters @ 16” oc toenailed to exterior walls and load bearing ridges. Solid blocked at walls
Roofing:	½” ply with 8d @ 6”/12”. Two layers of asphalt shingles.

Figure 22. 1960’s – 1970’s one-story house structural features

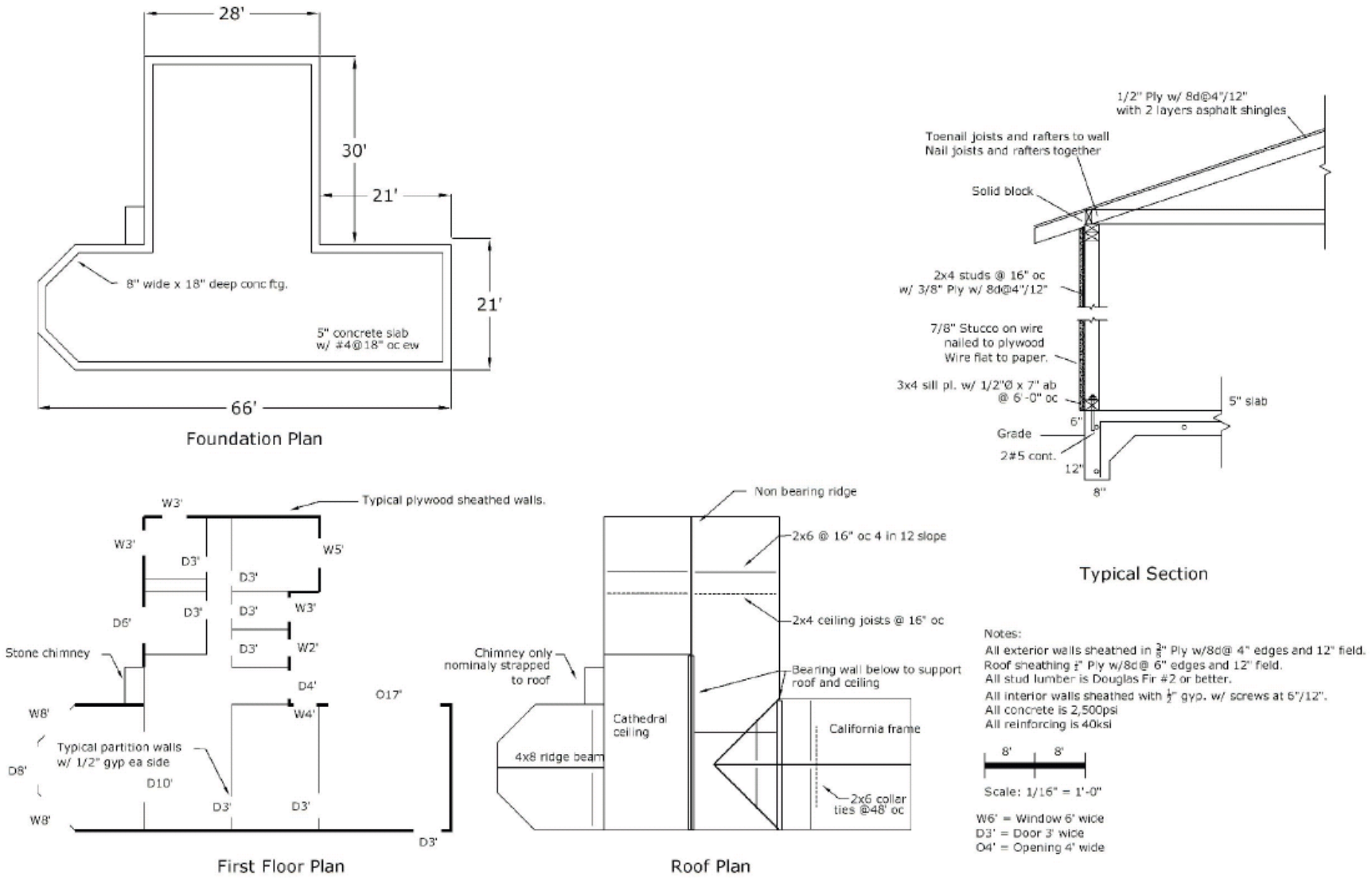

Figure 23. 1960's – 1970's one-story property, building sketches

12015 Morning Ave, Downey, 1964, 2sty, 2781 sf

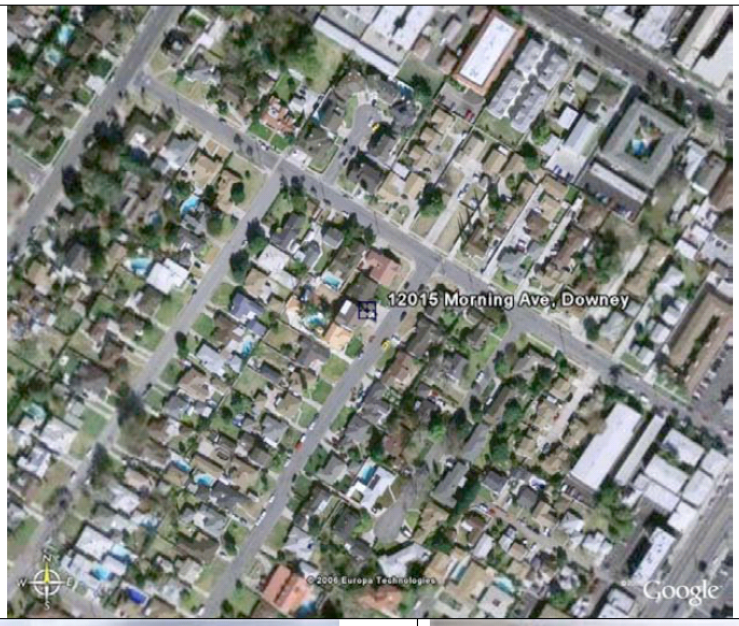

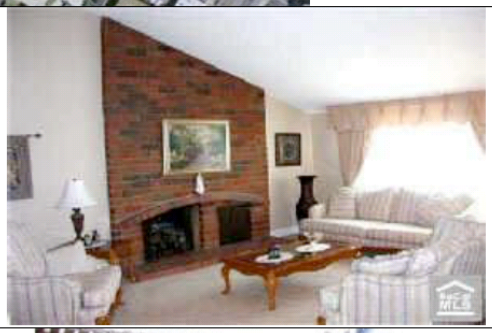

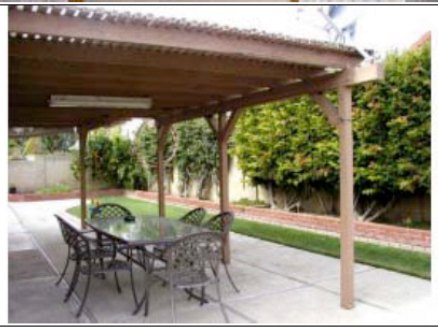

- Single Family Property
- Lot 9500 SF
- Year Built: 1964
- Master Suite,
- Kitchen, Dining
- Family Room, Living room

- Covered Patio,
- 4 bed + 4 bath
- Composition/Shingle Roofing
- Approximately 2781 sq. ft.
- Fireplace(s)
- 2 attached car garage

Figure 24. 1960's – 1970's two-story property

Element	Description
Foundation:	5” slab on grade with turned-down footing at perimeter and bearing walls
Sill plate:	3x4 with 1/2” anchor bolts at 4’-0” oc
First floor:	Slab on grade under hardwood planking
Exterior walls:	2x4 studs @ 16” oc to eight foot ceilings. 3/8” ply. nailed to all exterior wall faces with 8d @ 6”/12”. Stucco applied to exterior of wall with wire nailed flat to wall sheathing. No special hold downs or strapping details.
Interior walls:	½” gypsum wallboard with screws at ~6” oc ends. Walls are nailed to floor sheathing with 2-16d @ 16” oc.
Second Floor Framing	2x12 @ 12”-16” oc solid blocked at all ends, framing to bearing walls. ½” gypboard screwed to underside of joists. ¾” T&G ply unblocked nailed to joists w/ 10d@6”/12”.
First-Second floor wall connections	No special connection.
Second floor Ceiling:	2x6 ceiling joists @ 16” oc. with ½” gypboard screwed to underside.
Roof:	2x6 rafters @ 16” oc toenailed to exterior walls and load bearing ridges. Solid blocked at walls
Roofing:	½” ply with 8d @ 6”/12”. Two layers of asphalt shingles.

Figure 25. 1960’s – 1970’s two-story house structural features

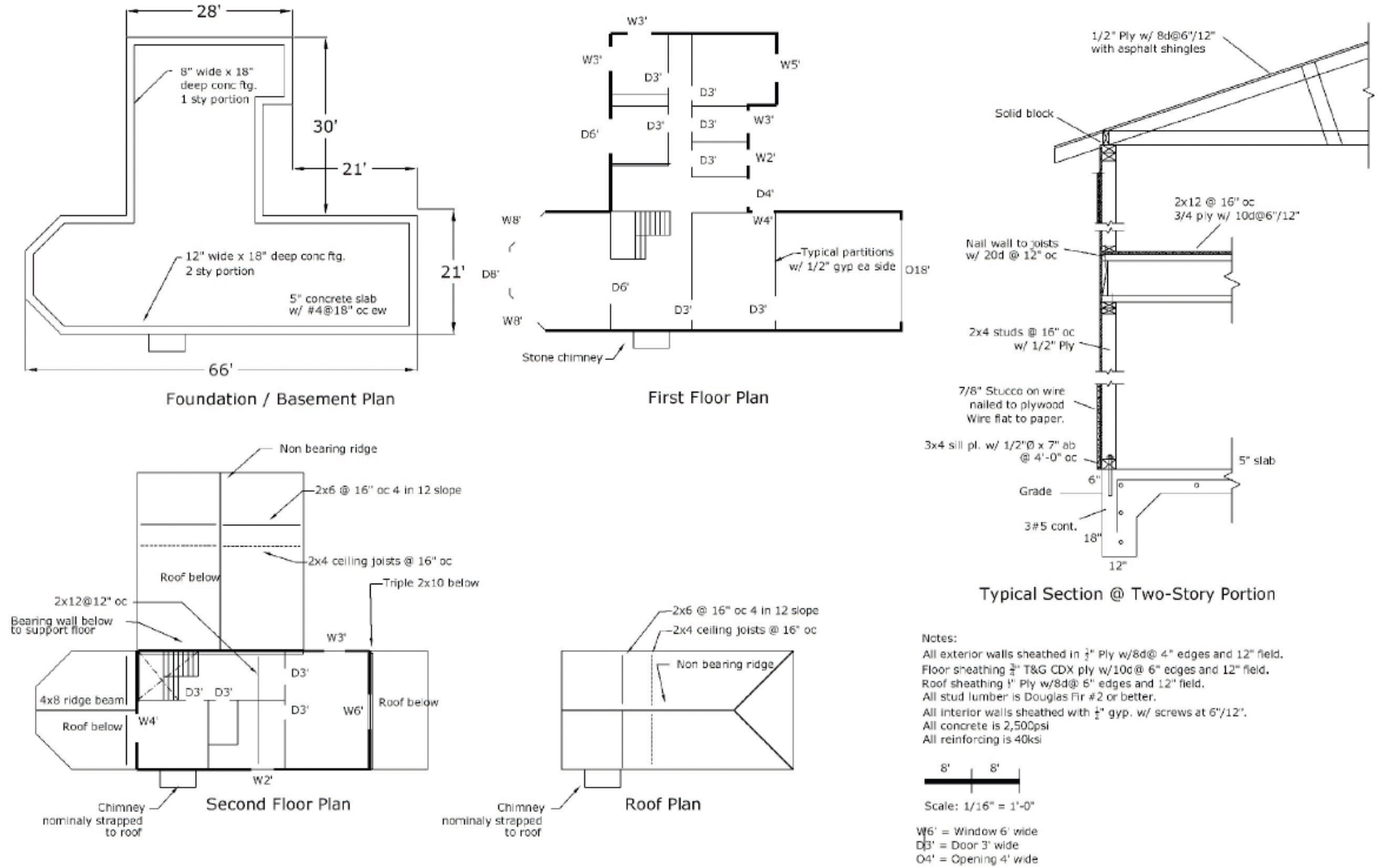

Figure 26. 1960's – 1970's two-story property, building sketches

9575 Palermo Way, Cypress, 1999, 2sty, 3,500 sf

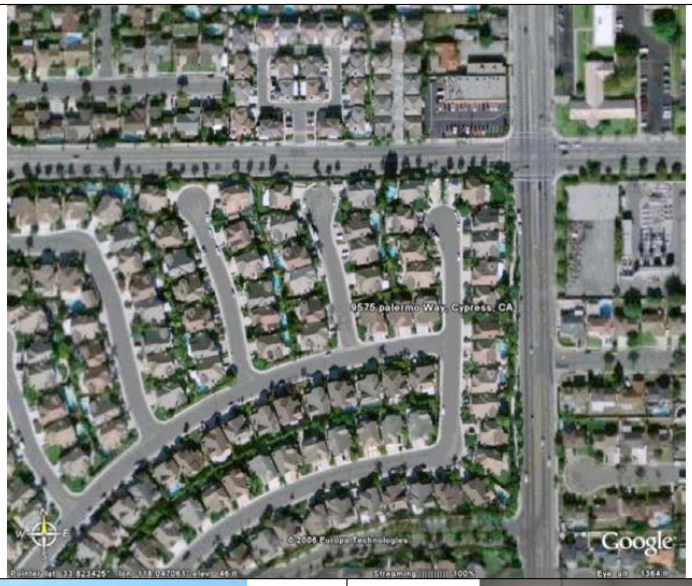

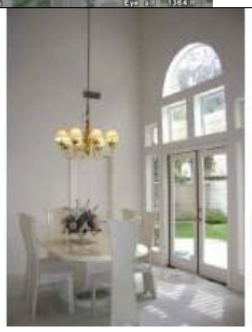

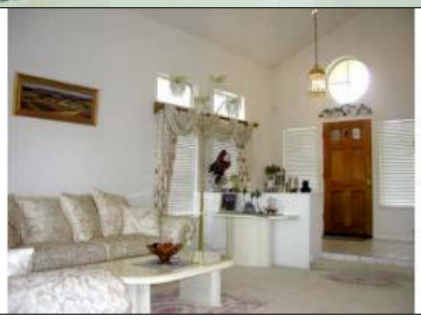

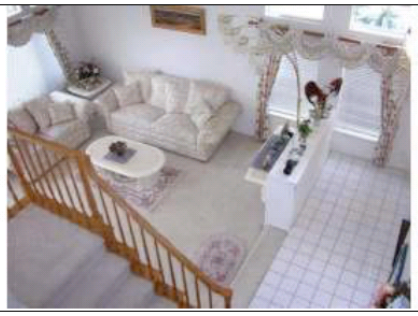

- Single Family Property
- Year Built: 1999
- Lot 6,000 SF
- Approximately 3,500 SF
- 5 bed + 4 bath
- Living room, Family room
- Fireplace(s)
- 3 car garage
- Master Suite,
- Kitchen,
- Separate Family Rm
- Concrete Tile Roofing

Figure 27. 1980's – 2000's property

4960 Ariano Dr, Cypress, 1991, 2sty, 2300 sf

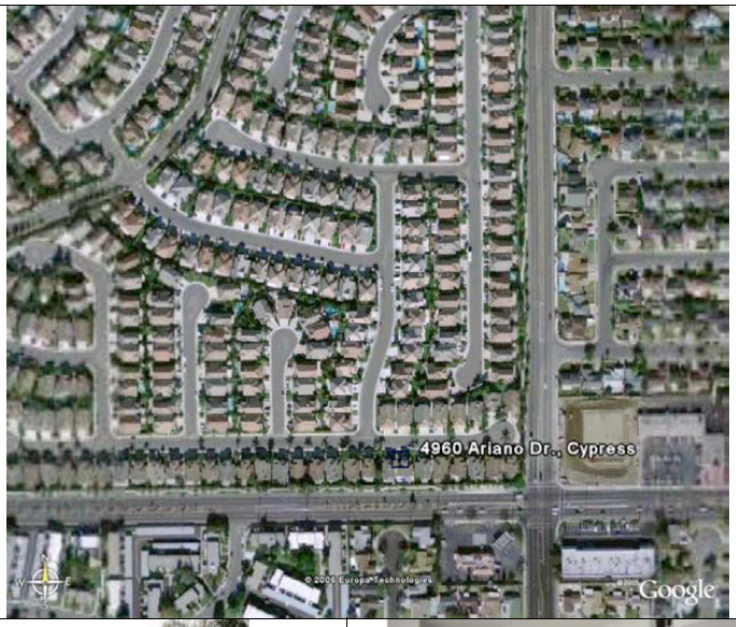

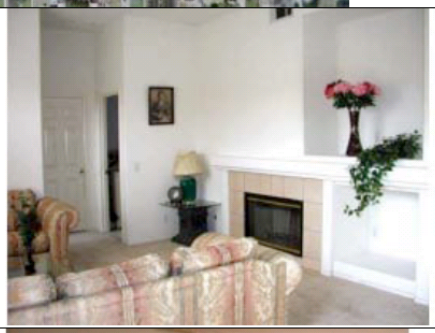

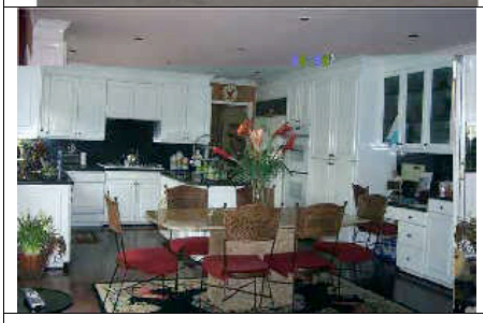

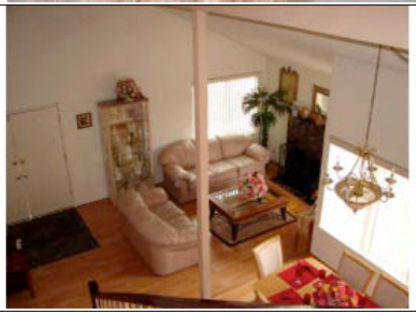

- Single Family Property
- Year Built: 1991
- Lot 5,000 SF
- Approximately 2300 sq. ft.
- 3 bed + 2.5 bath
- Living room, Dining room
- 3 car attached garage \
- Master Suite w/ Walk-In Closet,
- Family Rm, Living Rm,
- Formal Dining Rm,
- Cathedral-Vaulted Ceilings
- Roofing: Spanish Clay Tile roofing

Figure 28. 1980's – 2000's property

Element	Description
Foundation:	5” slab on grade with turned-down footing ad perimeter and bearing walls
Sill plate:	3x4 with 1/2” anchor bolts at 4’-0” oc
First floor:	Slab on grade under hardwood planking
Exterior walls:	2x4 studs @ 16” oc to nine foot ceilings. 3/8” ply. nailed to all exterior wall faces with 8d @ 6”/12”. Stucco applied to exterior of wall with wire flat against wall sheathing. Seismic wall panels include hold-down anchors at ends.
Interior walls:	½” gypsum wallboard with screws at ~6” oc ends. Walls are nailed to floor sheathing with 2-16d @ 16” oc.
Second Floor Framing	Manufactured TrussJoists @ 12”-16” oc solid blocked at all ends, framing into Parallam girders. ½” gypboard screwed to underside of TrussJoists. ¾” ply unblocked nailed to joists w/ 10d@4”/12”.
First-Second floor wall connections	No special connection.
Second floor Ceiling:	Cathedral ceilings at second floor made of prefabricated wood roof trusses @ 16” oc with ½” gypboard screwed to underside.
Roof:	2x4 prefabricated roof trusses @ 16” oc attached to exterior walls and load bearing ridges. Solid blocked at walls
Roofing:	5/8” ply with 10d @ 6”/12”. Concrete tile roofing.

Figure 29. 1980’s – 2000’s house, no special seismic detailing

Element	Description
Foundation:	5” slab on grade with turned-down footing ad perimeter and bearing walls
Sill plate:	3x4 with 5/8” anchor bolts at 4’-0” oc
First floor:	Slab on grade under hardwood planking.
Exterior walls:	2x4 studs @ 16” oc to nine foot ceilings. 1/2” OSB nailed to all exterior wall faces with 8d @ 4”/12”. Stucco applied to exterior of wall with wire held off from sheathing. Special Simpson or similar prefabricated wall units at front of house and at walls with large openings. Seismic wall panels include hold-down anchors at ends. All wall panels have Simpson CS straps around windows and doors. Steel moment frame around garage consisting of welded tubes designed to remain elastic at code forces. Tube column foundation condition considered partially restrained with 4 bolts.
Interior walls:	½” gypsum wallboard with screws at ~6” oc ends. Walls are nailed to floor sheathing with 2-16d @ 16” oc.
Second Floor Framing	Manufactured TrussJoists @ 12”-16” oc solid blocked at all ends, framing into Parallam girders. ½” gypboard screwed to underside of TrussJoists. ¾” ply unblocked nailed to joists w/ 10d@4”/12”.
First-Second floor wall connections	All special wall panels are strapped using Simpson MST straps between floors.
Second floor Ceiling:	Cathedral ceilings at second floor made of prefabricated wood roof trusses @ 16” oc with ½” gypboard screwed to underside.
Roof:	2x4 prefabricated roof trusses @ 16” oc attached to exterior walls and load bearing ridges. Solid blocked at walls with Simpson hurricane clips at ea truss.
Roofing:	5/8” OSB with 10d @ 4”/12”. Concrete tile roofing.

Figure 30 . 1980’s – 2000’s house, special seismic detailing

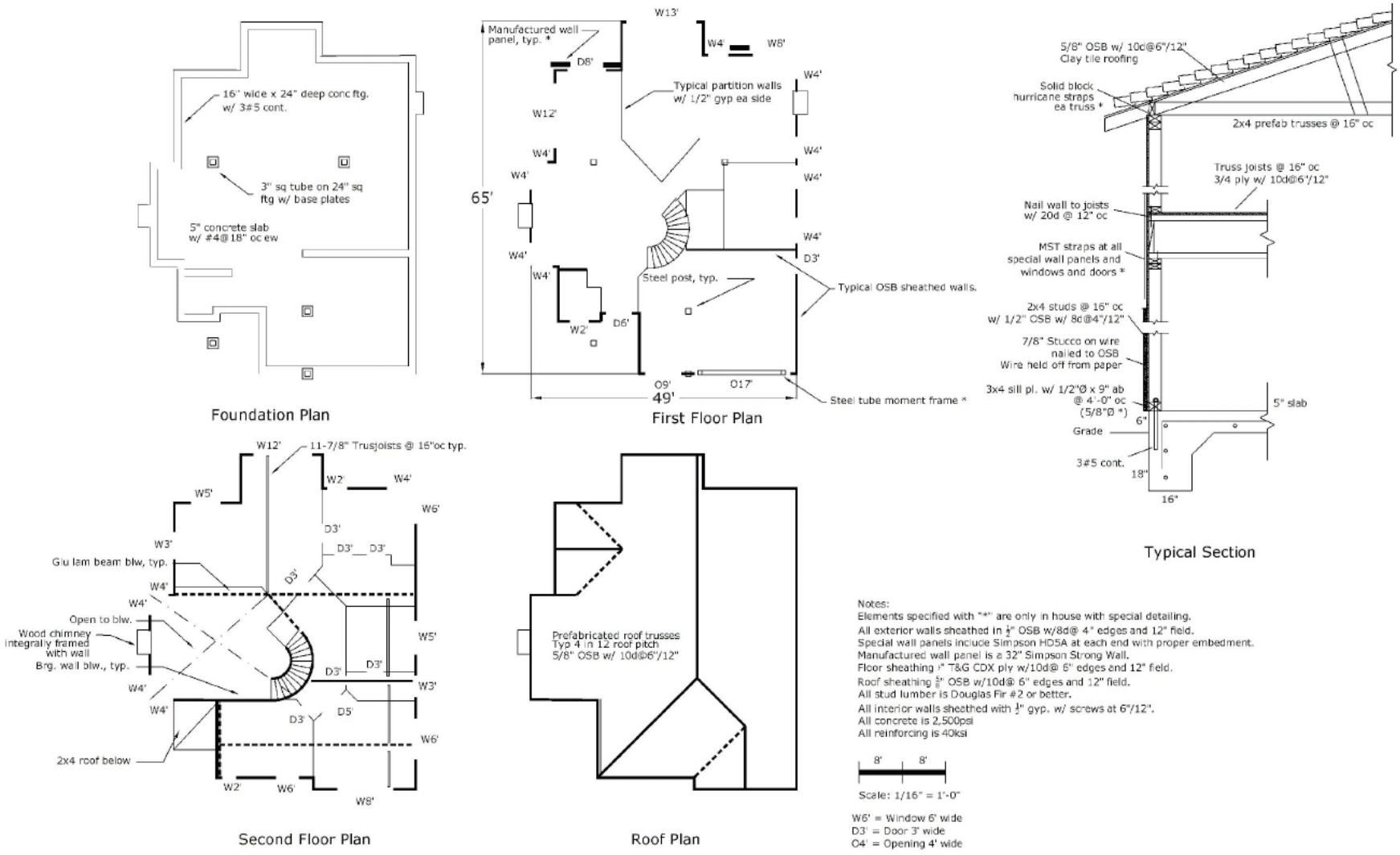

Figure 31. 1980's – 2000's property, building sketches

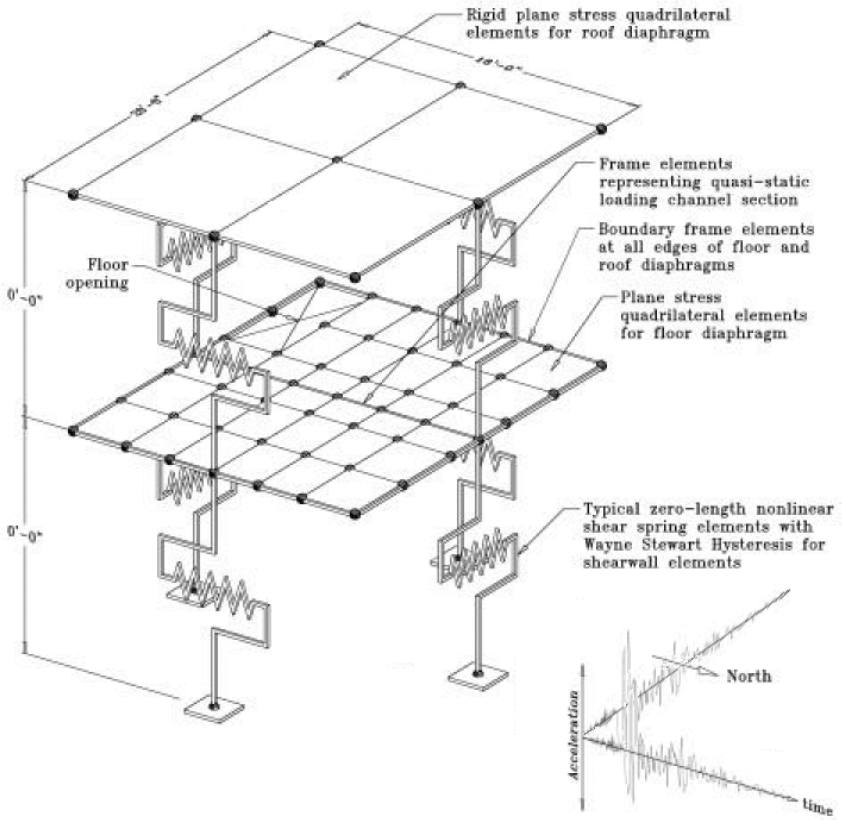

Figure 32. "Pancake" modeling of a 3-dimensional building in 2 plan dimensions, using zero-height springs to represent vertical (shearwall) elements; after Isoda et al. (2001)

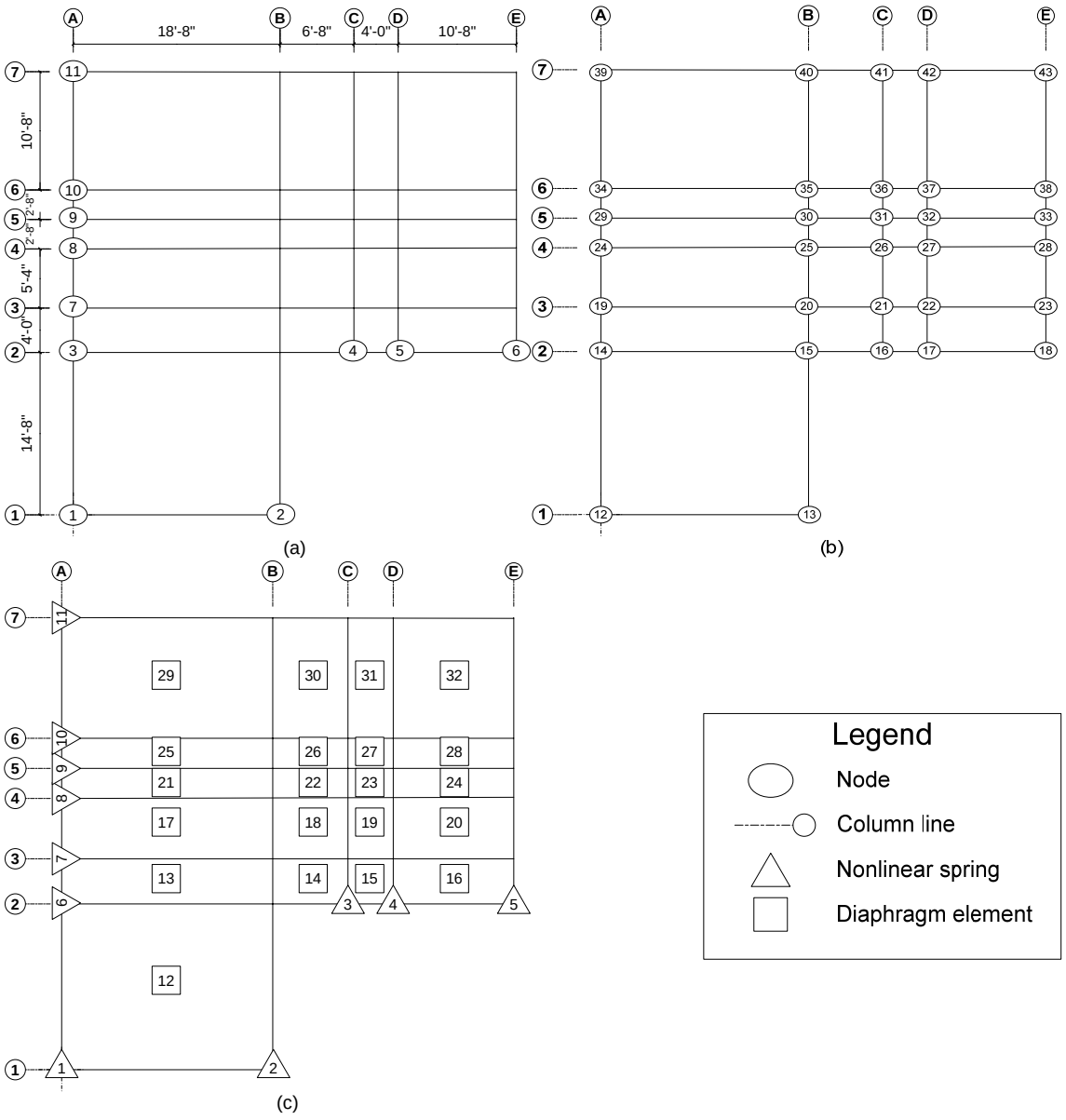

Figure 33. Configuration of structural model for 1940s-1950s index building: (a) foundation nodes, (b) ceiling/roof diaphragm nodes, and (c) nonlinear wall springs and quadrilateral diaphragm elements.

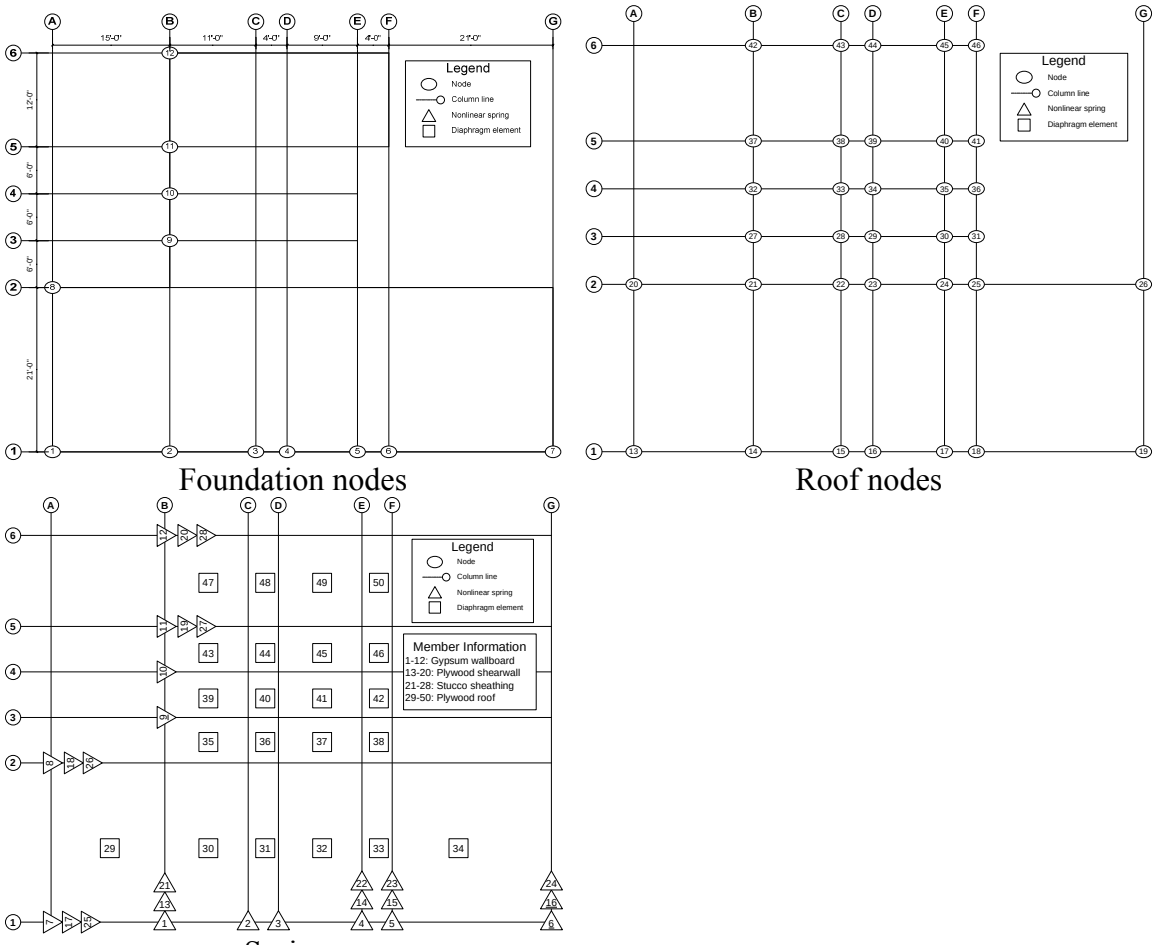

Figure 34. Structural model configuration for 1960s-1970s 1-story index building ("1960a").

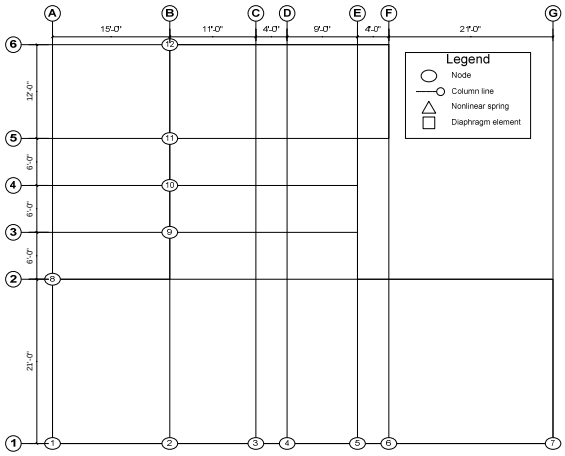

Foundation nodes

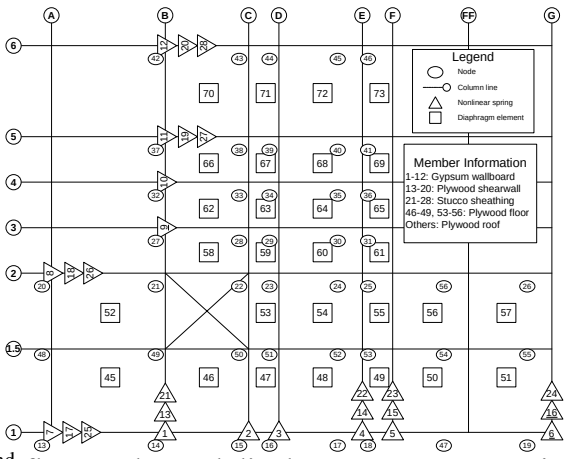

2nd floor nodes and diaphragm, 1st story springs

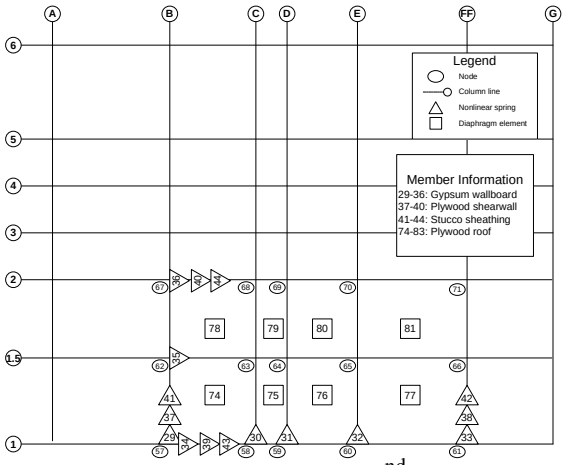

Roof nodes and diaphragm, 2nd story springs

Figure 35. Structural model configuration for 2-story 1960s-1970s index buildings ("1960b and 1960d"). In 1960d, some springs are set to dummy values to delete stucco.

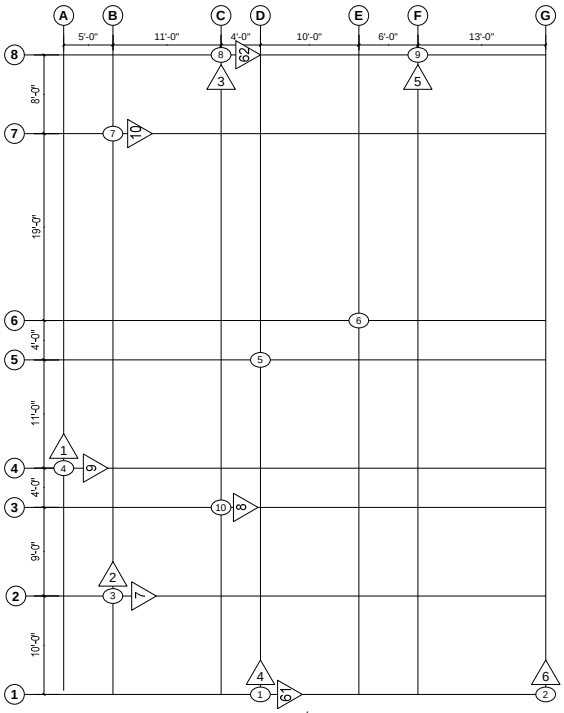

Foundation nodes, 1st-story wall springs

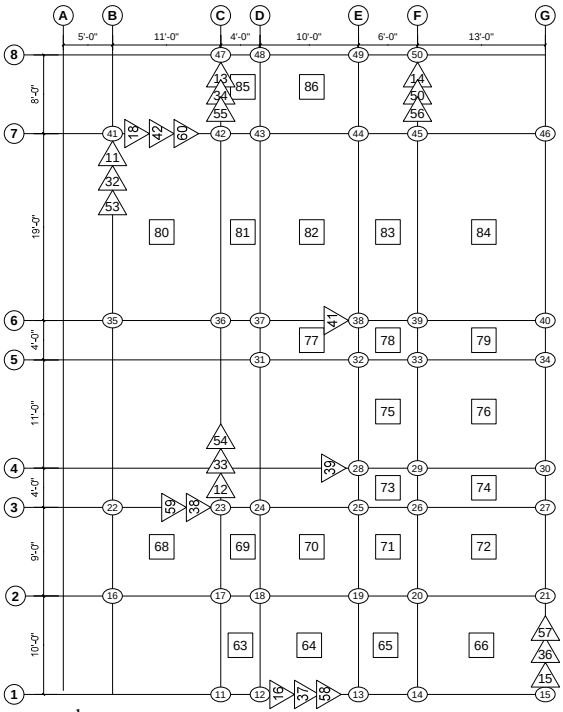

2nd floor nodes and diaphragm elements, 2nd-story wall springs

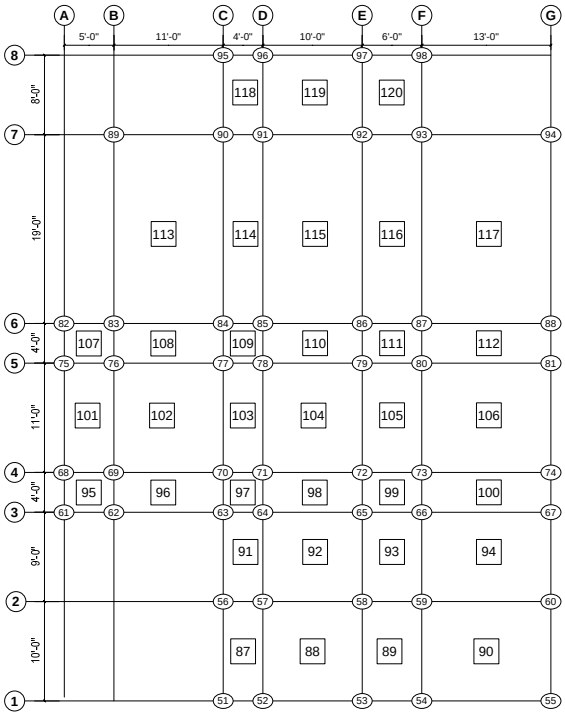

Roof nodes and diaphragm elements

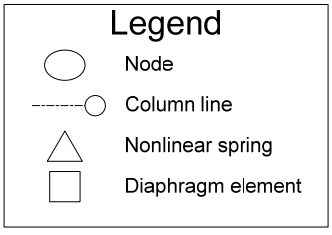

Figure 36. Structural model configuration for 1980s-2000s index buildings ("1980a" and "1980b"). In 1980a, some springs are set to dummy values to delete special seismic details.

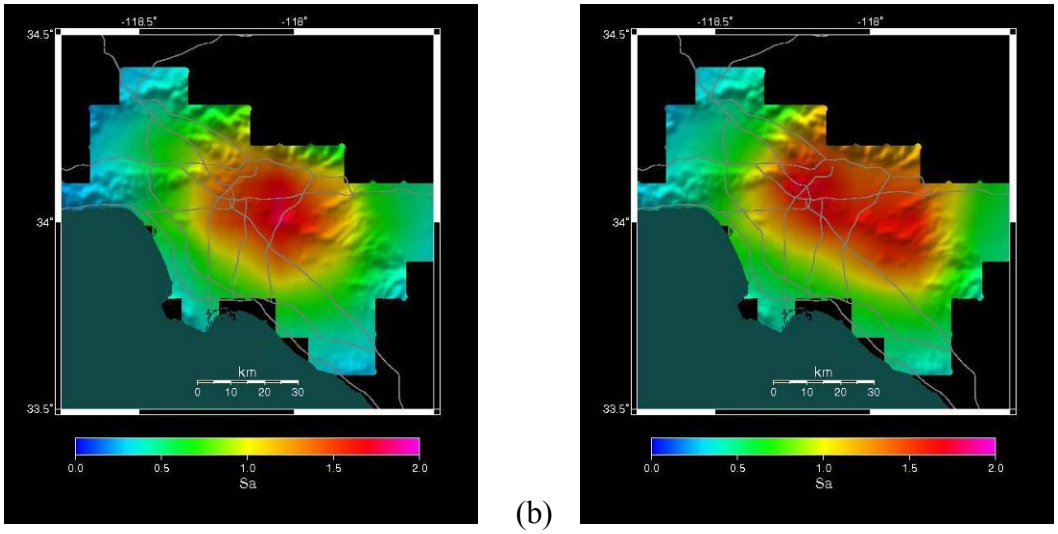

(a) End-to-end modeling (b) Attenuation-based modeling

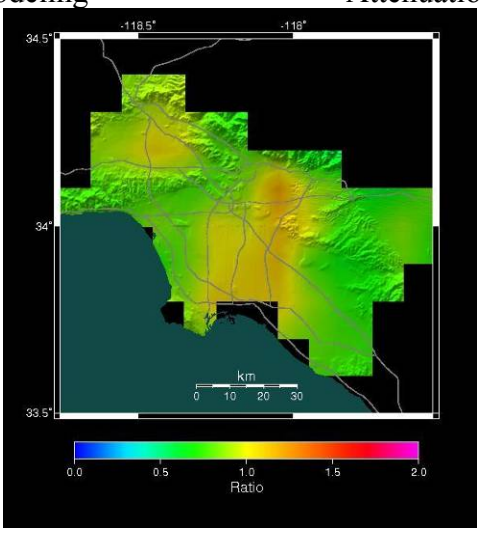

(c) Ratio

Figure 37. Mean S_a(0.3 sec, 5%) by (a) end-to-end modeling, (b) attenuation-based modeling, and (c) ratio of (a) to (b)

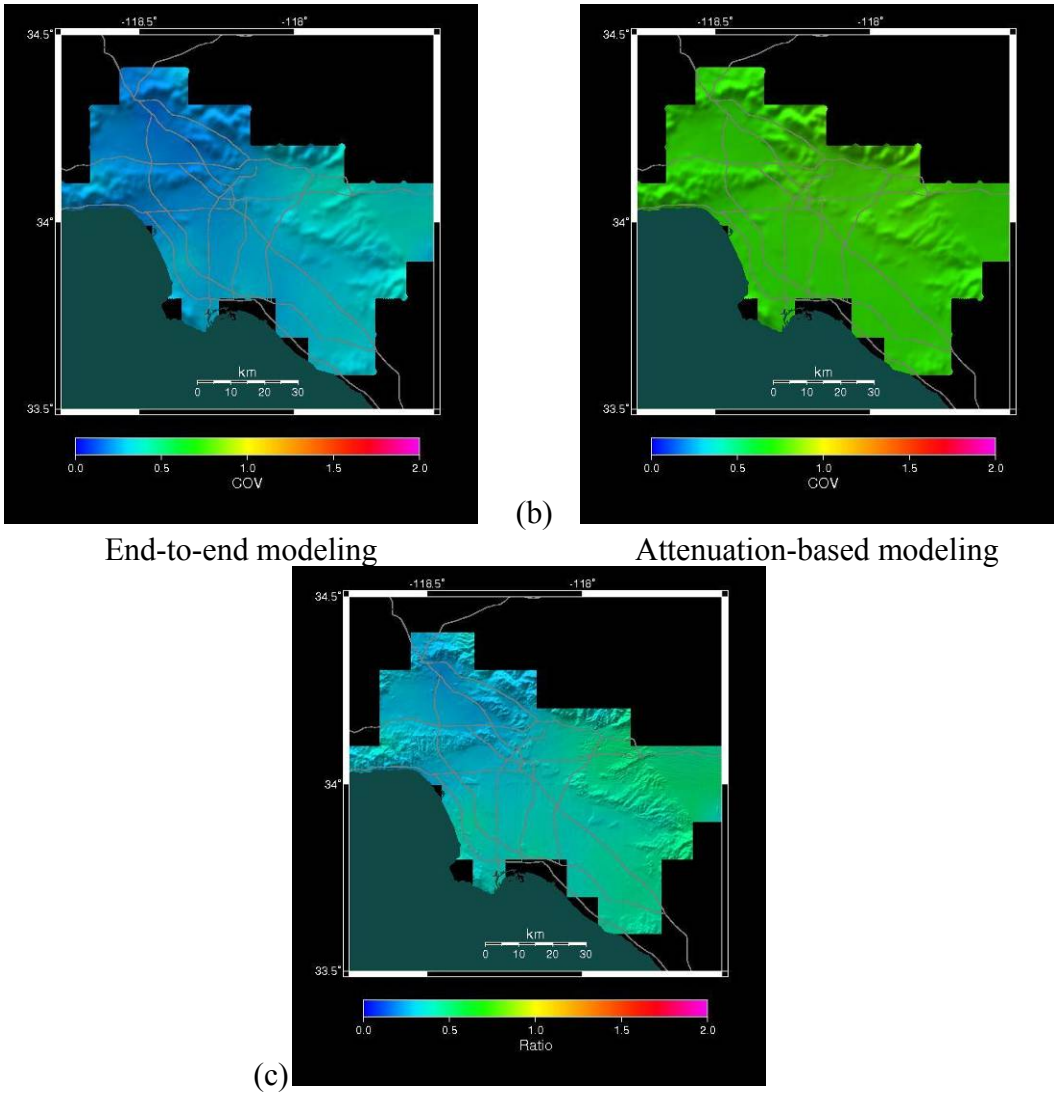

Figure 38. Coefficient of variation of S_a(0.3 sec, 5%) by (a) end-to-end modeling, (b) attenuation-based modeling, and (c) ratio of (a) to (b)

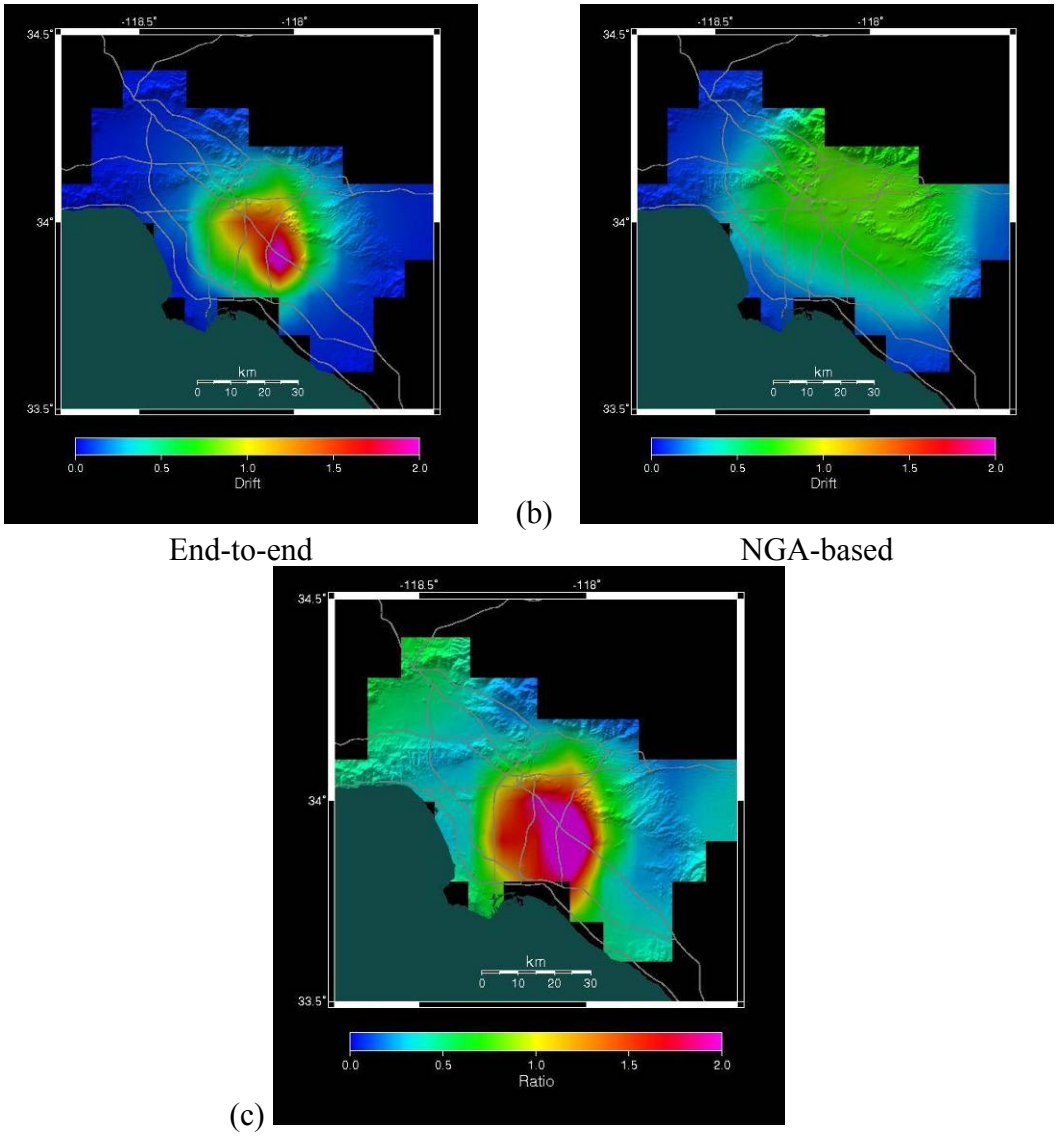

Figure 39. Average-wall 1st-story mean drifts for 1940s-1950s house by (a) end-to-end modeling, (b) attenuation-based modeling, and (c) ratio of (a) to (b).

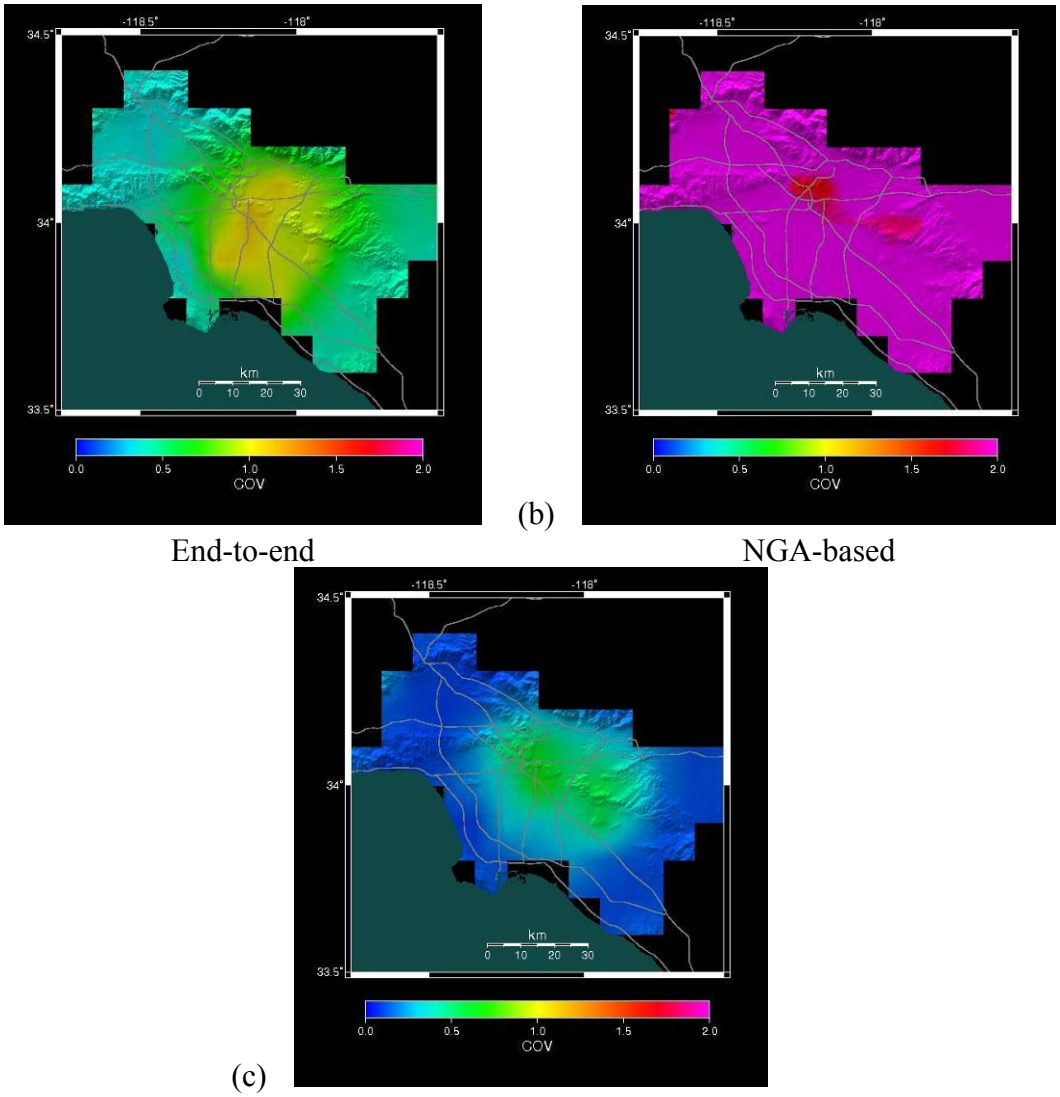

Figure 40. COV of average-wall 1st-story drifts for 1940s-1950s house by (a) end-to-end modeling, (b) attenuation-based modeling, and (c) ratio of (a) to (b).

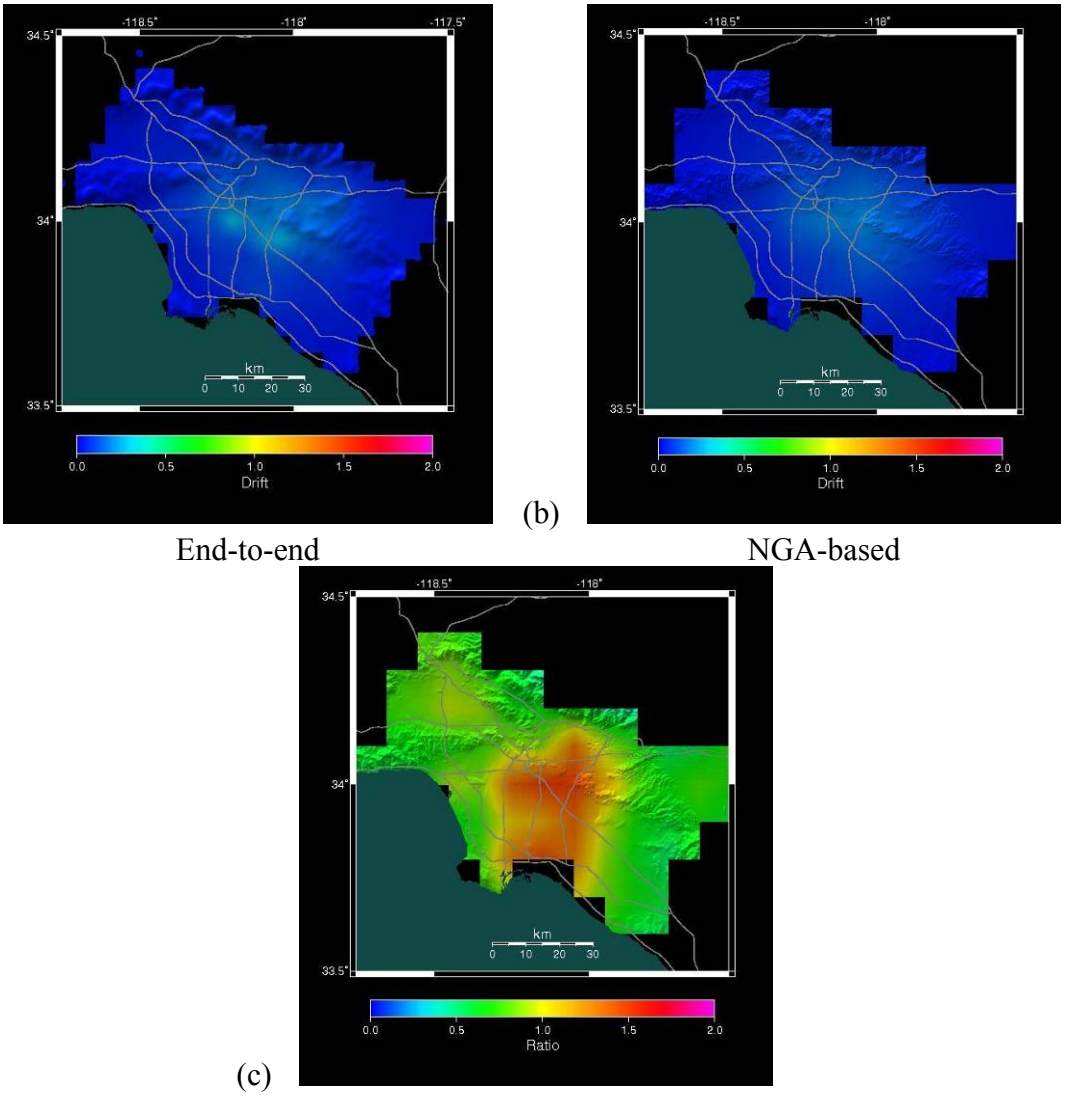

Figure 41. Average-wall 1st-story mean drifts for 1960a house by (a) end-to-end modeling, (b) attenuation-based modeling, and (c) ratio of (a) to (b).

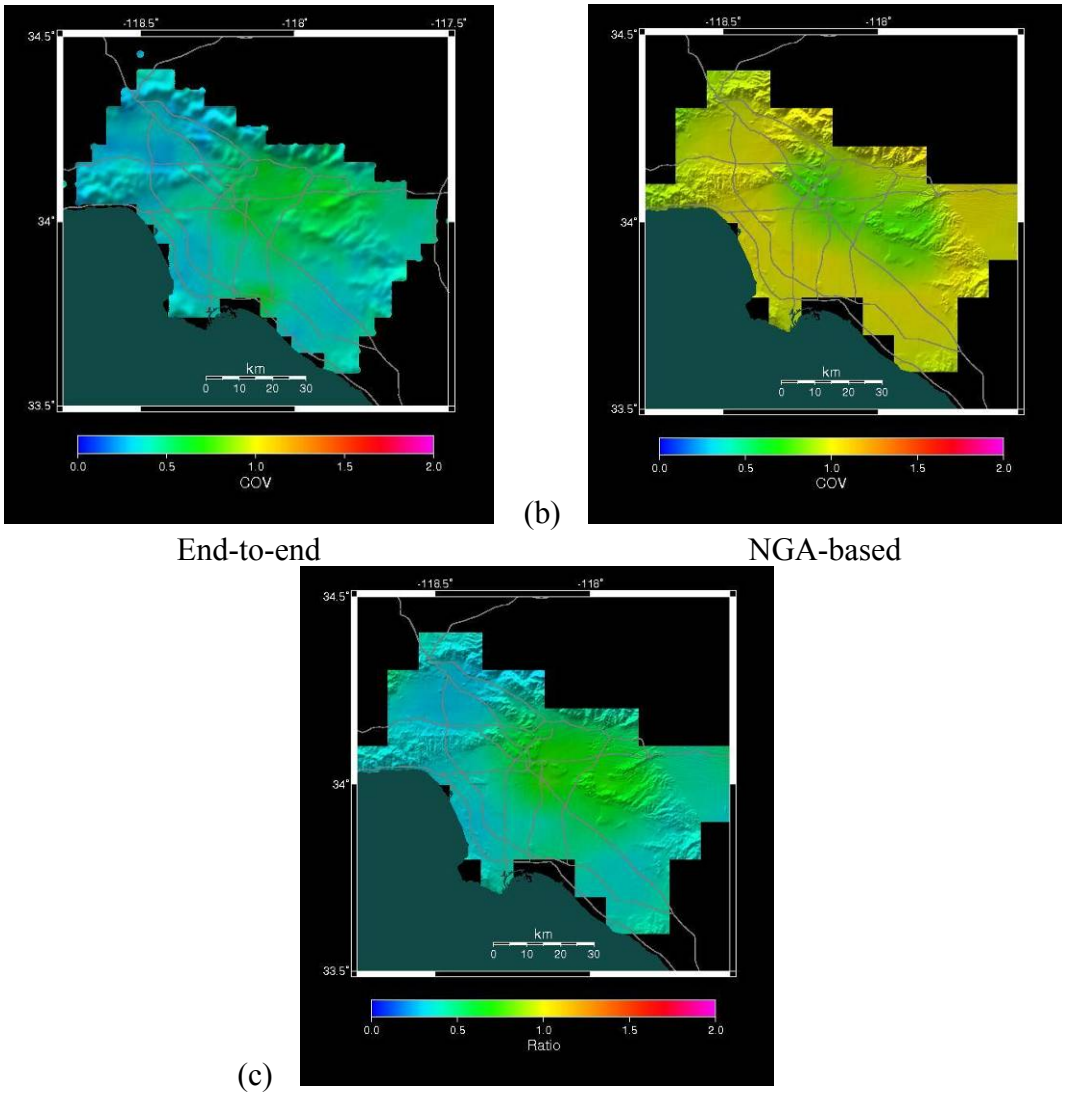

Figure 42. COV of average-wall 1st-story drifts for 1960a house by (a) end-to-end modeling, (b) attenuation-based modeling, and (c) ratio of (a) to (b).

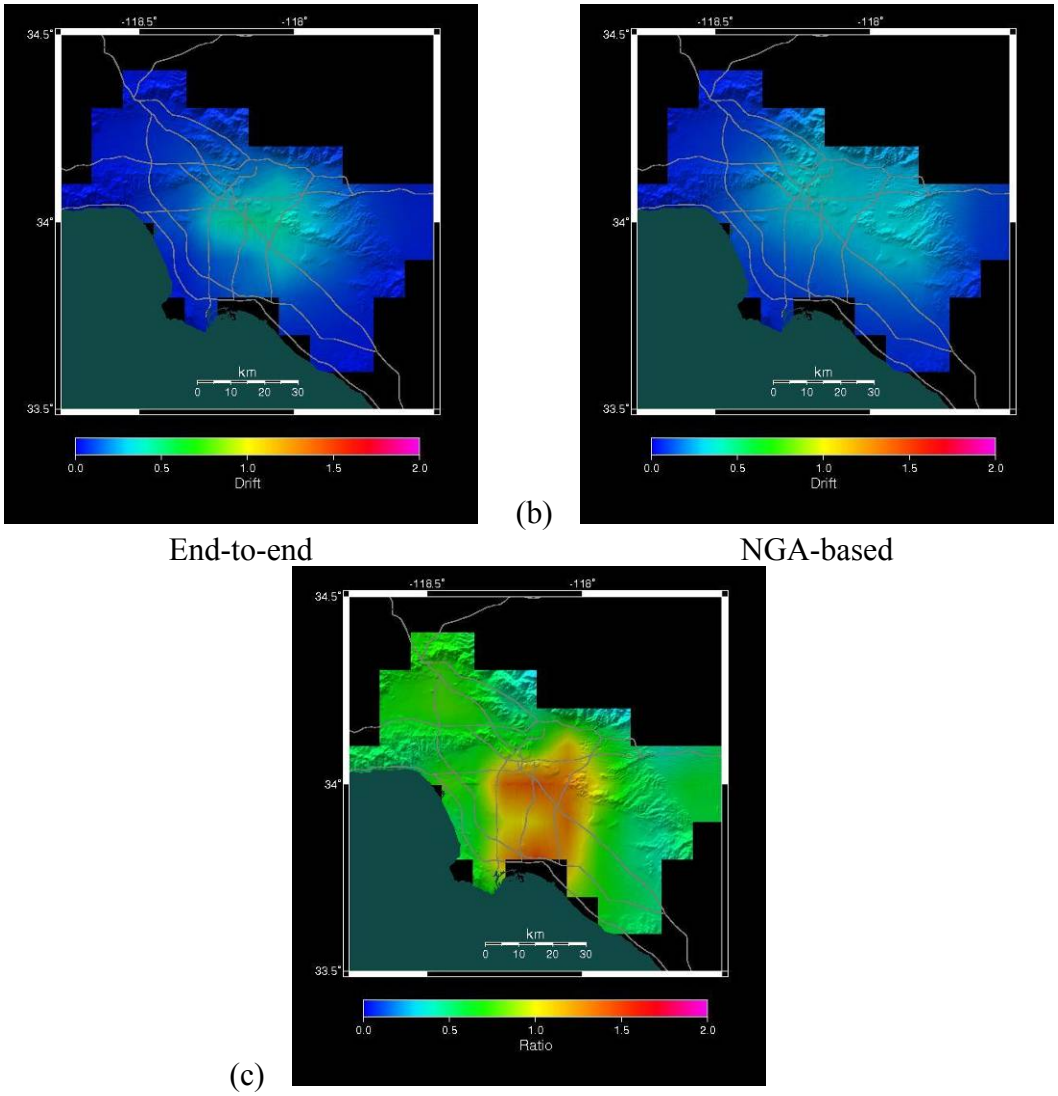

Figure 43. Average-wall 1st-story mean drifts for 2-story 1960s-1970s house ("1960b") by (a) end-to-end modeling, (b) attenuation-based modeling, and (c) ratio of (a) to (b).

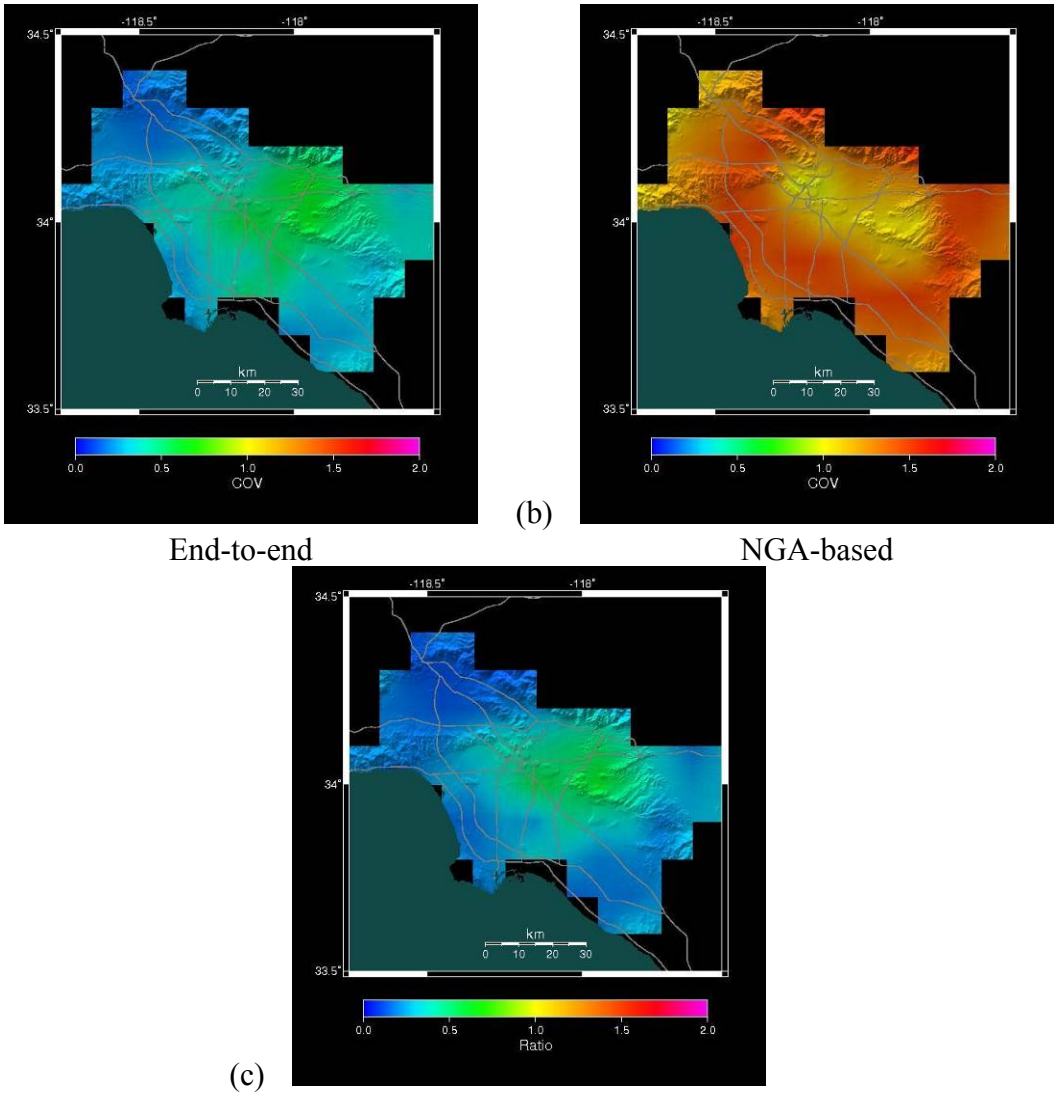

Figure 44. COV of average-wall 1st-story drifts for 2-story 1960s-1970s house ("1960b") by (a) end-to-end modeling, (b) attenuation-based modeling, and (c) ratio of (a) to (b).

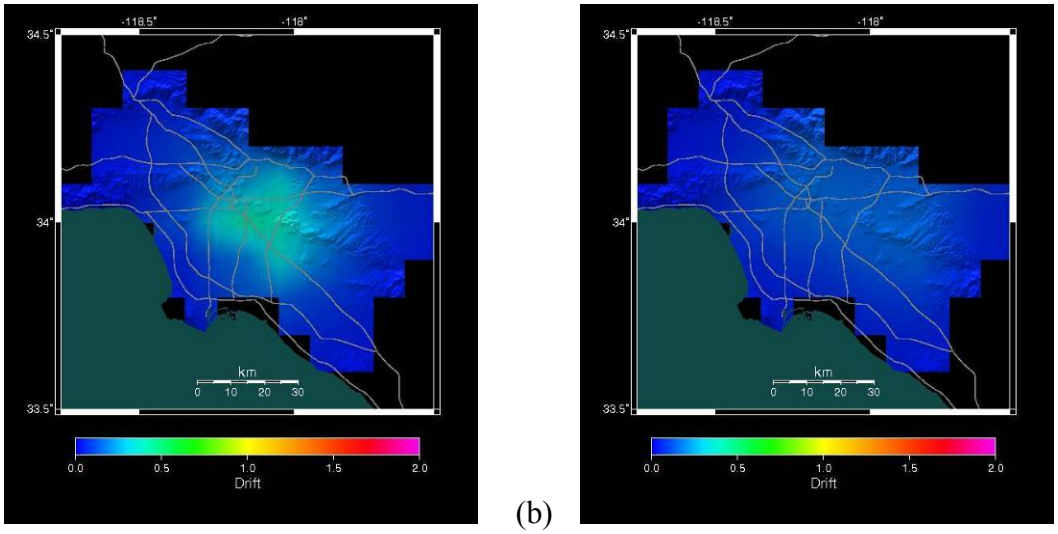

Figure 45. Average-wall 1st-story mean drifts for 1960s-1970s 2-story house with T1-11 siding and no stucco ("1960d") by (a) end-to-end modeling, (b) attenuation-based modeling, and (c) ratio of (a) to (b).

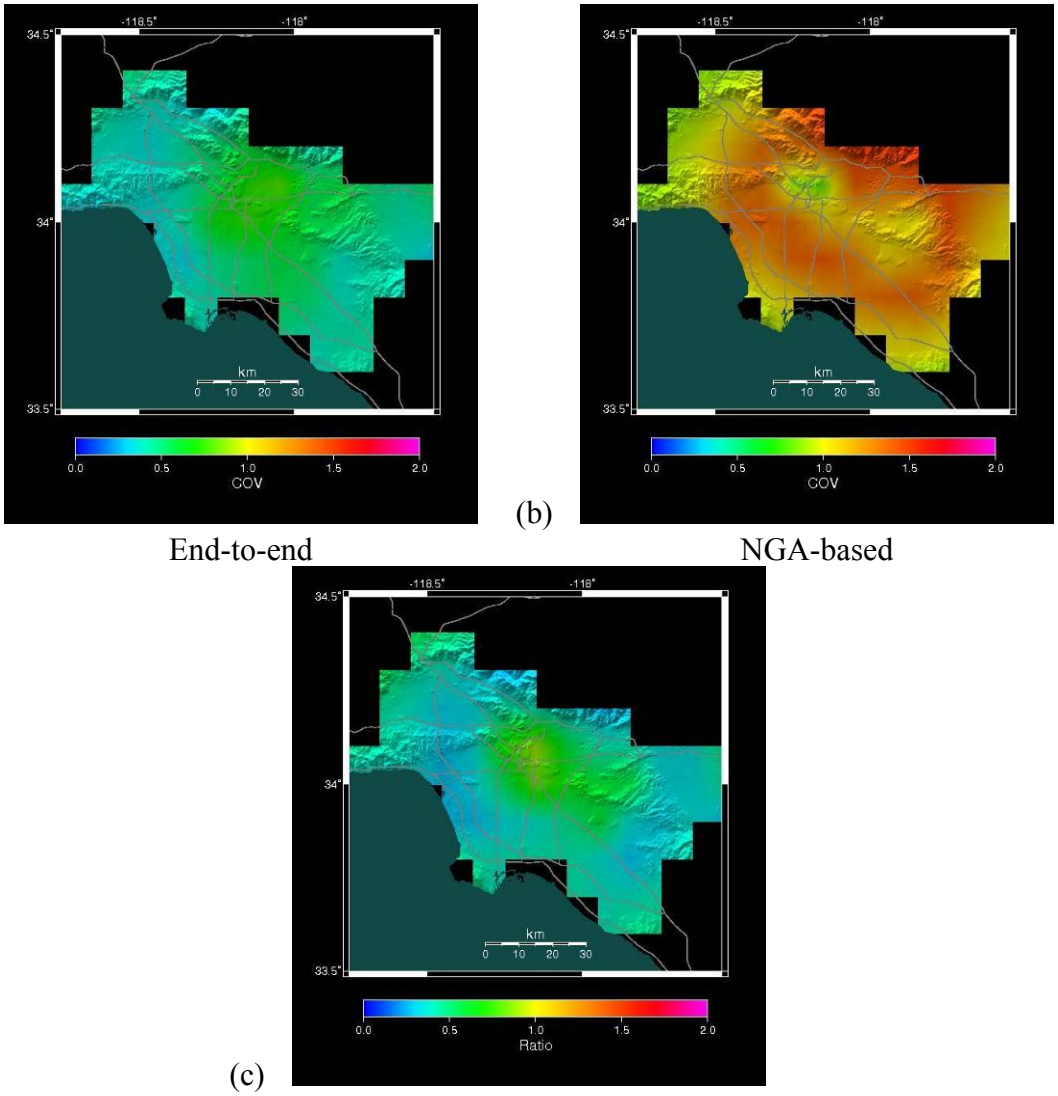

(a) End-to-end (b) NGA-based

(c) Ratio

Figure 46. COV of average-wall 1st-story drifts 1960s-1970s 2-story house with T1-11 siding and no stucco ("1960d") by (a) end-to-end modeling, (b) attenuation-based modeling, and (c) ratio of (a) to (b).

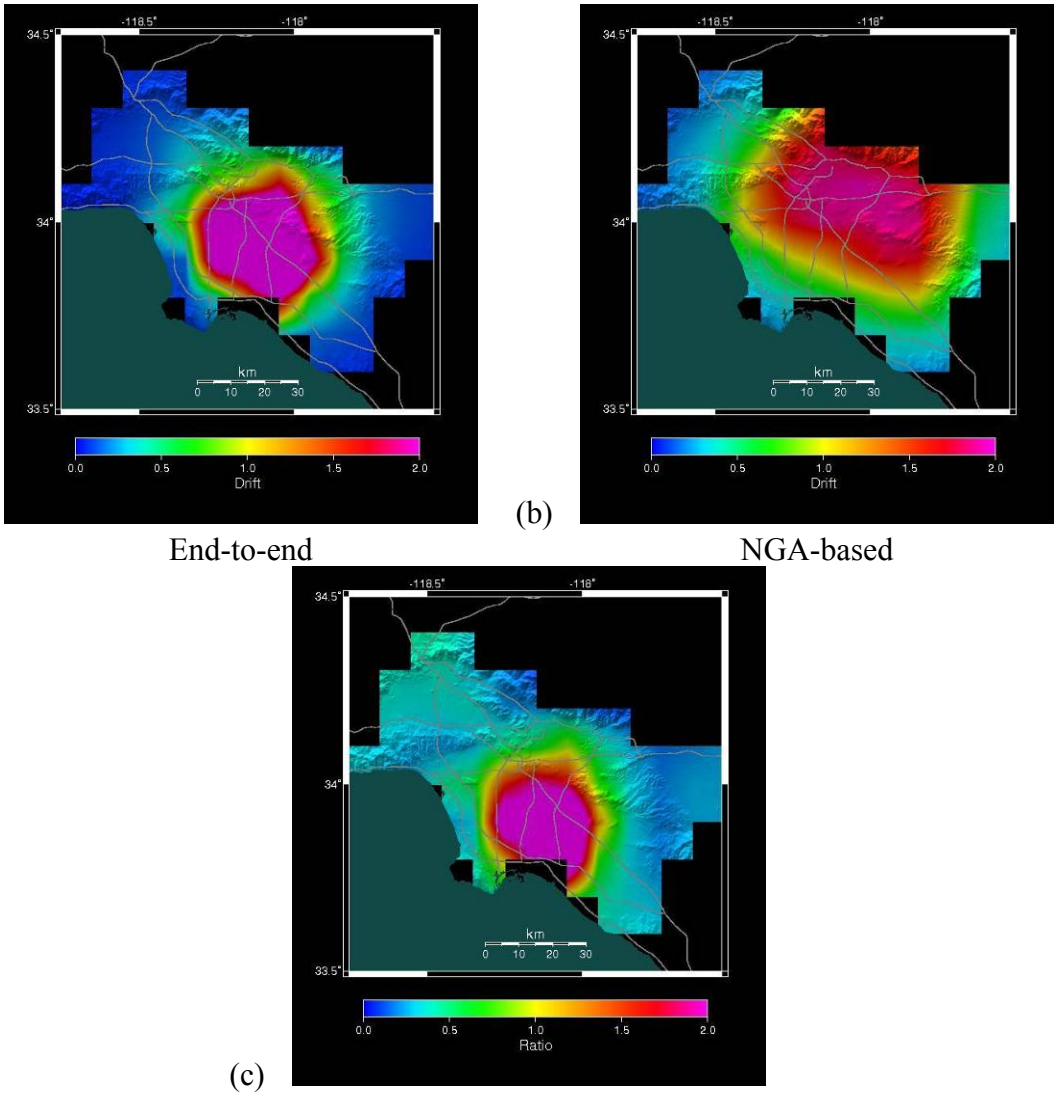

Figure 47. Average-wall 1st-story mean drifts for 1980s-2000s house ("1980a") by (a) end-to-end modeling, (b) attenuation-based modeling, and (c) ratio of (a) to (b).

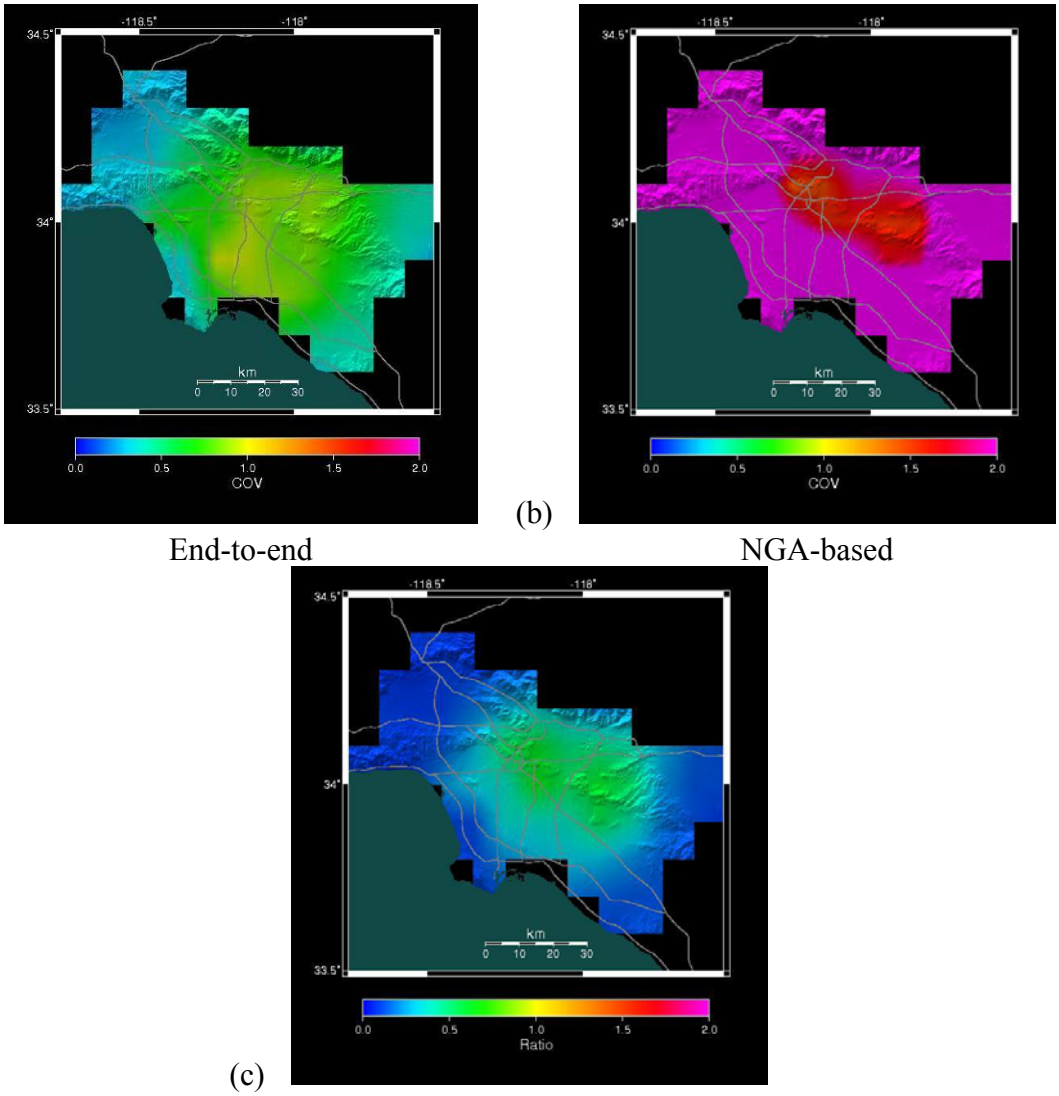

(a) End-to-end (b) NGA-based

(c) Ratio

Figure 48. COV of average-wall 1st-story drifts for 1980s-2000s house ("1980a") by (a) end-to-end modeling, (b) attenuation-based modeling, and (c) ratio of (a) to (b).

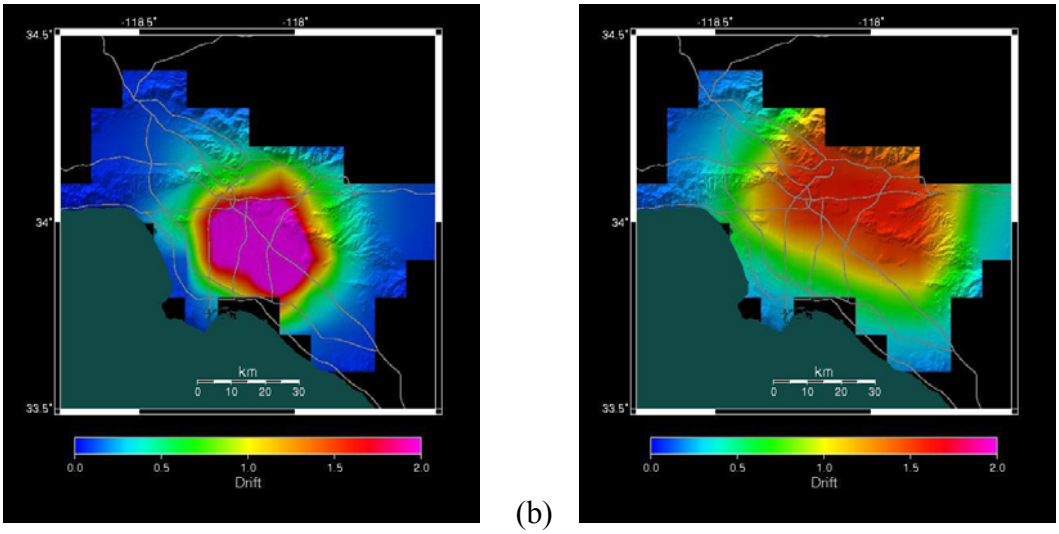

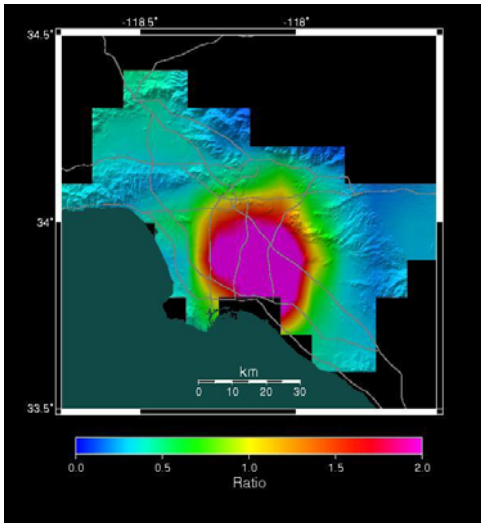

Figure 49. Average-wall 1st-story mean drifts for 1980s-2000s house with special seismic detailing ("1980b") by (a) end-to-end modeling, (b) attenuation-based modeling, and (c) ratio of (a) to (b).

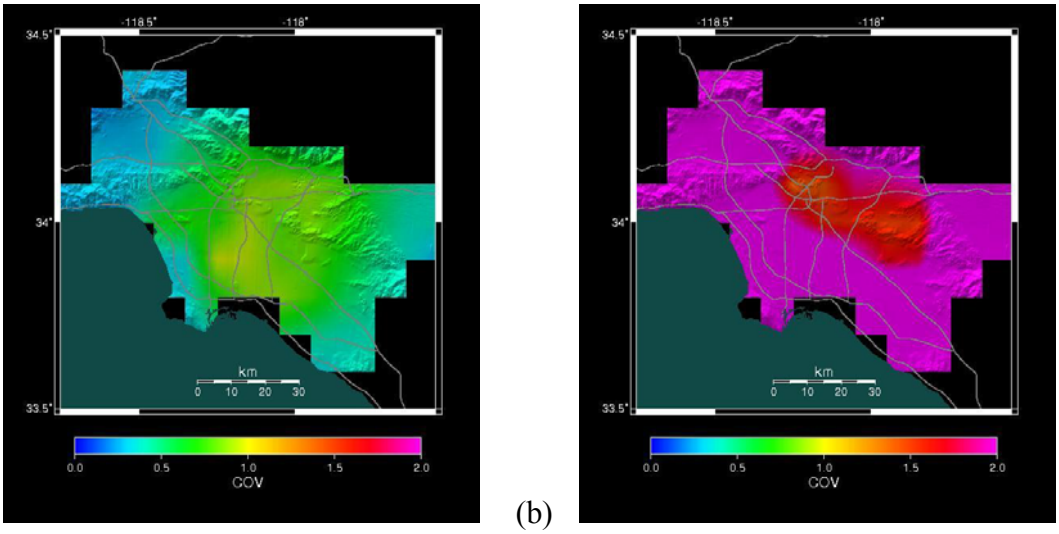

Figure 50. COV of average-wall 1st-story drifts for 1980s-2000s house with special seismic detailing ("1980b") by (a) end-to-end modeling, (b) attenuation-based modeling, and (c) ratio of (a) to (b).

APPENDIX 1: T1-11 SIDING SPRING PROPERTIES AND FRAGILITY FUNCTIONS

GIVEN

8-ft high woodframe shearwall sheathed with T1-11 siding, nailed at lap with ¼-in edge distance.

REQUIRED

Develop a SDOF nonlinear spring to represent the shearwall on a per-lf basis, formatted for use in Ruaumoko (Carr 2001). Also develop limit states and fragility functions.

SOLUTION

According to Rose (2000) of the American Plywood Association: "True T1-11 plywood siding is now 19/32" thick, grooves 1/4" deep. If you nail in the full-thick portion of panel (including edges), full allowable design shear values apply since panels are thicker (where nailed) than minimum nom. thickness specified in Table 23-II-I-1. Regularly, T1-11 plywood is nailed with 8d hot-galv. box nails (same shear values as 8d common nails). But if the panel is nailed along thinner shiplap edge, then use allowable design shear values for 5/16" panels since thickness of panel at point of nailing governs shear values."

Solution steps. Create a Ruaumoko spring and fragility functions by 3-step process:

1. Get similar connector parameters from Fonseca et al. (2002).
2. Input these with other shearwall parameters to CASHEW (Folz and Filiatrault 2000); model a 4x8 panel
3. Format CASHEW output for Ruaumoko on per-lf of wall basis. Assume typical as-built strength and stiffness is ~90% of values suggested by laboratory tests, to account for shiners & larger nail spacing, per advice from David McCormick and John Shipp for CUREE-Caltech Woodframe Project (Porter et al. 2002).
4. Define limit state 1 as first fracture of sheathing-to-framing connections, occurring at displacement at which ultimate force is reached (denoted here by DU), repaired by renailing. Limit state 2 as displacement at which force is reduced to 80% of ultimate, repaired by demolishing and replacing the shearwall.

Fonseca. Closest test was no. 48: 8d common nail connecting 3/8-in OSB and DF-L stud under wet/dry conditions, 3/8-in edge distance, 0 overdrive depth, loading perpendicular to grain (Table A1-1). Correct for use of ¼-in edge distance rather than 3/8-in tested distance by scaling parameters from test 48 by the ratio of two tests (1 and 85) that differ only by edge distance. There were no tests with 5/16-in thickness, so cannot correct for that factor. Connection parameters for each test and the "scaled" result are shown in Table A1-2. Parameters are explained graphically in Figure A1-1.

Table A1-1. Relevant coupon tests from Fonseca et al. (2002)

Test No.	Test Variable	Sheathing Panel	Wood Member	Moisture Condition	Fastener Type	Edge Distance	Overdrive Depth	Loading Direction	Samples
47	Fastener Common	3/8 OSB std	DF-L	Wet / Dry 8d	Common Nail	3/8"	0	Perpendicular	10
1	Control	7/16 OSB std	DF-L	Wet / Dry 8d	Cooler Nail	3/8"	0	Perpendicular	10
85	Edge Distance	7/16 OSB std	DF-L	Wet / Dry 8d	Cooler Nail	1/4"	0	Perpendicular	10

Table A1-2. Adjusting coupon test results to account for edge distance

Fonseca test:	47			1	85				
Comment:	Unscaled			3/8 edge	1/4 edge	Ratio		Scaled	
a	0.6000		a	0.6000	0.6000	100%	a	0.6000	
b	1.1000		b	1.1000	1.1000	100%	b	1.1000	
Fo	0.1506	kip	Fo	0.1233	0.0852	69%	Fo	0.1040	kip
Fl	0.0612	kip	Fl	0.0476	0.0309	65%	Fl	0.0397	kip
Du	0.2076	in	Du	0.2027	0.1011	50%	Du	0.1035	in
Ko [S0 in Fig1]	3.6695	kip/in	Ko	3.9163	3.1583	81%	Ko	2.9593	kip/in
r1	0.0578		r1	0.0761	0.2716	357%	r1	0.2061	
r2	-0.0842		r2	-0.1496	-0.6308	422%	r2	-0.3551	
r3	1.9690		r3	1.5292	1.6040	105%	r3	2.0653	
r4	0.0791		r4	0.0857	0.2524	295%	r4	0.2331	

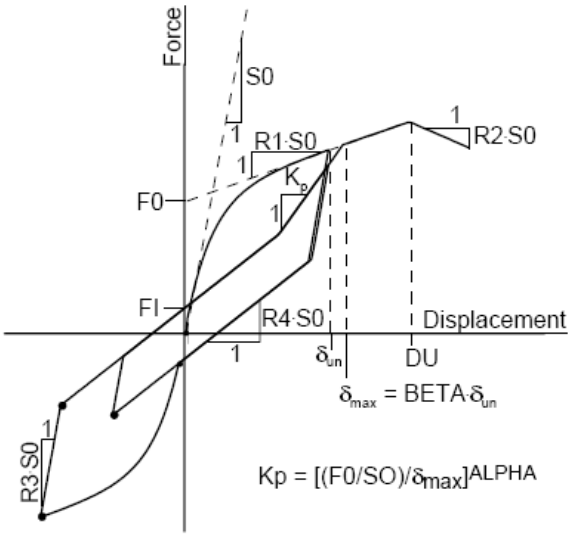

Figure A1-1. Connection parameters (Folz and Filiatrault 2000).

CASHEW. Use scaled connector data with the following input for CASHEW:

Table A1-3. CASHEW input parameters

Wall ht	8	ft
Wall width	4	ft
Sheathing	T1-11	
Thick	0.3125	in (nailed at shiplap edge)
Nail	8d	
Edge vert	0.25	in
Edge T&B	0.75	in
Edge sp	6	in
Panel sp	6	in
Pl thick	1.75	in
G	360	ksi

Formatted CASHEW input. See Folz and Filiatrault (2000) for detailed explanation of input file format. Summary explanations are shown at right after exclamation points. Units are kips and inches.

Table A1-4. Formatted CASHEW input

```
T1-11 0.313in 4ftx8ft 8d@6in edge 6in panel                                  ! 2-4.1. Title
2                                                                            ! 2-4.2. Control Param
95.125          1                                                            ! 2-4.3. Shear Wall Config
1               48          96          0.3125          24  48  2  4  360   ! 2-4.4. Panel Geom, Properties.
1                                                                            ! 2-4.5. Connector Properties
0.104029        0.039692    0.103517                                           ! Fo, Fl, Du,
2.959264        0.20605     -0.355122   2.065336    0.233118                   ! Ko, r1, r2, r3, r4
0.6             1.1                                                          ! a, b
1                                                                            ! 2-4.6. Connector Placement
-47.125         -23.75      23.75       6                                    ! Line 1: x, y0, y1, spacing
47.125          -23.75      23.75       6                                    ! Line 2
-23.75          -41.125     41.125      6                                    ! Line 3
-7.75           -41.125     41.125      6                                    ! Line 4
7.75            -41.125     41.125      6                                    ! Line 5
23.75           -41.125     41.125      6                                    ! Line 6
```

CASHEW output and Ruaumoko input. Use CASHEW output. Scale initial stiffness, yield strength, and ultimate strength by 0.25 (to reflect per-lf strength and stiffness) and again by 0.90 (to reflect as-built strength and stiffness). Results are shown below. Units are kips and inches.

Table A1-5. CASHEW output and equivalent Ruaumoko (Carr 2001) input

CASHEW output	Ruaumoko input	Value	Scale factor for Ruaumoko
Initial wall stiffness	KX or KY	4.75E+00	x 0.25 x 0.9
Ultimate lateral load	FU	1.46E+00	x 0.25 x 0.9
Displacement @ ultimate load	not used	5.33E-01	
CUREe protocol displacement DELTA	not used	3.82E-01	
SDOF system ID under cyclic loading:	not used		
WS0 [S0 in Fig1]	not used	4.58E+00	
WR1 [r1]	RF	2.23E-01	
WR2 [r2]	PTRI	-8.29E-01	
WR3 [r3]	PUNL	1.64E+00	
WR4 [r4]	not used	4.17E-01	
WF0 [Fo]	See FY below	1.09E+00	
WFI [FI]	FI	2.98E-01	0.25 FY, per Wayne Stewart
WDULT [Du]	not used	5.33E-01	
WALPHA	ALPHA	-7.05E-01	
WBETA	*B*	8.12E-01	
	FY = WF0/(1 – WR1)	1.40	x 0.25 x 0.9

Validation of spring parameters: comparison with Pardoen et al. (2000) lab tests. The most similar full-scale specimens tested by Pardoen et al. (2000) were their group 1, comprising 3/8 STR I on one side, connected with 8d hand driven common nails at 6 in OC with ½-in edge distance, 8d at 12 in OC in panels, 8 lf specimens. Mean initial stiffness was 11.2 kip/in, roughly 1.2 times the above on a per-lf basis. Mean yield strength was 3.4 kip, about 1.2x the above on a per-lf basis. Mean ultimate strength was 5.5 kip, about 1.9x the above on a per-lf basis. Given the greater edge distance in the Pardoen tests, one would expect relatively greater overstrength. Mean displacement at ultimate was 1.4 in, almost 3x that of the above, also not surprising given double the edge distance. These comparisons tend to support the stiffness and strength estimates by CASHEW.

Fragility functions. Median peak transient drift ratio for limit state 1 occurs at Du/height, or 0.523 in/96 in = 0.00545. Median peak transient drift ratio for limit state 2 occurs at (Du – 0.2Fu/(S0xR2))/height = 0.00616. For distribution, assume both fragility functions have lognormal distribution, consistent with common structural and nonstructural elements. For logarithmic standard deviation, note that Pardoen et al. (2000) tests had coefficient of variation of drift at yield and drift at ultimate, within tests, of generally 0.1 to 0.3, suggesting a typical value of 0.2. To account for variability in contractor judgment relating drift limit states to repair requirements SRSS in another 0.2, and for uncertainty in assigning these limit states to these drift levels, SRSS in 0.25, for a total logarithmic standard deviation of $(2*0.2^2 + 0.25^2)^{0.5} = 0.38$, or approximately 0.4.

Validation of fragility parameters. A β value of 0.4 is in line with common nonstructural components, per ATC-58 (Porter et al. 2007) and is the default value proposed by Kennedy (1999).

CONCLUSIONS

An analytical model of T1-11 siding was created from coupon tests of the fasteners and a finite element model of the system of fasteners, studs, and sheathing panels. The analytical model agrees reasonably well with laboratory tests of similar full-scale shearwall specimens (generally within 20%). Fragility functions were created based on the limits states of first fastener tearthrough and extensive fastener tearthrough, and by equating these limit states with displacement at ultimate strength and when strength is reduced to 80% of ultimate.

APPENDIX 2: DETAILED DISCUSSION OF DAMPING RATIOS

Camelo et al. (2001) performed forced-vibration tests, ambient-vibration tests, and post-earthquake system-ID analysis of a number of woodframe buildings. Figure shows the damping ratio calculated from 16 seismic records taken from instrumented woodframe buildings, plotted against the calculated 5%-damped elastic spectral acceleration response of the base excitation. (The damping ratios were calculated using the Caltech software MODE-ID, see e.g., Beck 1978) The triangles represent the damping ratios calculated from these 16 records. The solid line is a regression line fit to the data. One could reasonably call the levels of excitation in the figure "pre-yield," i.e., having little if any contribution from hysteretic energy dissipation that would be calculated in a structural model. The zero-intercept—here, 10%—is a reasonable estimate of the elastic damping ratio, to which one can later add hysteretic energy dissipation during the structural analysis.

A mean viscous damping ratio of 10% for woodframe buildings is not out of line with other authors' estimates: Newmark and Hall (1982, pg 54) suggest 15-20% for wood structures with nailed joints at or just below the yield point. The HAZUS developers (NIBS and FEMA 2003 pg 5-68) adopt Newmark and Hall (1982) for these ratios. Camelo et al. cite a number of authors who estimate woodframe damping ratios from cyclic and static load tests. For example, 13 to 27% (Seo et al. 1981), 1.4 to 2.4% (Hirashima 1988), 4 to 9% (Yokel et al. 1973).

Regarding the uncertainty in viscous damping, consider again the Camelo et al. (2001) data shown in Figure A2-1. The logarithmic standard deviation of the residual (which measures the variability of the data about the regression line) is approximately 0.3. To this logarithmic standard deviation is added (actually SRSS'd) an additional logarithmic standard deviation of 0.3 to account for variability in damping ratio between competing system-ID methods, yielding a total coefficient of variation of 0.4 (i.e., $0.3^2 + 0.3^2 \approx 0.4^2$). This additional logarithmic standard deviation is calculated by comparing the damping ratios for 26 records analyzed by both McVerry (1979) and Hart and Vasdevan (1975); additional detail can be provided.

Regarding the form of the distribution used for the viscous damping ratio, it was hypothesized that a lognormal cumulative distribution function could be used to idealize the distribution. From information-theory principles, given a variable that must take on a positive value, and given a median and a measure of uncertainty (here, the logarithmic standard deviation), the lognormal imposes the least information (i.e., maximizes uncertainty, or makes the least "assumptions" about the data). In addition to this information-theory justification for the lognormal, the Lilliefors (1963) goodness-of-fit test was performed on the Camelo et al. (2001) data to check how well the residual actually matched the lognormal (more precisely, how well the natural logarithm of the residual matched the normal distribution). The data passed the test at the 5% significance level, meaning that the lognormal distribution adequately fits the Camelo et al. (2001) data. (Lilliefors is a stricter version of the Kolmogorov-Smirnov goodness-of-fit test,

appropriate where the data are used to calculate the parameters of the distribution being fit. If an idealized distribution passes the Lilliefors test, it passes the K-S test as well.)

Regarding the selection of 5% and 18% as the lower- and upper bounds of the distribution of damping ratio, these values come from calculating the 4^{th} and 96^{th} percentiles of the lognormal distribution with median of 10% and a logarithmic standard deviation of 0.4, i.e., roughly median ± sqrt(3) standard deviation bounds.

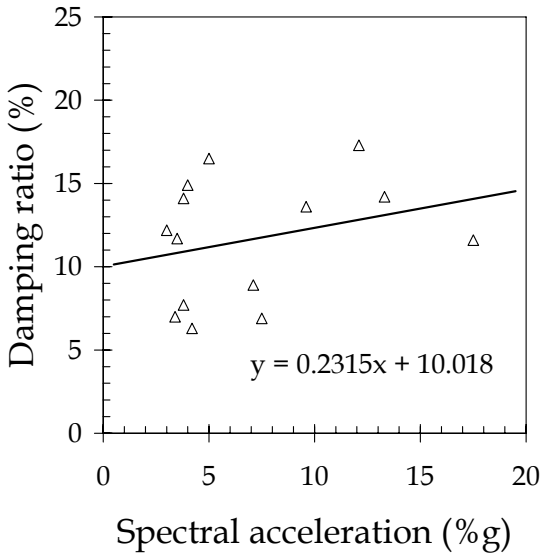

Figure A2-1. Damping ratio calculated from system-ID analysis of 16 earthquake records in woodframe buildings (data taken from Camelo et al. 2001).

APPENDIX 3: DETAILED DISCUSSION OF MOMENT MATCHING

The accuracy and superiority of moment matching are demonstrated in Rosenblueth (1975), Julier and Uhlman (2002), and recent work by Ching et al. (2004), and the reader is referred to these publications for detailed discussion. Ching et al. (2004) is the longest and most detailed of these publications, presenting moment matching's mathematical basis as well as a number of illustrations of general mathematical problems as well as performance-based earthquake engineering problems, and unlike the other two references compare moment matching with Monte Carlo simulation and another method called first-order-second-moment (FOSM).

Two simple mathematical problems are shown in Figure A3-1. Imagine a function Y that depends only on one variable, X. In this case, X is normally distributed with mean of 0 and standard deviation of 1.0. In the left-hand pair of figures, $Y = X^2$; in the right, $Y = X^4$. The upper figures show how well the various methods estimate the mean of Y; the lower, variance. In both problems, one generally has to generate 1,000 to 10,000 samples of X and calculate Y for each sample, to be fairly confident of being within 5 to 10% of the true mean and variance of Y, compared with 5 samples using moment matching (the red line). (The reader can ignore the blue "FOSM" lines.)

Ching et al. (2004) show that the estimates of drift provided here using moment matching are equivalent to a 5^{th}-order Taylor-series expansion of drift and a 2nd-order Taylor-series expansion of the variance of drift, while requiring only $2n+1$ simulations, where n is the number of random variables being simulated. (More samples of each variable can be used for arbitrarily greater accuracy.) We treat 4 random variables (rise time, rupture velocity, damping and a combined factor for member strengths and stiffnesses), requiring nine simulations per house and gridpoint. The reader will get a better sense of the superiority of moment matching over Monte Carlo by noting in Figure A3-1 how well Monte Carlo performs with 10 or even 100 simulations and just one basic random variable.

Each simulation—whether by Monte Carlo or moment matching—requires a nonlinear time-history structural analysis for 70 seconds of input ground motion. We are analyzing seven index houses at each of 648 gridpoints (five initial designs plus two added recently to address concerns about how well trends in drift in these sample index buildings match loss trends in general populations of houses). The initial calculations for the first house employed 2 orientations of the building. Thus the total computational effort using moment matching is therefore 648 x 9 x 2 + 6 x 649 x 9 = 47,000 nonlinear time-history structural analyses, requiring roughly 500 hours—20 days—of dedicated computer time. Since the accuracy achieved in the mean and variance of drift (and later, loss) is probably greater than Monte Carlo simulation with 10 times the number of simulations, moment matching appears to be not simply superior, but of the two approaches the only practical way to estimate mean and variance of drift and loss with any degree of confidence.

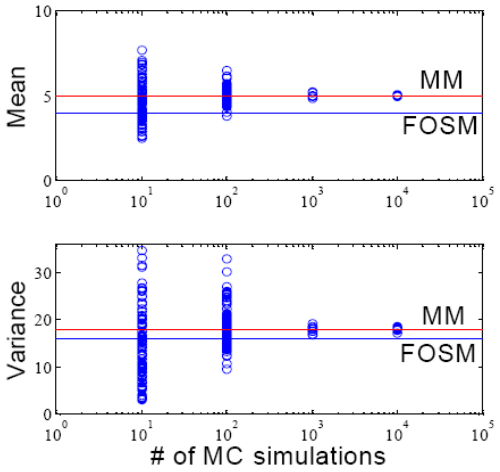

Figure 3-4. Estimation result for $Y=X^2$

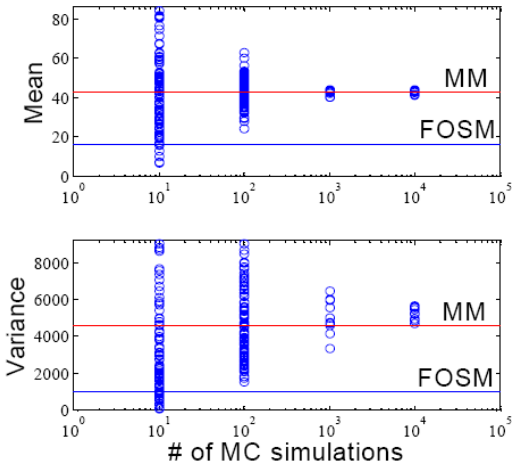

Figure 3-5. Estimation result for $Y=X^4$

Figure A3-1. Two illustrations of how quickly moment matching converges relative to Monte Carlo simulation. Each blue circle is an estimate of the mean or variance of the function $Y = X^2$ or $Y = X^4$, where X is a Gaussian random variable with mean = 0 and standard deviation = 1.0. Each circle employs between 100 and 10,000 simulations of X and Y. MM refers to the moment-matching estimate using 5 samples. FOSM refers to first-order-second-moment. Moment matching is not limited to Gaussian random variables (neither is Monte Carlo).

APPENDIX 4: MAPS OF WORST-WALL 1ST-STORY DRIFT

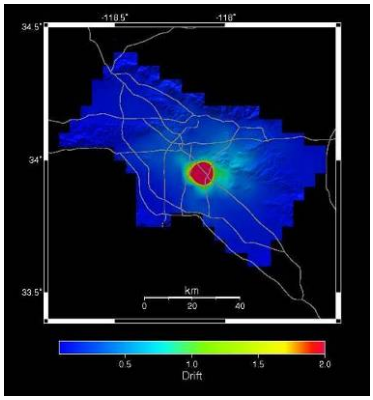

Low rupture velocity

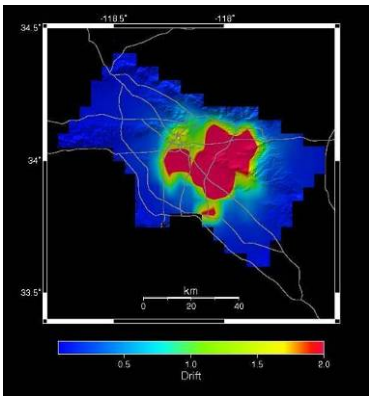

Low rise time

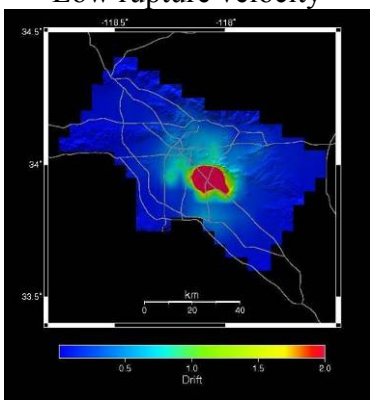

Nominal values

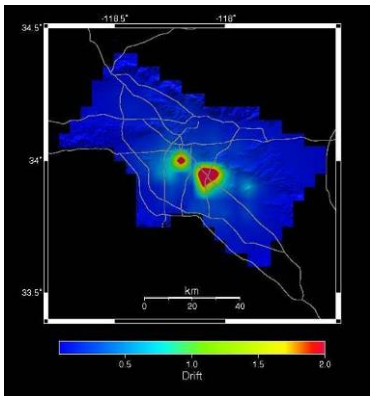

High rise time

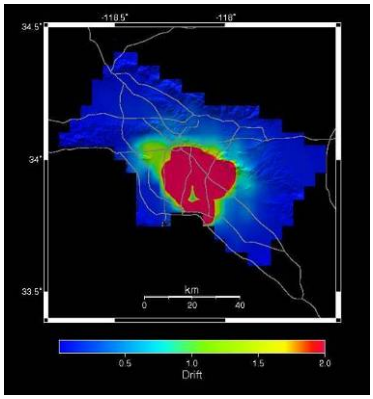

High rupture velocity

Figure A4-1. Peak drift, in., 1940s-1950s index building, worst wall, 0° X-axis

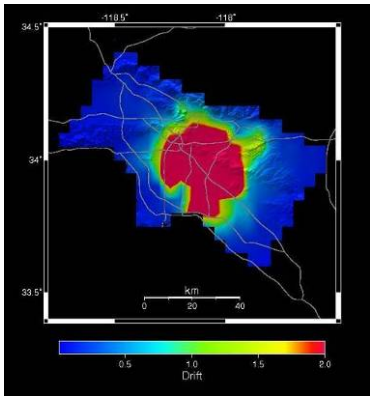

Low strength and stiffness

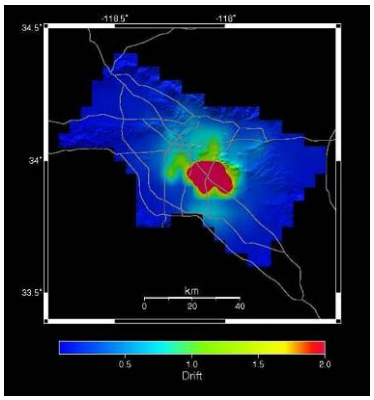

Low damping

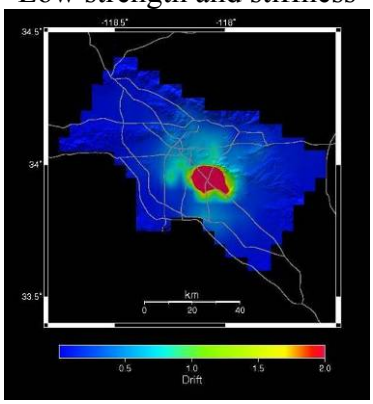

Nominal values

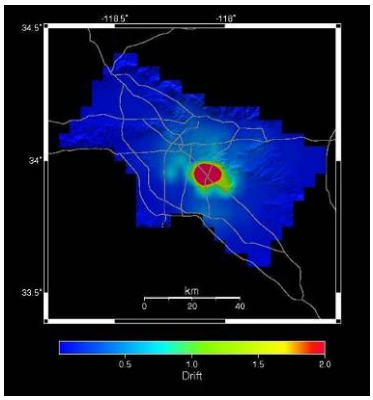

High damping

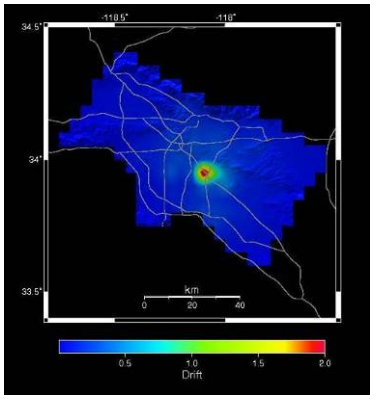

High strength and stiffness

Figure A4-1 (cont). Peak drift, in., 1940s-1950s index building, worst wall, 0° X-axis

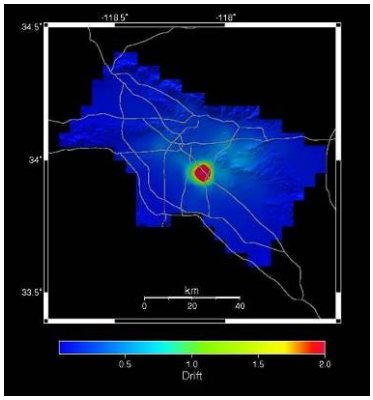

Low rupture velocity

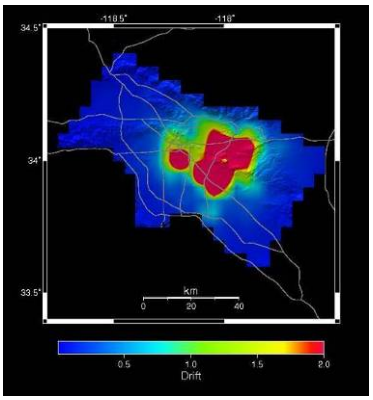

Low rise time

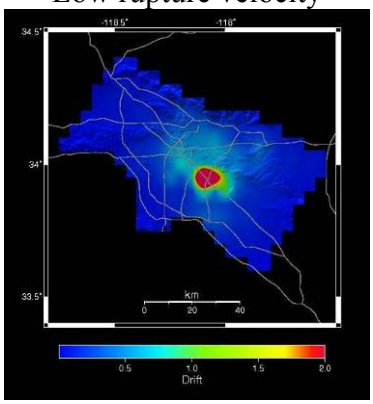

Nominal values

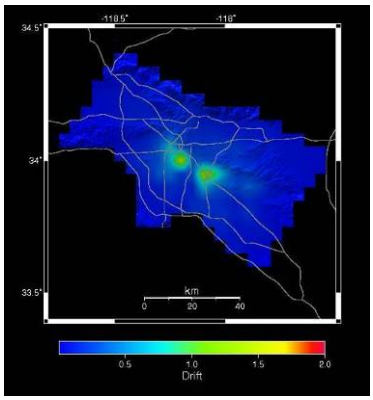

High rise time

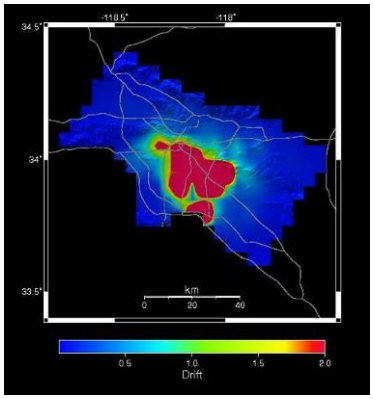

High rupture velocity

Figure A4-1 (cont). Peak drift, in., 1940-1950s index building, worst wall, 90° X-axis

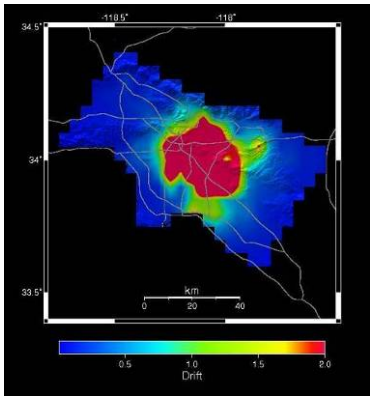

Low strength and stiffness

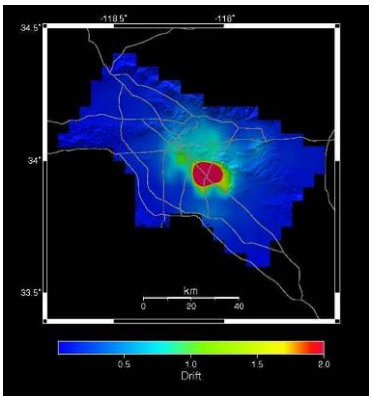

Low damping

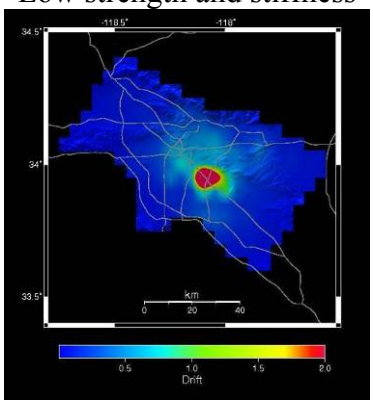

Nominal values

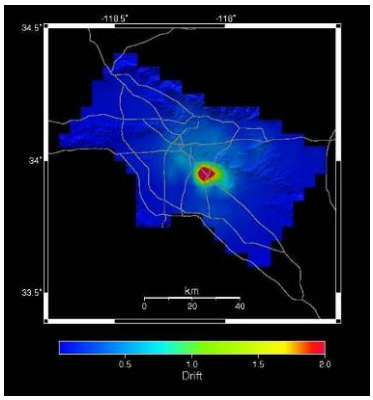

High damping

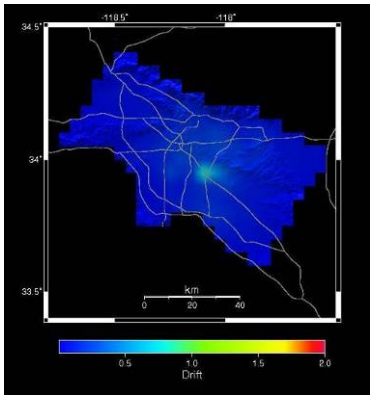

High strength and stiffness

Figure A4-1 (cont). Peak drift, in., 1940-1950s index building, worst wall, 90° X-axis

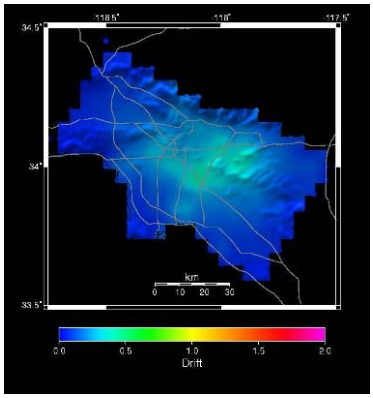

Low rupture velocity

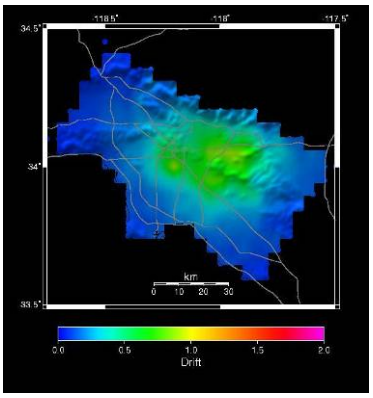

Low rise time

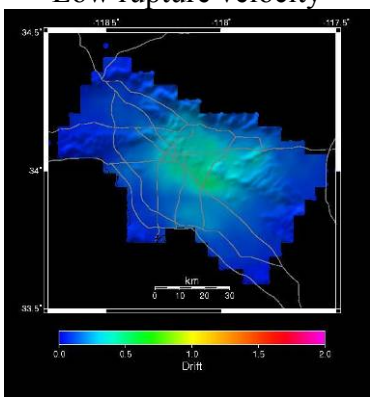

Nominal values

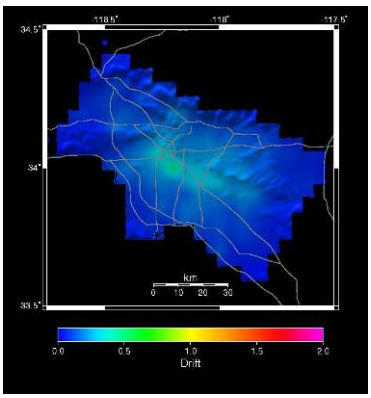

High rise time

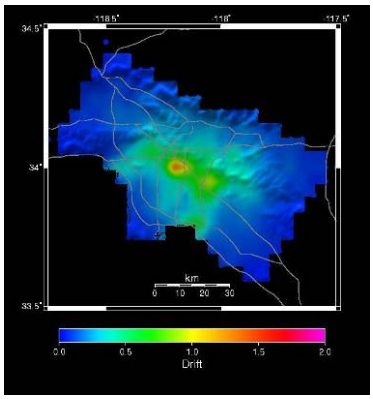

High rupture velocity

Figure A4-2. Peak transient drift, in., 1960s 1-story building ("1960a"), worst wall

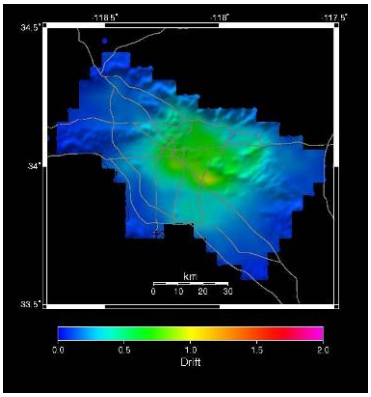

Low strength and stiffness

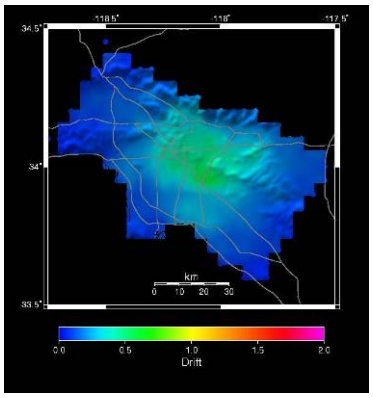

Low damping

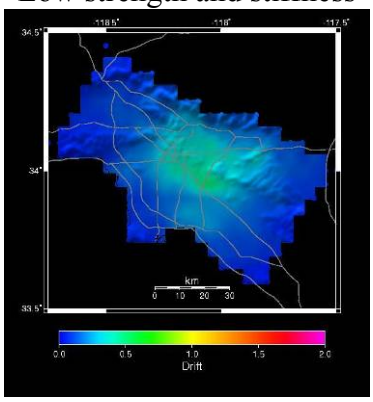

Nominal values

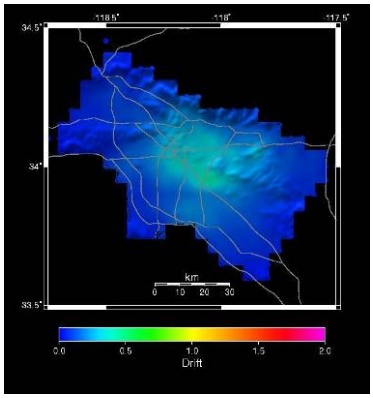

High damping

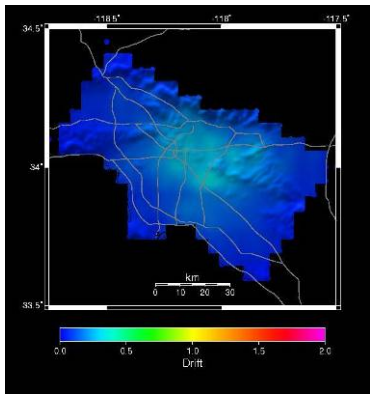

High strength and stiffness

Figure A4-2 (cont.). Peak drift, in., 1960s 1-story building ("1960a"), worst wall

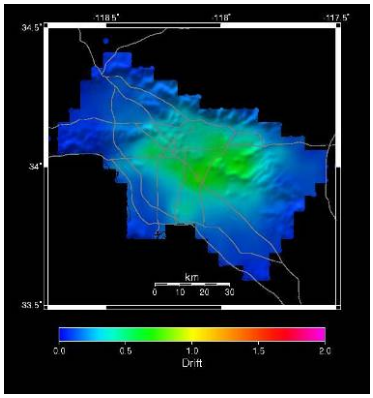

Low rupture velocity

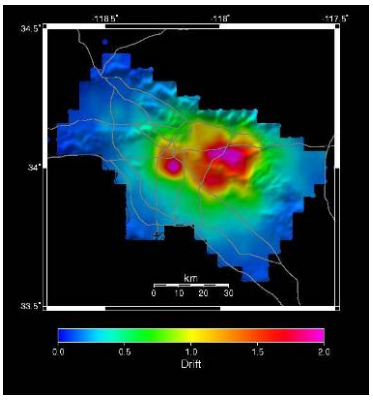

Low rise time

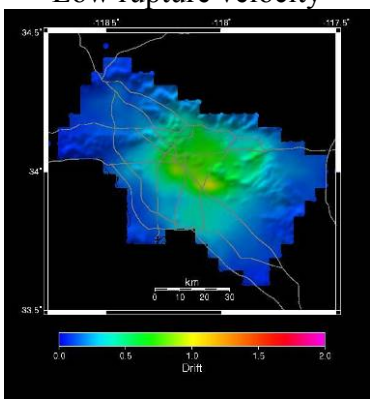

Nominal values

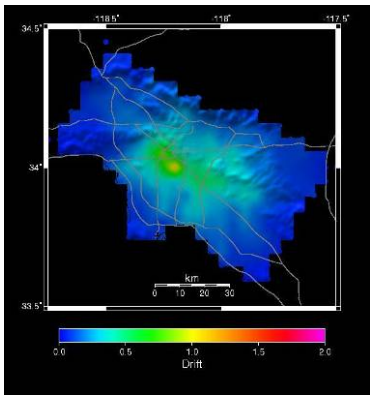

High rise time

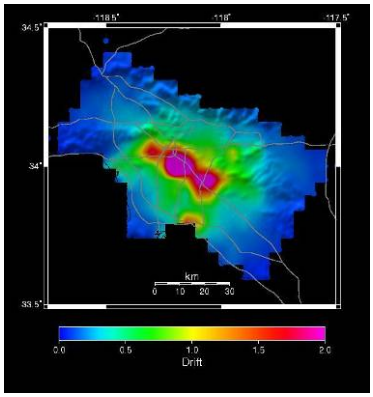

High rupture velocity

Figure A4-3. Peak 1st-story drift, in., 1960s 2-story building ("1960b"), worst wall

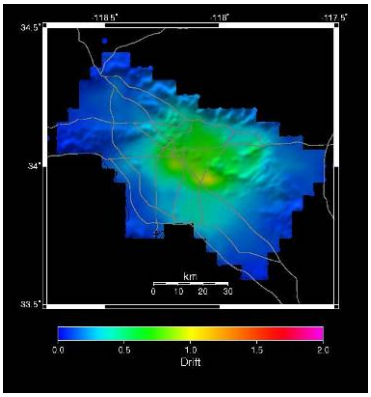

Low strength and stiffness

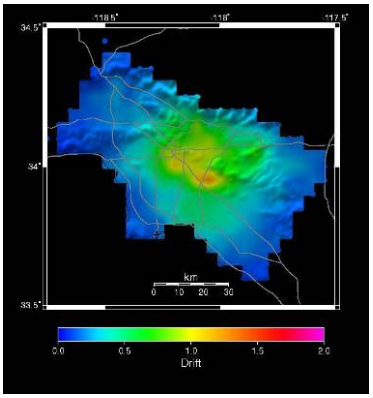

Low damping

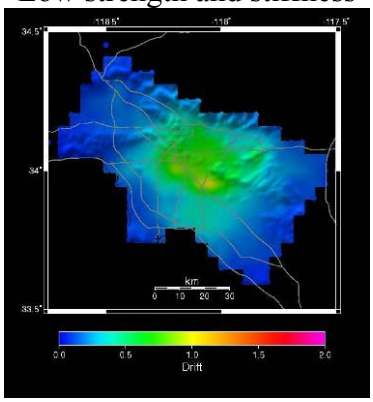

Nominal values

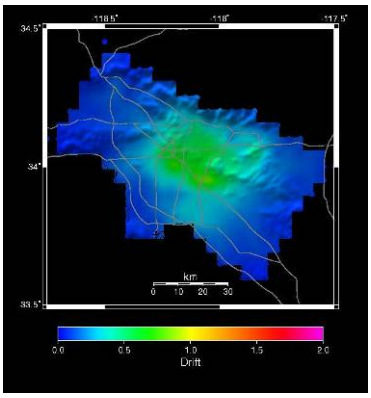

High damping

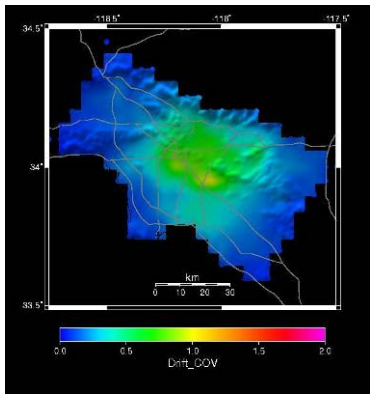

High strength and stiffness

Figure A4-3 (cont). Peak 1st-story drift, in., 1960-1970s 2-story building ("1960b"), worst wall

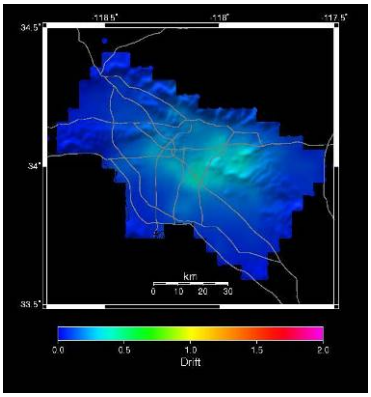

Low rupture velocity

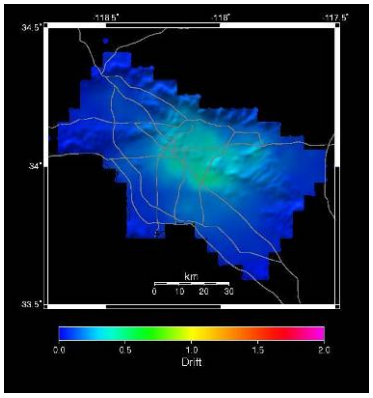

Low rise time

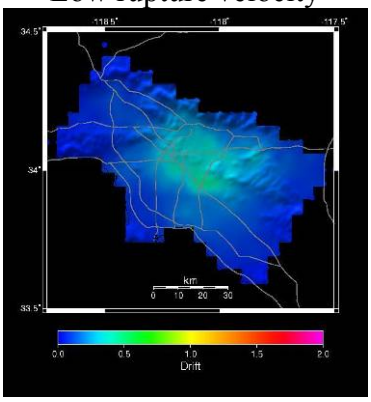

Nominal values

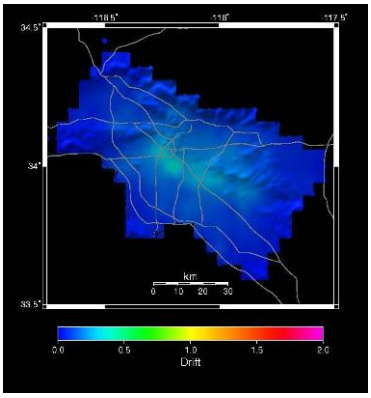

High rise time

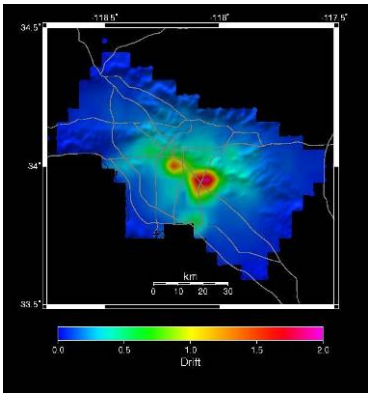

High rupture velocity

Figure A4-4. Worst-wall 1st-story drift, in., 1960s 2-story building with T1-11 ("1960d")

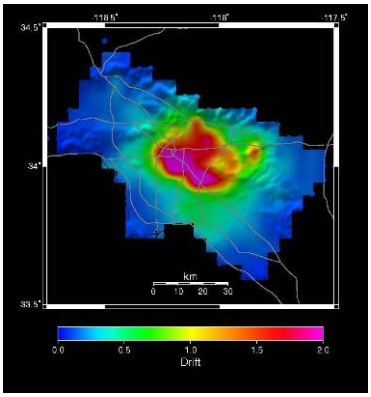

Low strength and stiffness

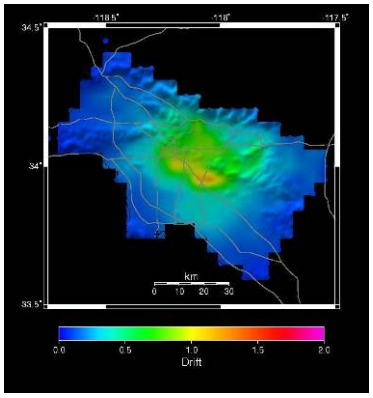

Low damping

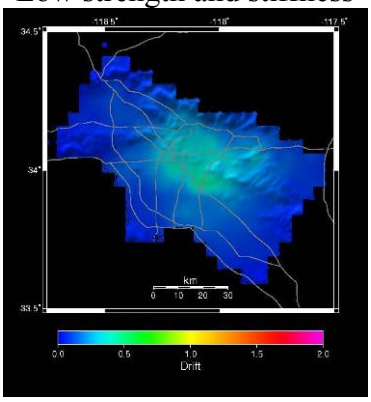

Nominal values

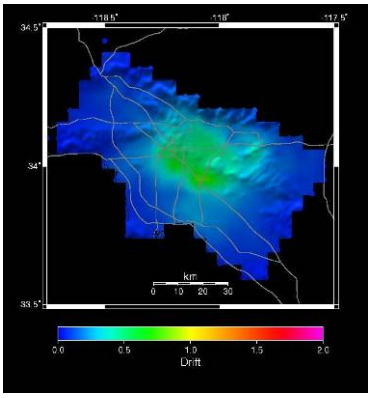

High damping

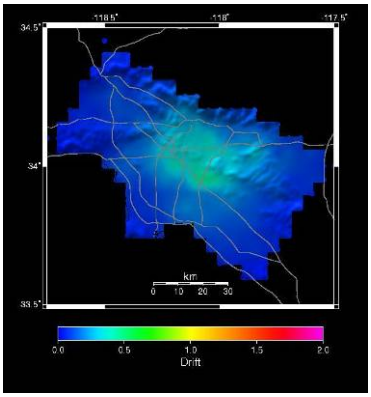

High strength and stiffness

Figure A4-4 (cont). Worst-wall 1st-story drift, in., 1960s 2-story with T1-11 ("1960d"),

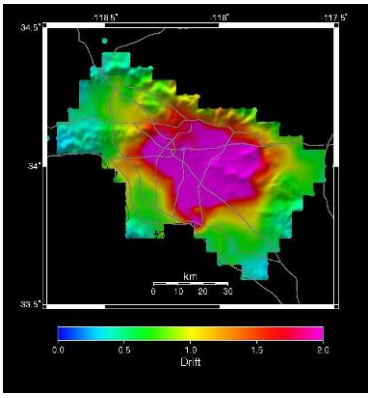

Low rupture velocity

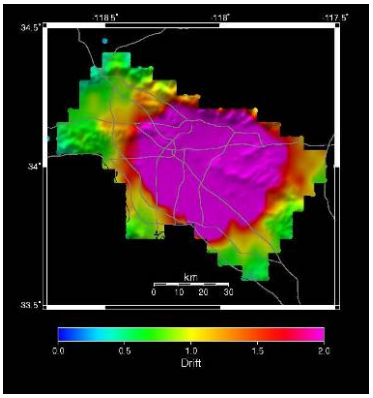

Low rise time

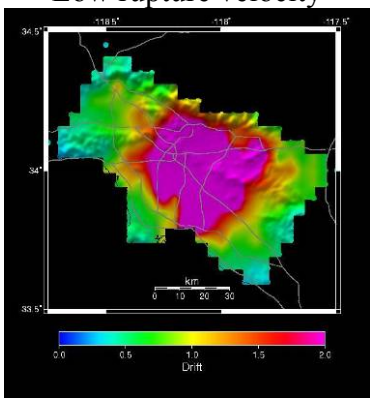

Nominal values

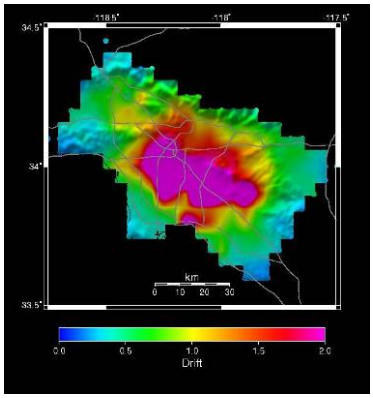

High rise time

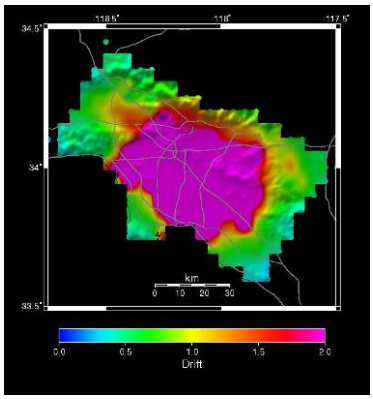

High rupture velocity

Figure A4-5. Peak 1st-story drift, in., 1980s-2000s building, no special seismic detailing ("1980a"), worst wall

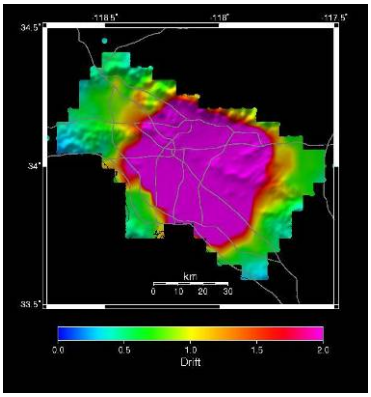

Low strength and stiffness

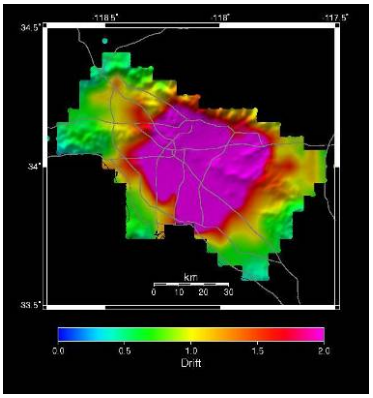

Low damping

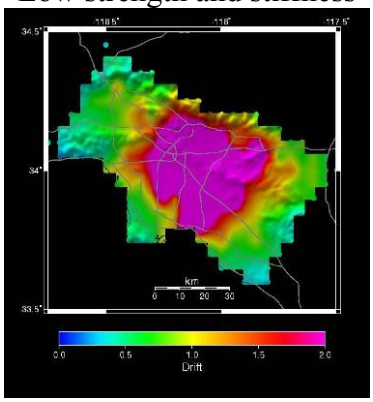

Nominal values

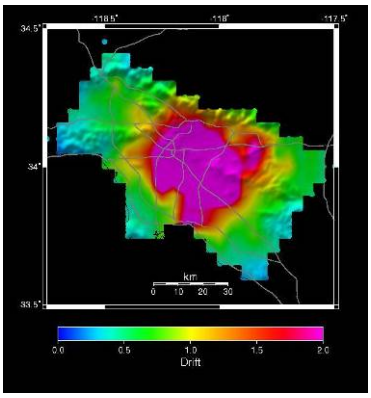

High damping

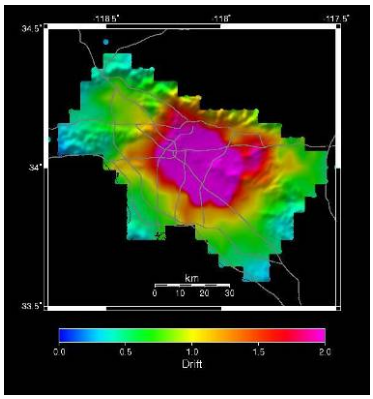

High strength and stiffness

Figure A4-5 (cont). Peak 1st-story drift, in., 1980s-2000s index building, no special seismic detailing ("1980a"), worst wall

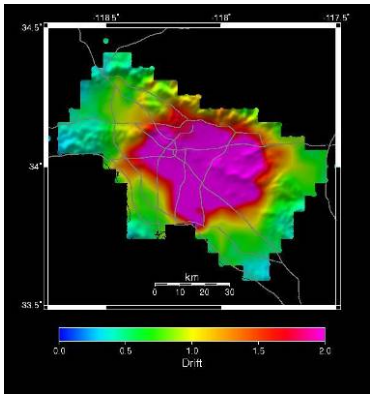

Low rupture velocity

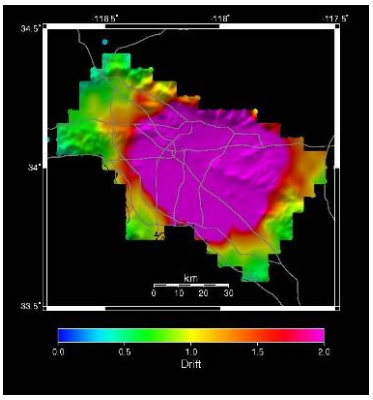

Low rise time

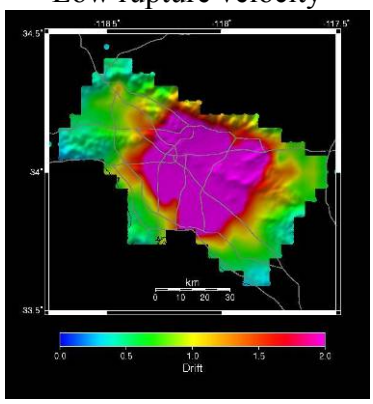

Nominal values

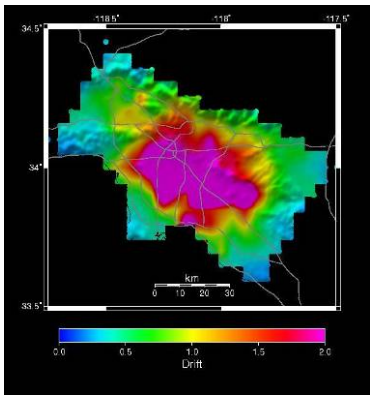

High rise time

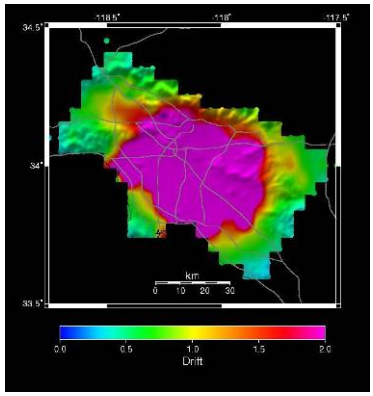

High rupture velocity

Figure A4-6. Peak transient 1st-story drift, inches, 1980-2000 index building with special seismic detailing ("1980b"), worst wall

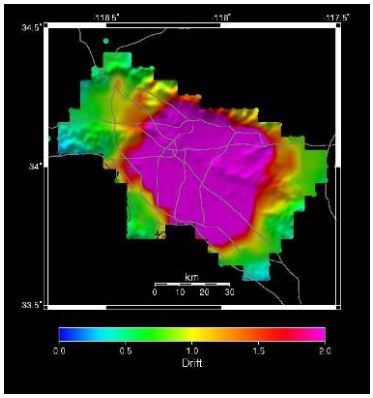

Low strength and stiffness

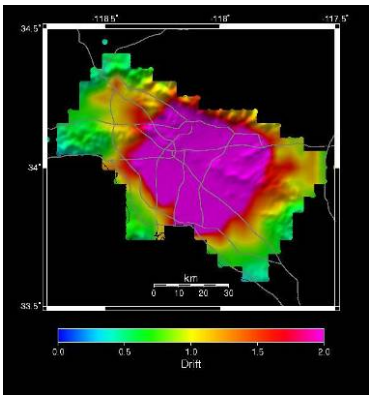

Low damping

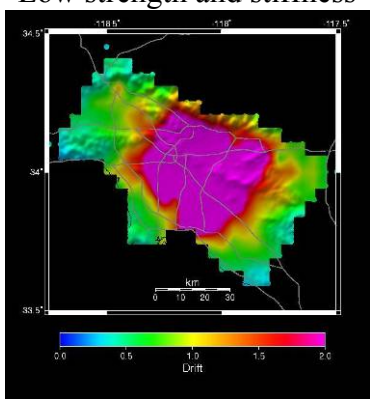

Nominal values

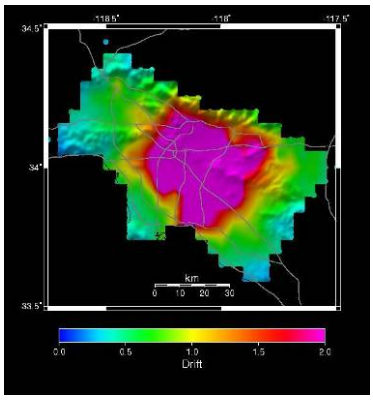

High damping

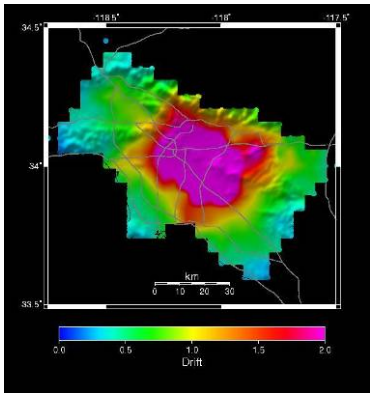

High strength and stiffness

Figure A4-6 (cont). Peak transient 1st-story drift, inches, 1980-2000 index building with special seismic detailing ("1980b"), worst wall

APPENDIX 5: MAPS OF AVERAGE-WALL 1ST-STORY DRIFT

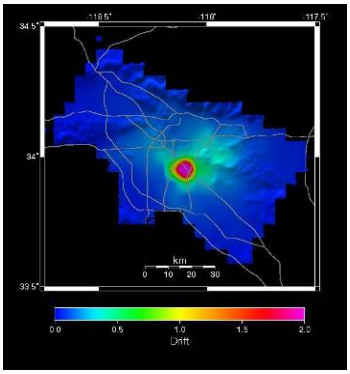

Low rupture velocity

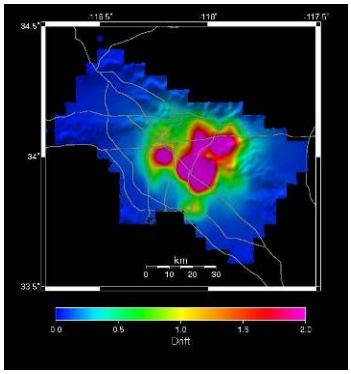

Low rise time

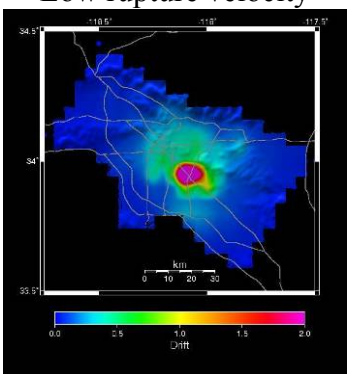

Nominal values

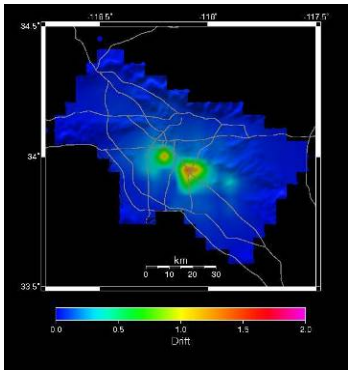

High rise time

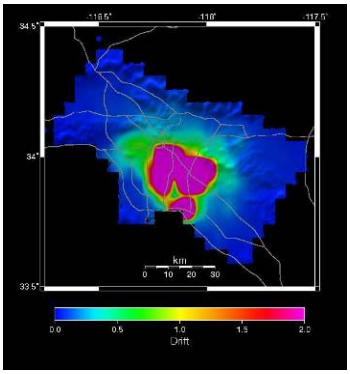

High rupture velocity

Figure A5-1. 1940s-1950s house average-wall 1st story drift simulations

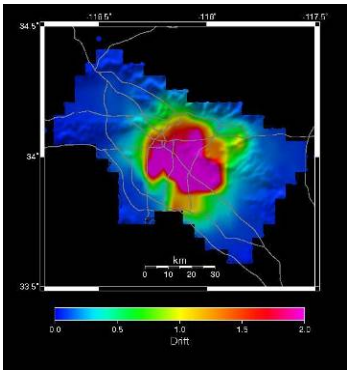

Low strength and stiffness

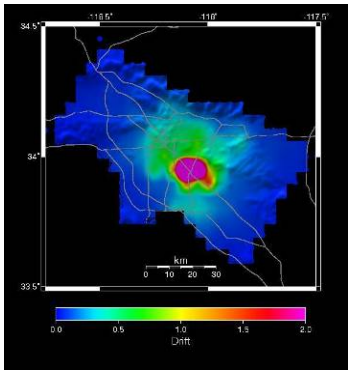

Low damping

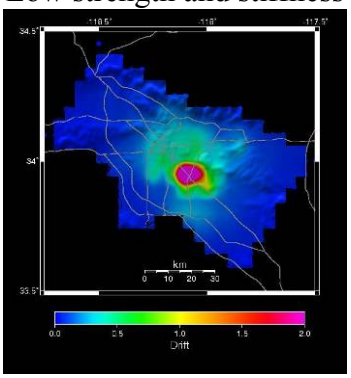

Nominal values

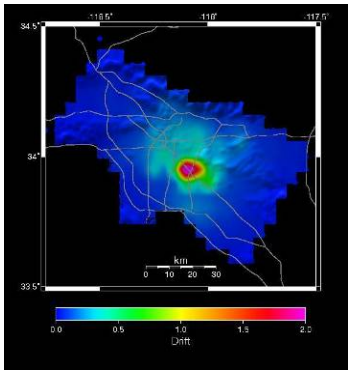

High damping

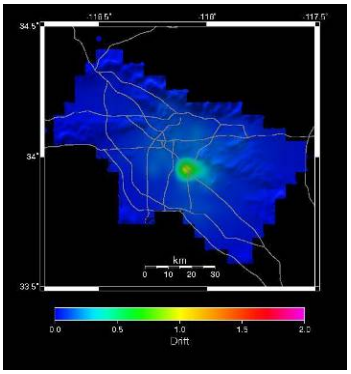

High strength and stiffness

Figure A5-1 (cont). 1940s-1950s house average-wall 1st story drift simulations

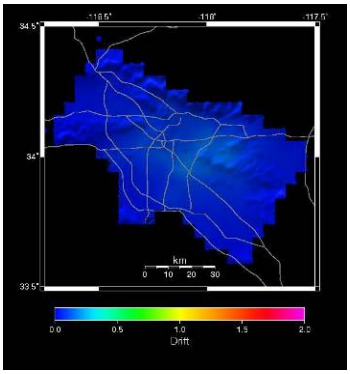

Low rupture velocity

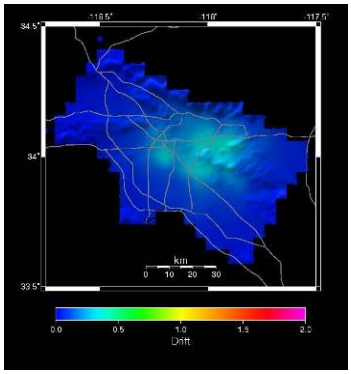

Low rise time

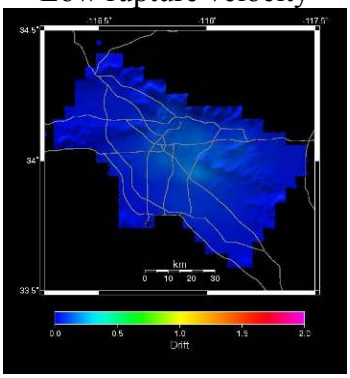

Nominal values

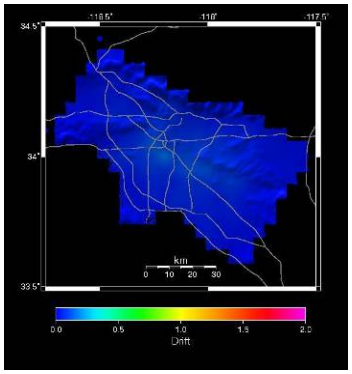

High rise time

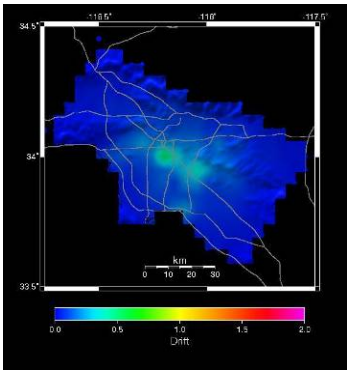

High rupture velocity

Figure A5-2. 1960a house average-wall 1st story drift simulations

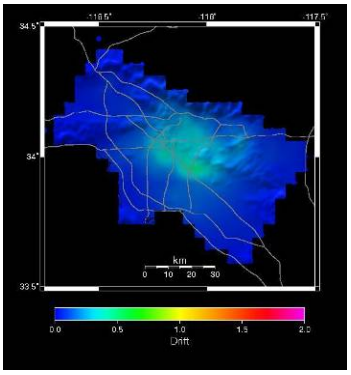

Low strength and stiffness

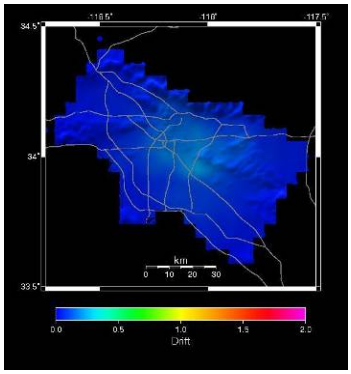

Low damping

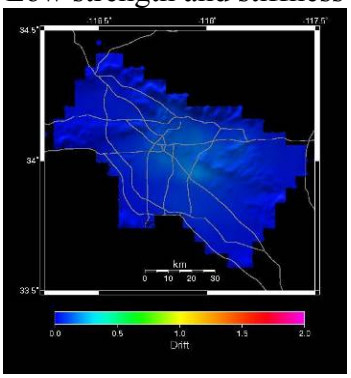

Nominal values

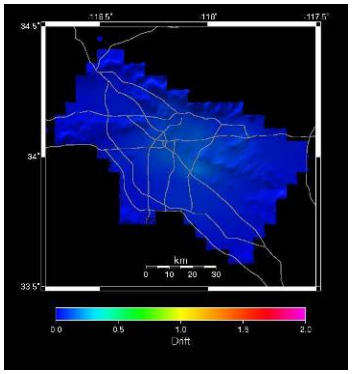

High damping

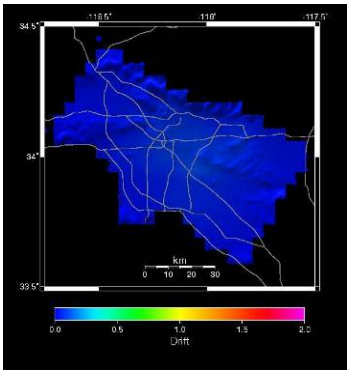

High strength and stiffness

Figure A5-2 (cont). 1960a house average-wall 1st story drift simulations

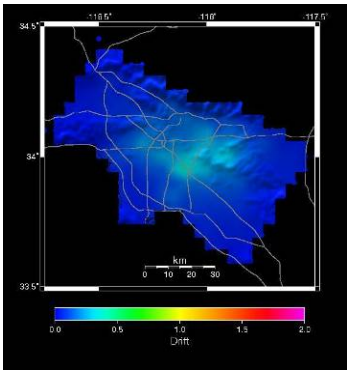

Low rupture velocity

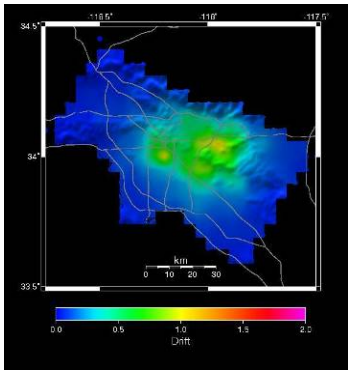

Low rise time

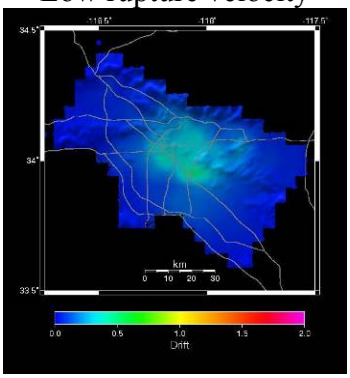

Nominal values

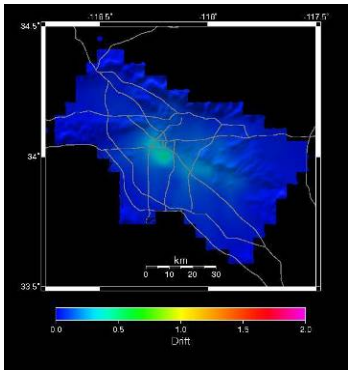

High rise time

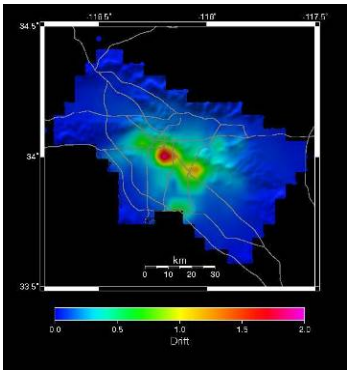

High rupture velocity

Figure A5-3. 1960b house average-wall 1st story drift simulations

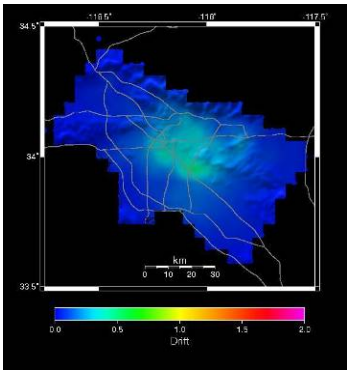

Low strength and stiffness

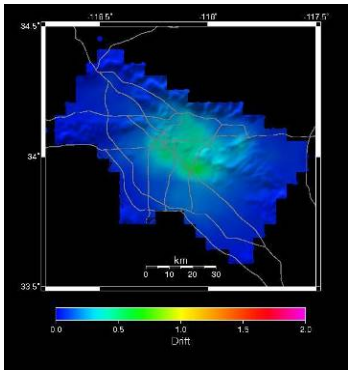

Low damping

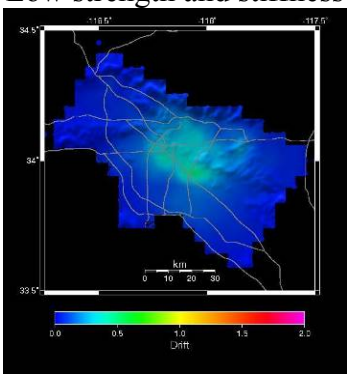

Nominal values

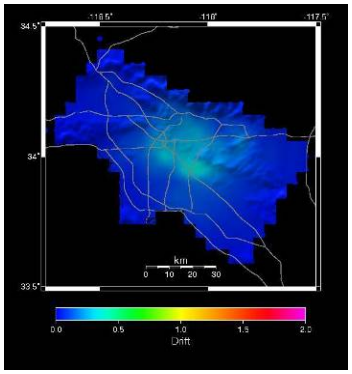

High damping

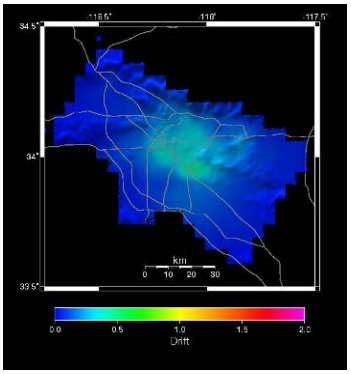

High strength and stiffness

Figure A5-3 (cont). 1960b house average-wall 1st story drift simulations

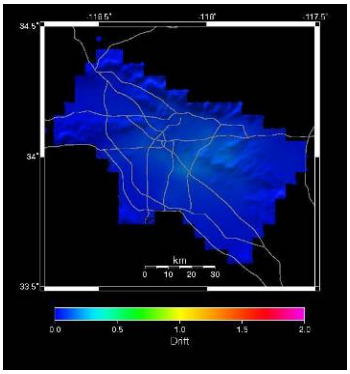

Low rupture velocity

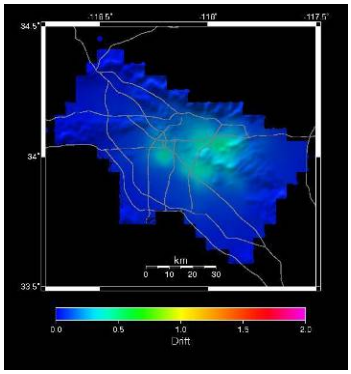

Low rise time

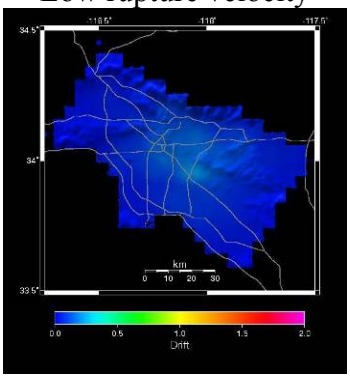

Nominal values

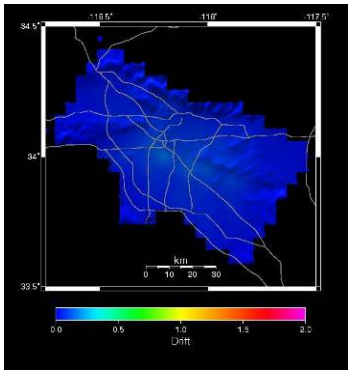

High rise time

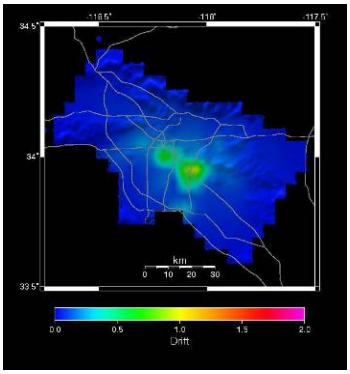

High rupture velocity

Figure A5-4. 1960d house average-wall 1st story drift simulations

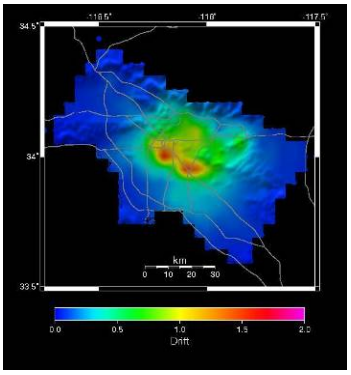

Low strength and stiffness

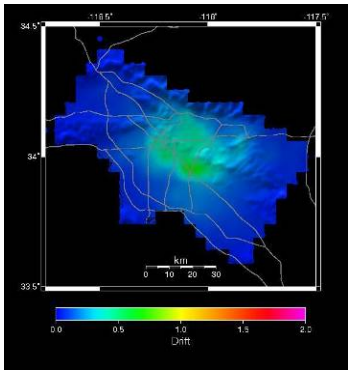

Low damping

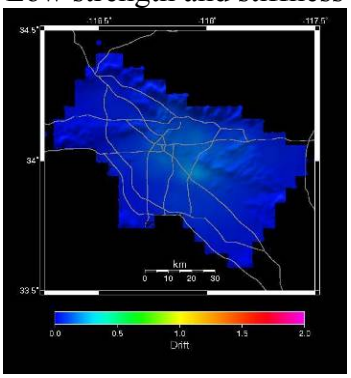

Nominal values

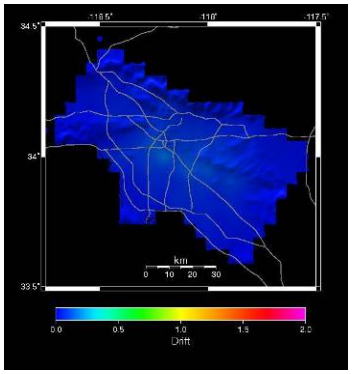

High damping

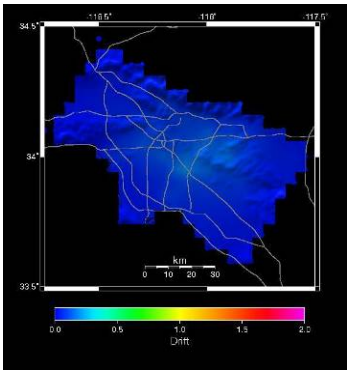

High strength and stiffness

Figure A5-4 (cont). 1960d house average-wall 1st story drift simulations

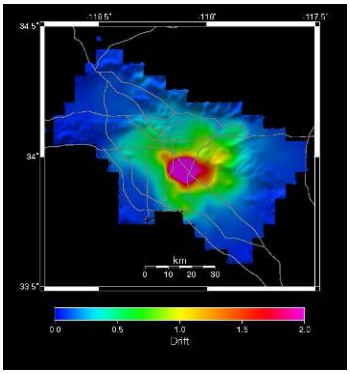

Low rupture velocity

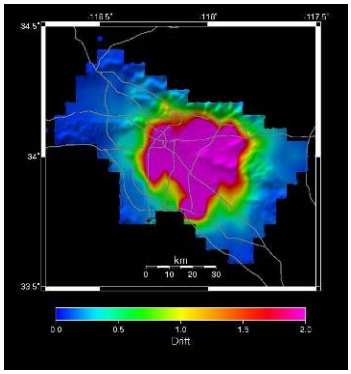

Low rise time

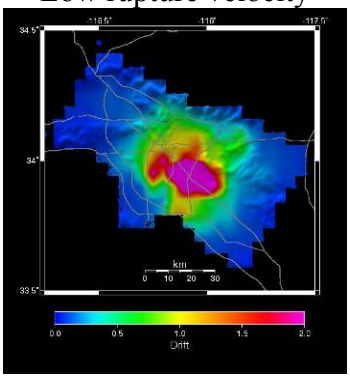

Nominal values

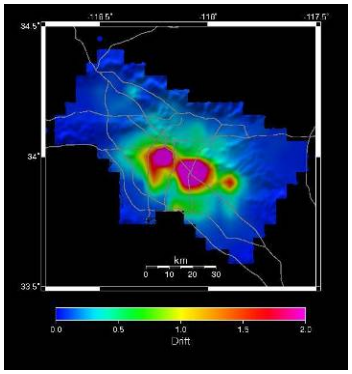

High rise time

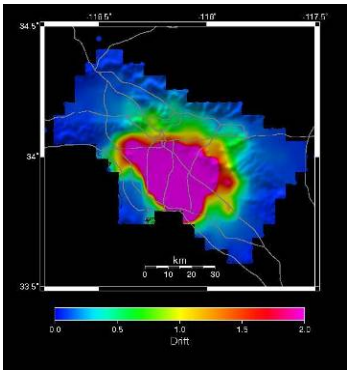

High rupture velocity

Figure A5-5. 1980a house average-wall 1st story drift simulations

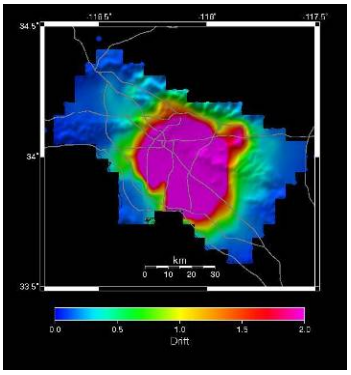

Low strength and stiffness

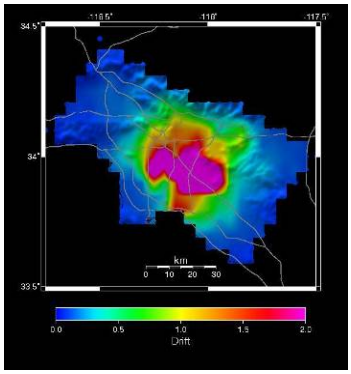

Low damping

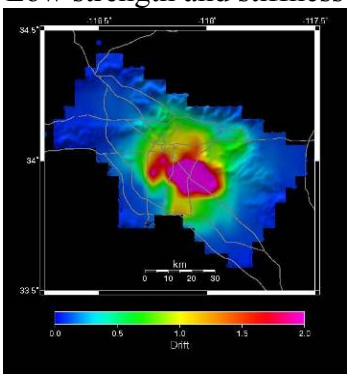

Nominal values

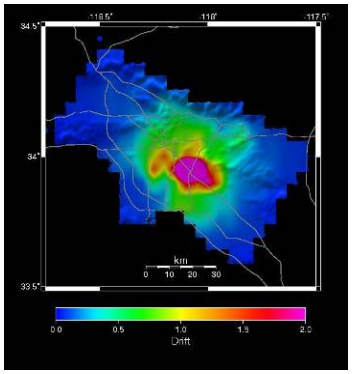

High damping

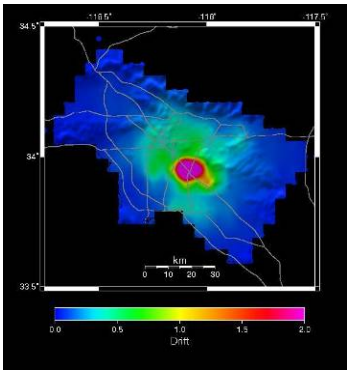

High strength and stiffness

Figure A5-5 (cont). 1980a house average-wall 1st story drift simulations

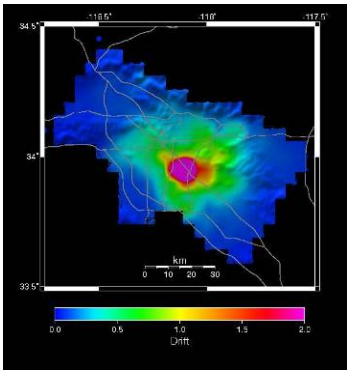

Low rupture velocity

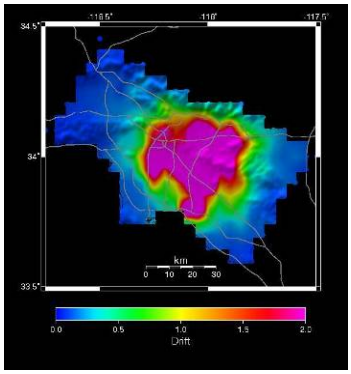

Low rise time

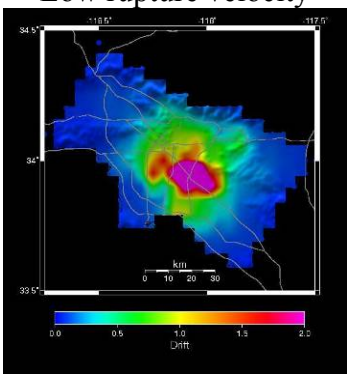

Nominal values

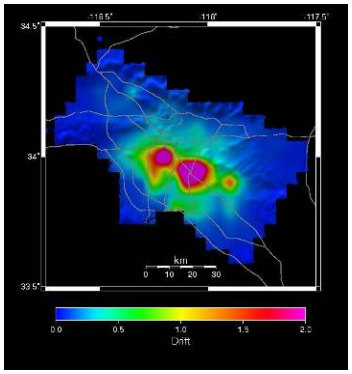

High rise time

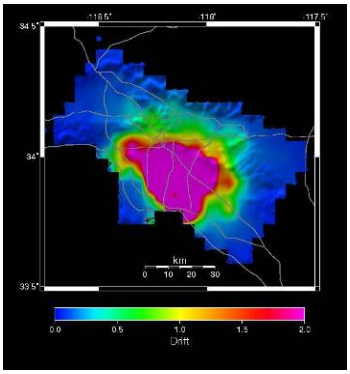

High rupture velocity

Figure A5-6. 1980b house average-wall 1st story drift simulations

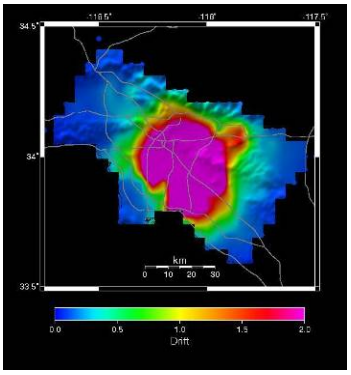

Low strength and stiffness

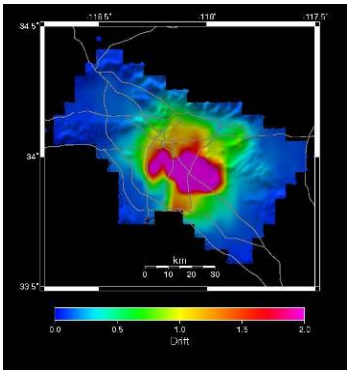

Low damping

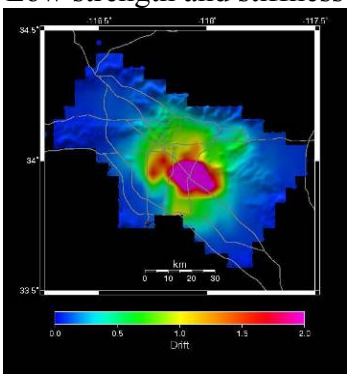

Nominal values

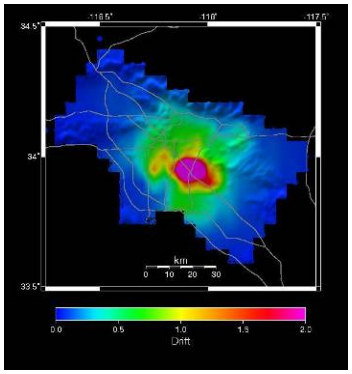

High damping

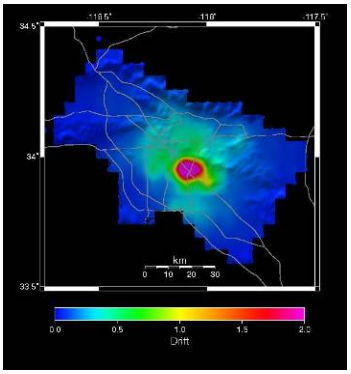

High strength and stiffness

Figure A5-6 (cont). 1980b house average-wall 1st story drift simulations

APPENDIX 6: COMPARISON OF AVERAGE-WALL AND WORST-WALL 1ST-STORY DRIFT

(a) 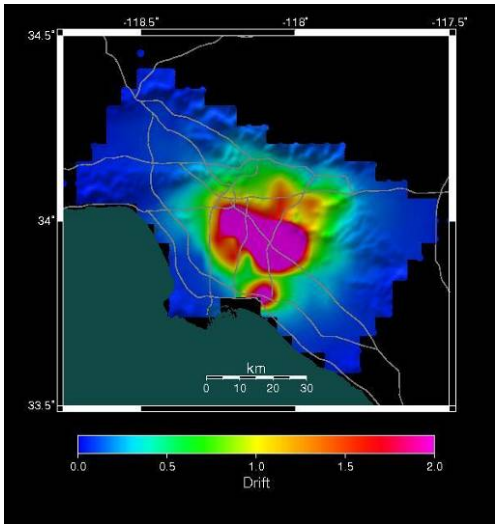

(b) 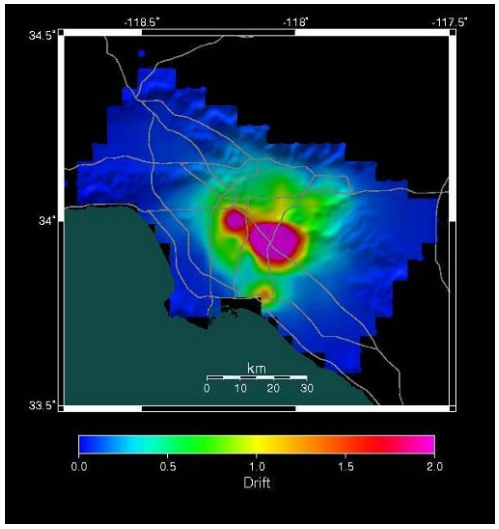

A6-1. Mean drift, in., 1940s-1950s building (a) worst wall; (b) average wall

(a) 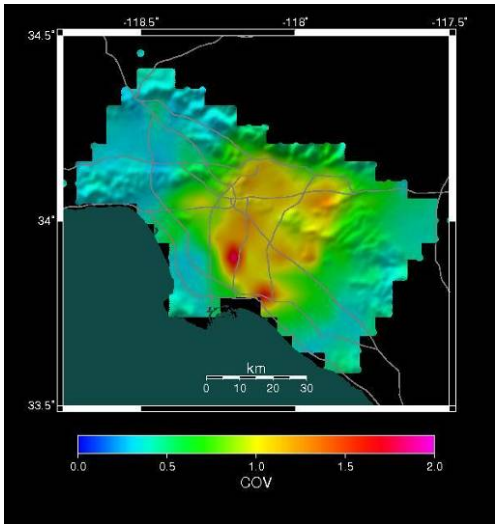

(b) 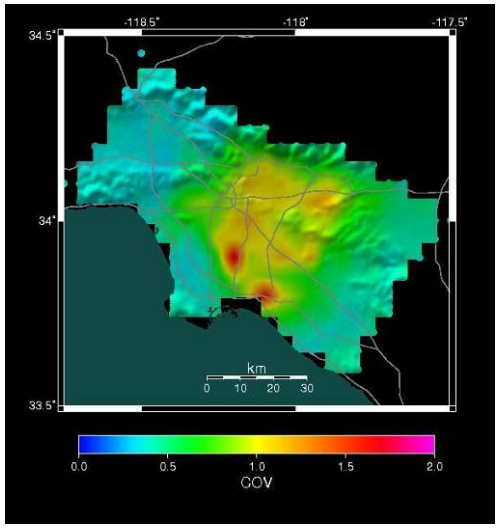

A6-2. Coefficient of variation of drift for 1940s-1950s building (a) worst wall; (b) average wall

(a) 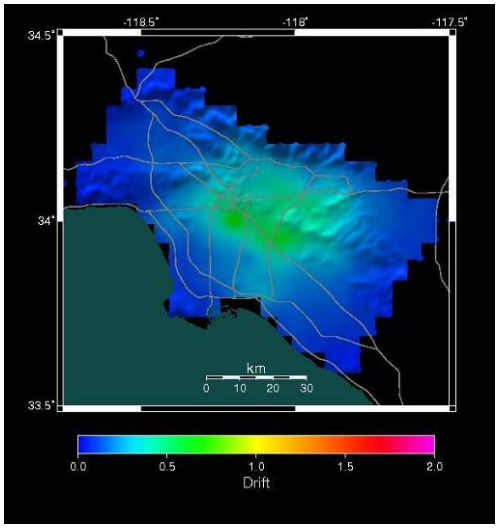

(b) 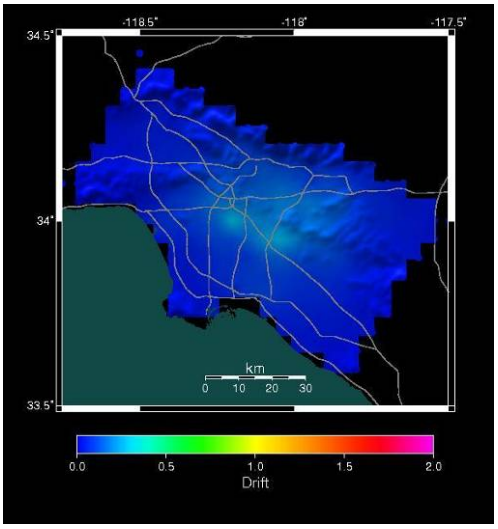

A6-3. Mean drift, in., 1960s 1-story building ("1960a"), (a) worst wall (b) average wall

(a) 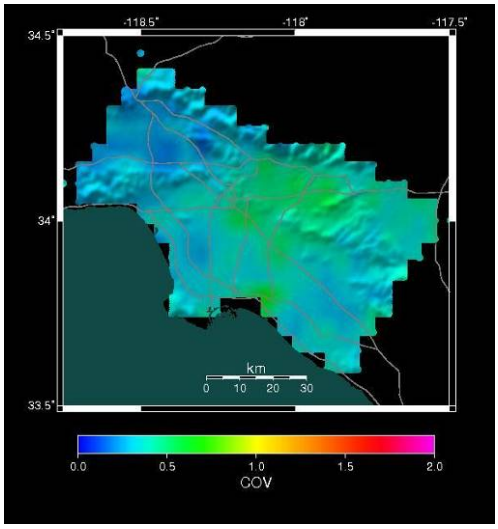

(b) 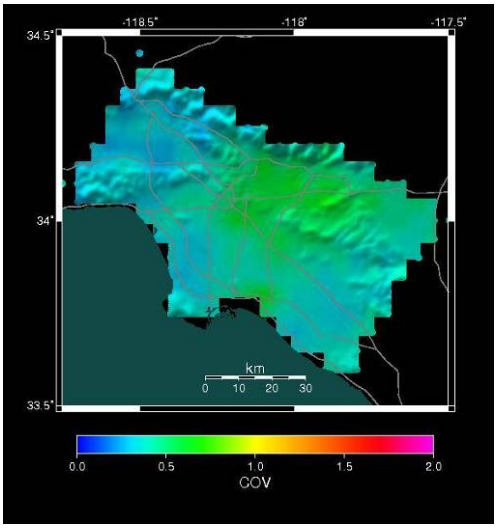

A6-3. Coefficient of variation of drift, 1960s 1-story building ("1960a"), (a) worst wall (b) average wall

(a) 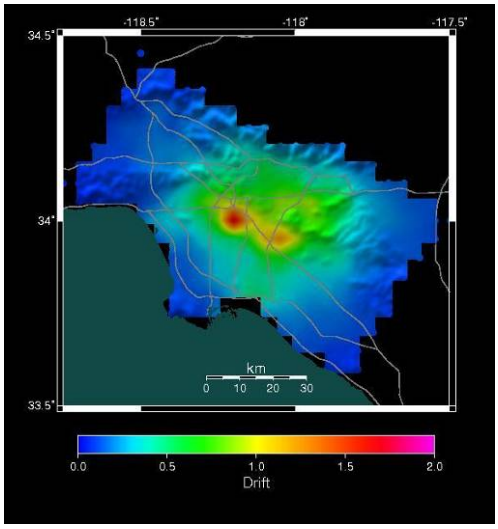

(b) 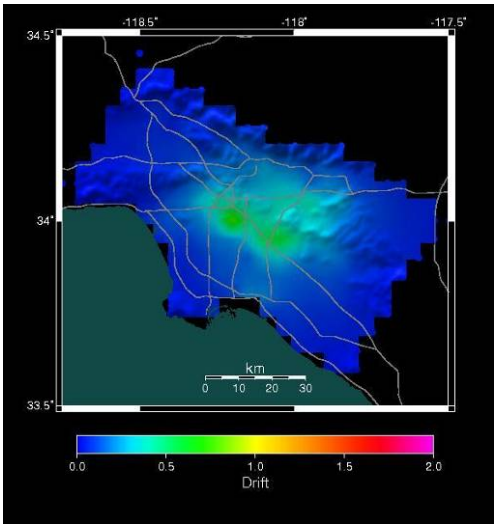

A6-4. Mean transient 1st-story drift, in., 1960s 2-story building ("1960b") (a) worst wall, (b) average wall

(a) 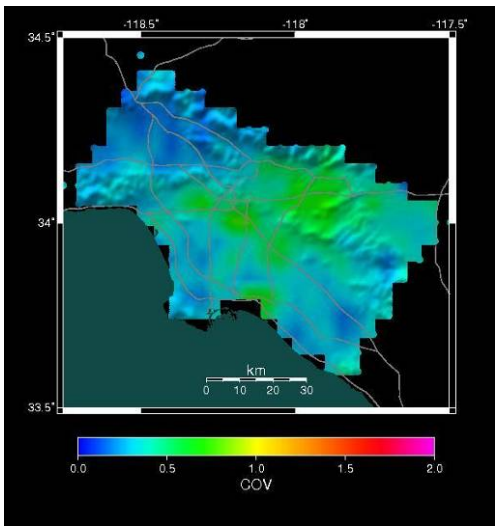

(b) 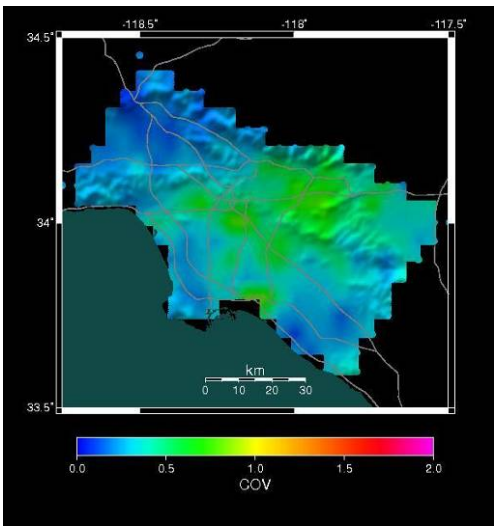

A6-5. Coeff. of variation of 1st-story drift, 2-story 1960s building ("1960b") (a) worst wall, (b) average wall

(a) 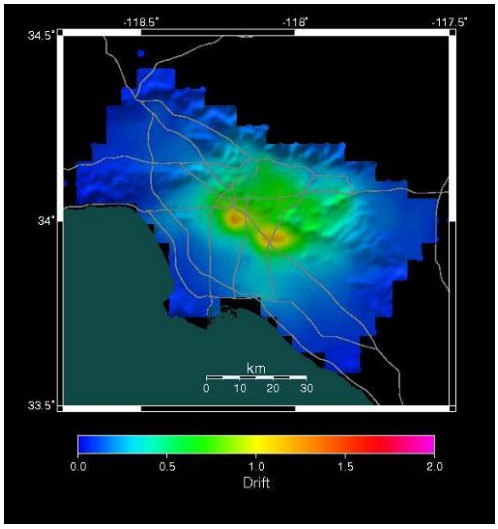

(b) 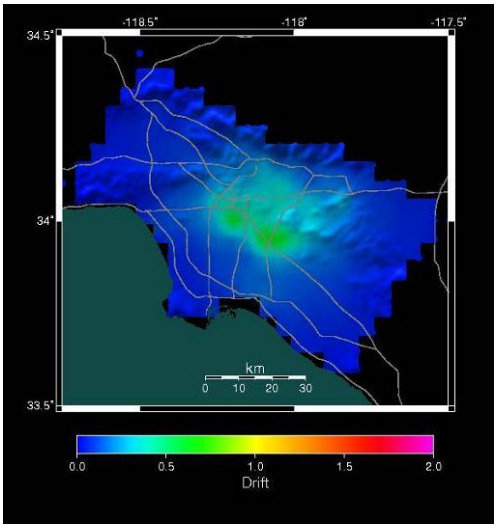

A6-6. Mean transient 1st-story drift, in., 1960s 2-story building with T1-11 and no stucco ("1960d") (a) worst wall, (b) average wall

(a) 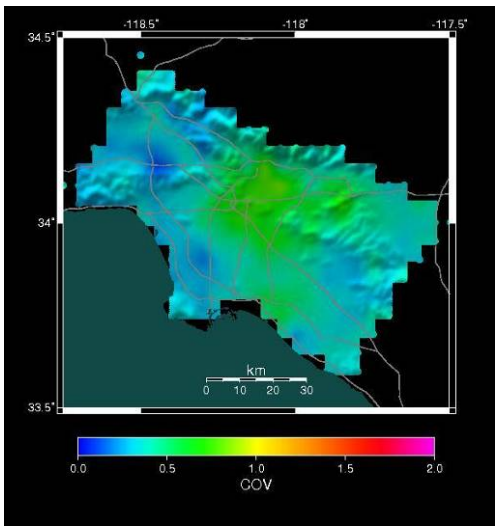

(b) 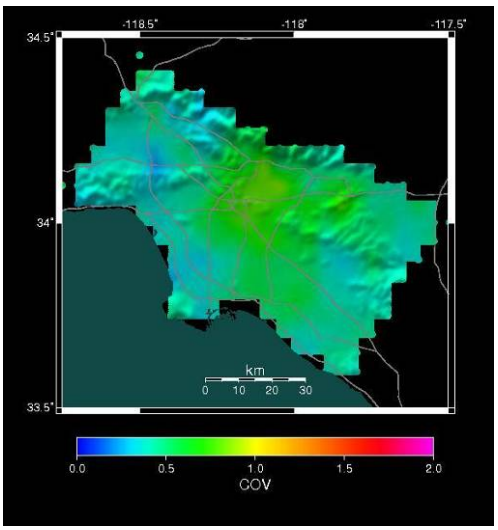

A6-7. Coeff. of variation of 1st-story drift, 1960s 2-story building with T1-11 and no stucco ("1960d") (a) worst wall, (b) average wall

(a) 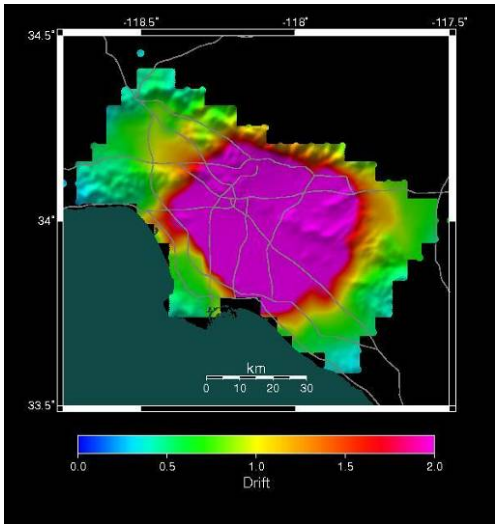

(b) 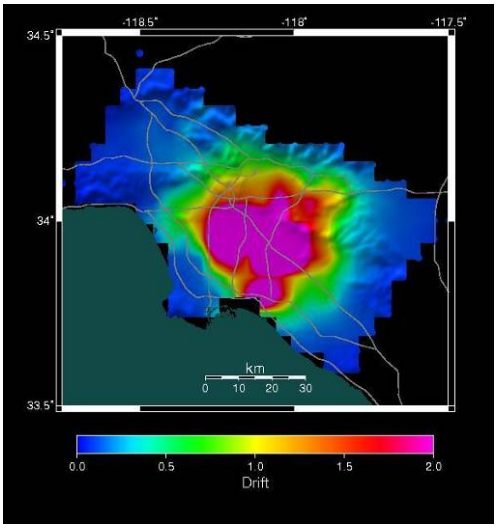

A6-8. Mean transient 1st-story drift, in., 1980-2000s building, no special seismic detailing ("1980a") (a) worst wall, (b) average wall

(a) 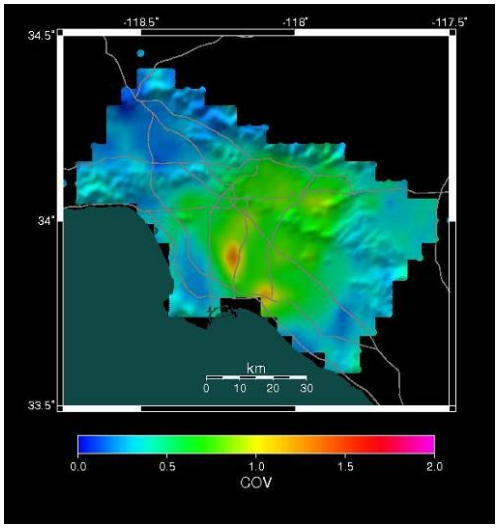

(b) 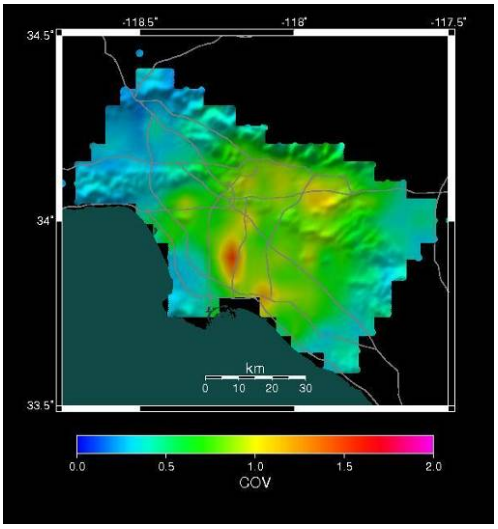

A6-9. Coefficient of variation of transient 1st-story drift for 1980-2000s index building, no special seismic detailing ("1980a") (a) worst wall (b) average wall

(a) 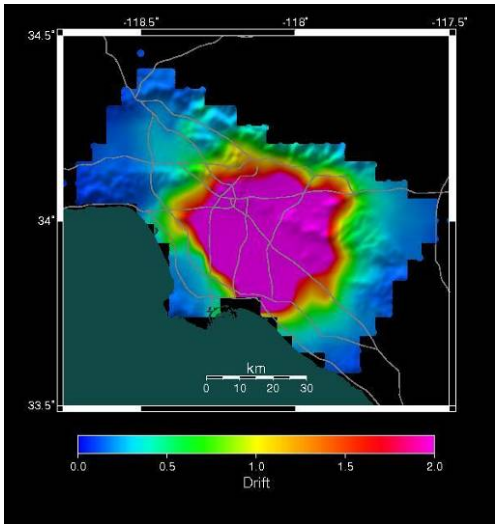

(b) 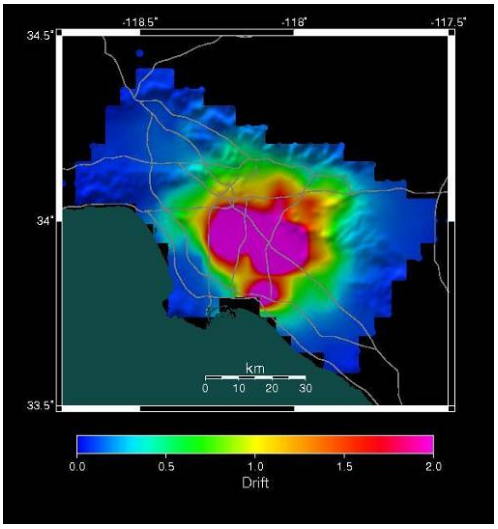

A6-10. Mean transient 1st-story drift, inches, 1980-2000 index building with special seismic detailing ("1980b"), (a) worst wall, and (b) average wall

(a) 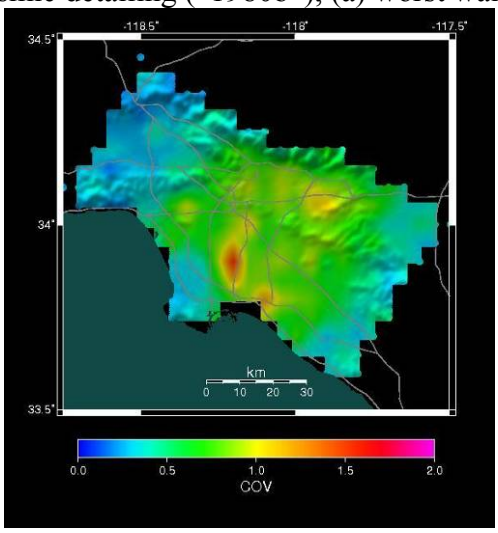

(b) 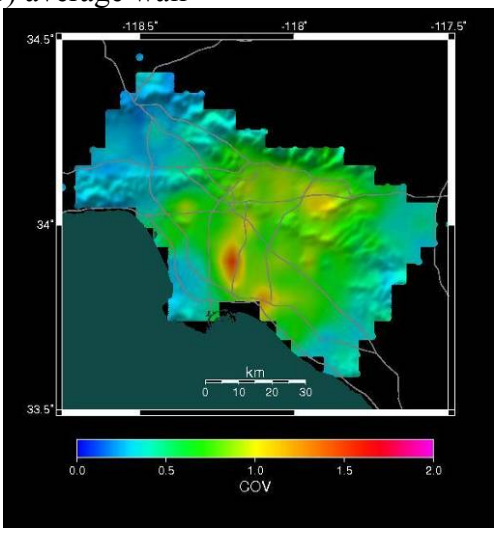

A6-11. Coeff. of variation, transient 1st-story drift for 1980-2000 building with special seismic detailing ("1980b"), (a) worst wall, and (b) average wall